EFFECT OF SEX ON EXPERIMENTAL DIABETIC NEPHROPATHY AND THE RENIN-ANGIOTENSIN SYSTEM. ROLE OF ACE2

Thesis submitted by

Sergi Clotet Freixas

For the degree of Doctor of Biochemistry, Molecular Biology and Biomedicine

Directors

Dr. Julio Pascual Santos

Dr. Mª José Soler Romeo

Dr. Marta Riera Oliva

Tutor

Dr. Assumpció Bosch

PhD Student

Sergi Clotet Freixas

Department of Biochemistry and Molecular Biology
Universitat Autònoma de Barcelona

Barcelona, July 2016

5. RESULTS

5.A. SEX DIFFERENCES IN DIABETIC NEPHROPTAHY AND CIRCULATING AND RENAL RAS. ROLE OF MALE SEX HORMONES

5.A.I. Effect of sex and diabetes on physiological parameters

We studied sex differences in diabetic nephropathy and RAS after 19 weeks of type 1 diabetes. During this period, blood glucose and BW were monitored every 2 weeks under fasting conditions. As shown in Figure 39A, all groups receiving STZ showed significantly increased blood glucose levels as compared to their controls. This was already observed in the first measure (2 weeks after the administration of the second dose of STZ), and maintained throughout all the follow-up. Within the diabetic groups, males showed accentuated hyperglycemia as compared to females during the first 12 weeks of follow-up. Interestingly, blood glucose levels in GDX diabetic males dramatically decreased from week 2 to week 8 of follow-up. From this point, this group showed attenuated hyperglycemia in comparison to the non-gonadectomized diabetic males, with blood glucose values still higher as compared to the GDX controls.

Hyperglycemia was accompanied by a significant decrease in BW in all the experimental groups (Figure 39B). As expected, control and diabetic males showed a clearly higher BW as compared to females throughout all the follow-up. In turn, gonadectomy significantly reduced BW in both, control and diabetic males.

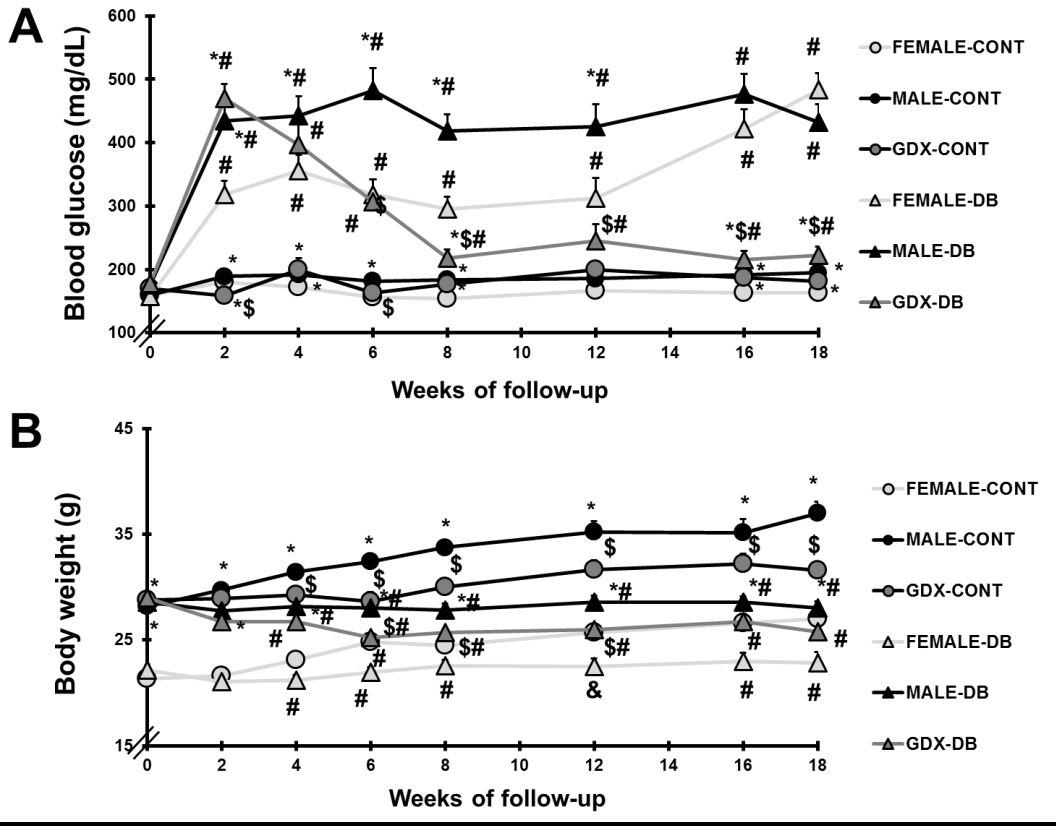

Figure 39. Blood glucose and body weight monitoring in all experimental groups. Y axis represents blood glucose levels (A) and body weight values (B). Time of follow-up is expressed in weeks and depicted in the X axis. Data are expressed as mean ± SEM. *p<0.05 vs. female; #p<0.05 vs. control; $p<0.05 vs. Non-GDX males.

Differences between groups in blood glucose levels and BW were also observed at the end of follow-up, when these parameters were assessed under non-fasting conditions (Figure 40A,B). In control mice, male sex was associated to augmented kidney and heart weights as compared to females (Figure 40C,E). This increase was not observed in GDX males. In turn, diabetes was accompanied by renal hypertrophy in terms of KW/BW ratio in all experimental groups (Figure 40D), and decreased heart weight in females and intact males (Figure 40E).

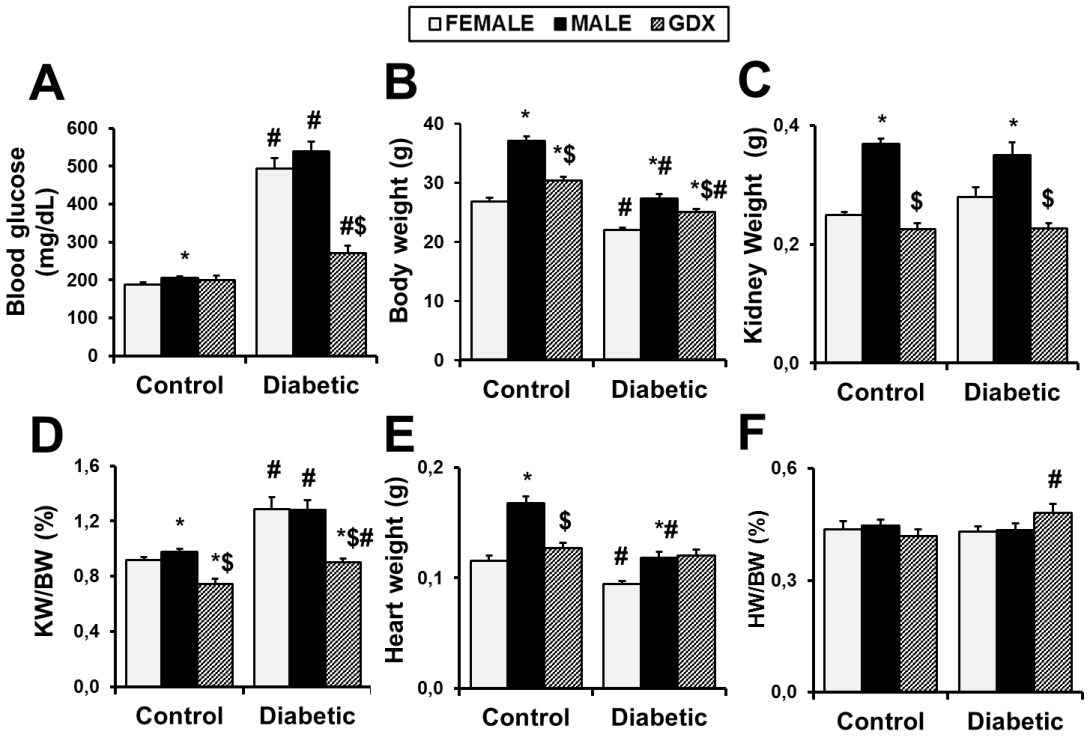

Figure 40. Physiological parameters. Sex effect on blood glucose levels (A), body weight (BW, B), kidney weight (KW, C), KW/BW (D), heart weight (HW, E) and HW/BW (F) were studied after 19 weeks of diabetes. Data are expressed as mean ± SEM. *p<0.05 vs. female; #p<0.05 vs. control; $p<0.05 vs. Non-GDX males.

In this study, diabetes did not significantly alter blood pressure in any of the studied groups (Figure 41A,B). Diabetic females showed a modest but not significant increase in SBP and DBP as compared to their controls, achieving the highest values among all diabetic groups. The decrease in heart weight observed in diabetic females and males was accompanied by a diminished heart rate. In turn, gonadectomy significantly increase heart rate in both, control and diabetic mice (Figure 41C).

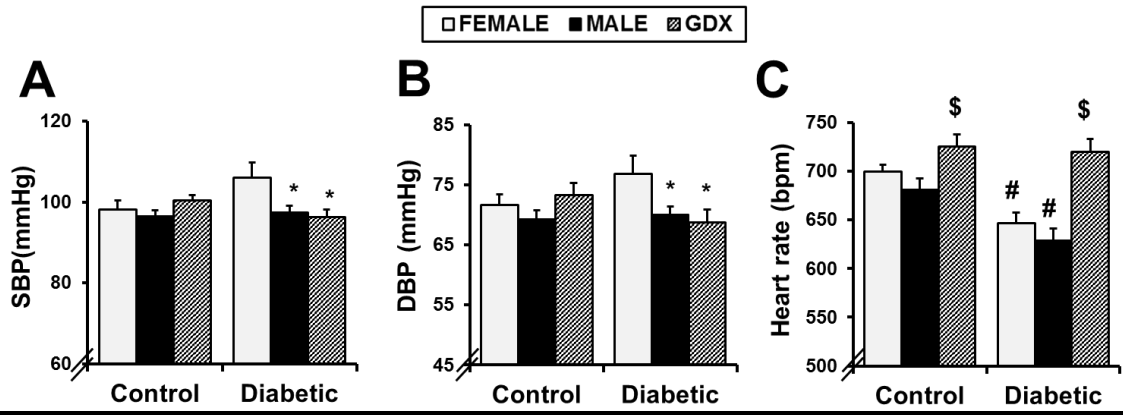

Figure 41. Blood pressure and heart rate. Sex effects on systolic (A) and diastolic (B) blood pressure and heart rate (C) were studied after 19 weeks of diabetes. Data are expressed as mean ± SEM. *p<0.05 vs. female; #p<0.05 vs. control; $p<0.05 vs. Non-GDX males.

5.A.II. Effect of sex and diabetes on glomerular injury

To evaluate the impact of sex hormones in the diabetic glomeruli, several functional and histological hallmarks of diabetic nephropathy associated to this compartment were studied. Specifically, changes in GFR, UAE, glomerular tuft area and mesangial area were analyzed.

5.A.II.1. Glomerular functional parameters

Diabetes was accompanied by increased UAE (Figure 42B) in female and male mice. In addition, GFR (Figure 42A) was significantly increased only in diabetic males as compared to control males. Interestingly, GDX prevented the increase of GDX and albuminuria in diabetic males.

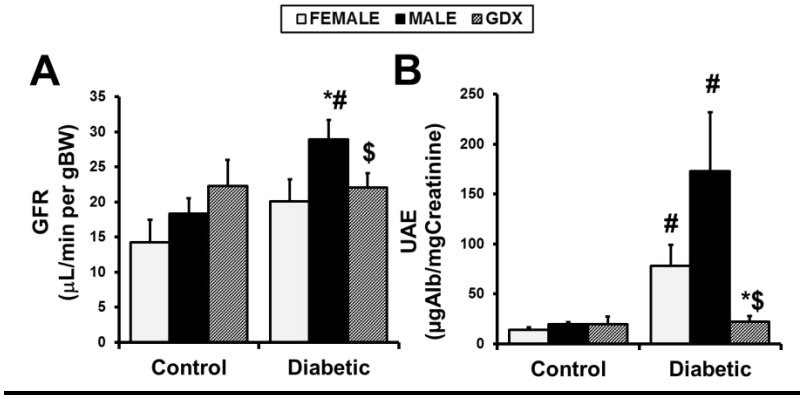

Figure 42. Assessment of glomerular function. Sex effects on glomerular filtration rate (GFR, A) and urinary albumin excretion (UAE, B) were studied after 19 weeks of diabetes. Data are expressed as mean ± SEM. *p<0.05 vs. female; #p<0.05 vs. control; $p<0.05 vs. Non-GDX males.

5.A.II.2. Glomerular histology

5.A.II.2.1. Glomerular tuft area and mesangial area

Sex differences in glomerular morphometry were observed even under physiologic conditions. Specifically, control male mice showed significantly lower glomerular tuft area (Figure 43A,B) and mesangial area (Figure 43A,C) as compared to females. Diabetes significantly increased glomerular tuft area, mesangial area and mesangial index only in males (Figure 43A-D). Surprisingly, gonadectomy increased mesangial area and mesangial index to values that were comparable to females (Figure 43A,C,D).

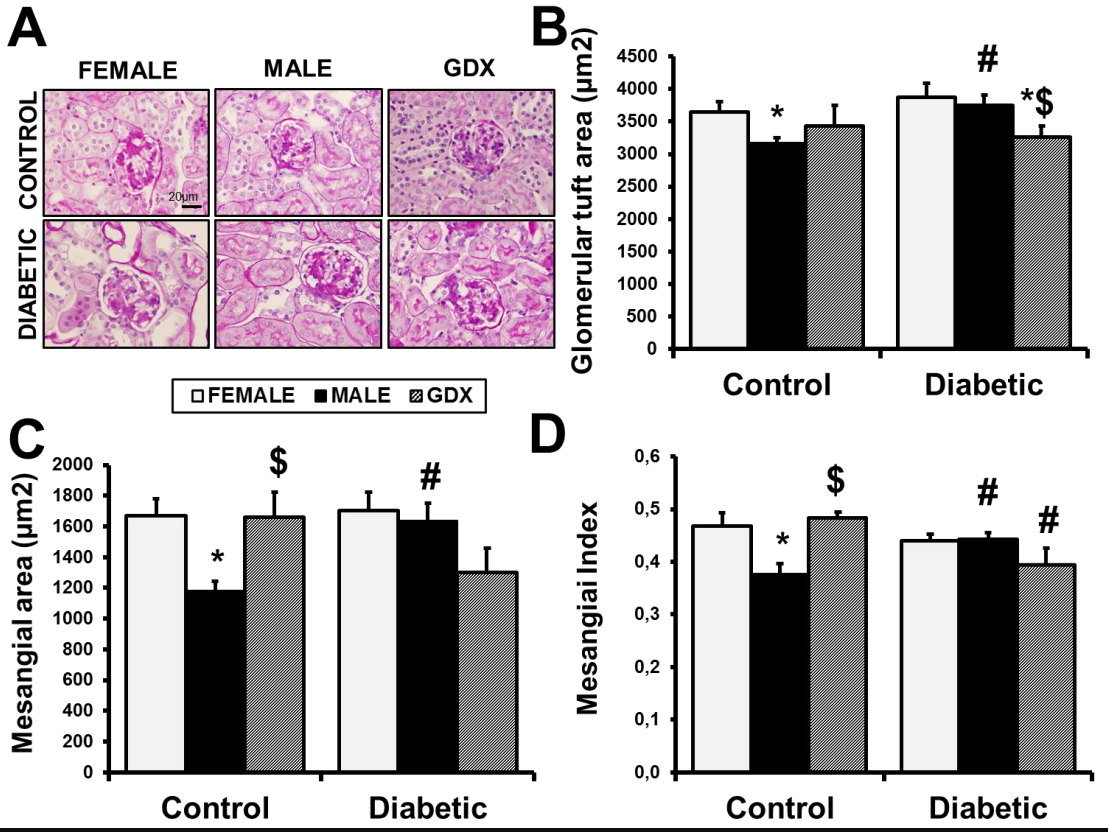

Figure 43. Glomerular morphometry. Panel A shows representative photomicrographs depicting glomerular morphometric changes in PAS-stained stained sections from all the experimental groups. Scale Bar = 20µm. Original magnification x40. On these images, sex effects on glomerular tuft area (B), mesangial area (C) and mesangial index (D) were studied. Data are expressed as mean ± SEM. *p<0.05 vs. female; #p<0.05 vs. control; $p<0.05 vs. Non-GDX males.

5.A.II.2.2. Bowman's capsule epithelialization

Qualitative evaluation of Bowman's capsule width revealed that male sex was associated to a higher degree of epithelialization of the glomerular capsule (Figure 44). Focusing our attention on the urinary pole of the glomeruli, we first noticed that control

females had none or just a few epithelial cells recovering the inner side of the capsule. Control males, however, showed a clear, wide and continuous layer of epithelial cells in the majority of their glomeruli. This layer was composed for at least 5-6 cells and coated the inner side of Bowman's capsule along half of its perimeter, approximately. Interestingly, this morphologic characteristic was not observed in control GDX males.

The morphology of the Bowman's capsule was also altered in the context of diabetes. Diabetic males did not show the epithelization of the capsule observed in their controls. In turn, several glomeruli from diabetic females showed a thickening of the capsule. This thickening was based on a hyperplasic process consisting on dysregulated growth and accumulation of cluttered and stacked cells, distributed in one or more layers. In some cases, thickening of the capsule was accompanied by the presence of one or more PAS positive fibers, suggesting periglomerular collagen accumulation. To a lesser extent, this hyperplasic and pro-fibrotic process was also observed in diabetic GDX mice.

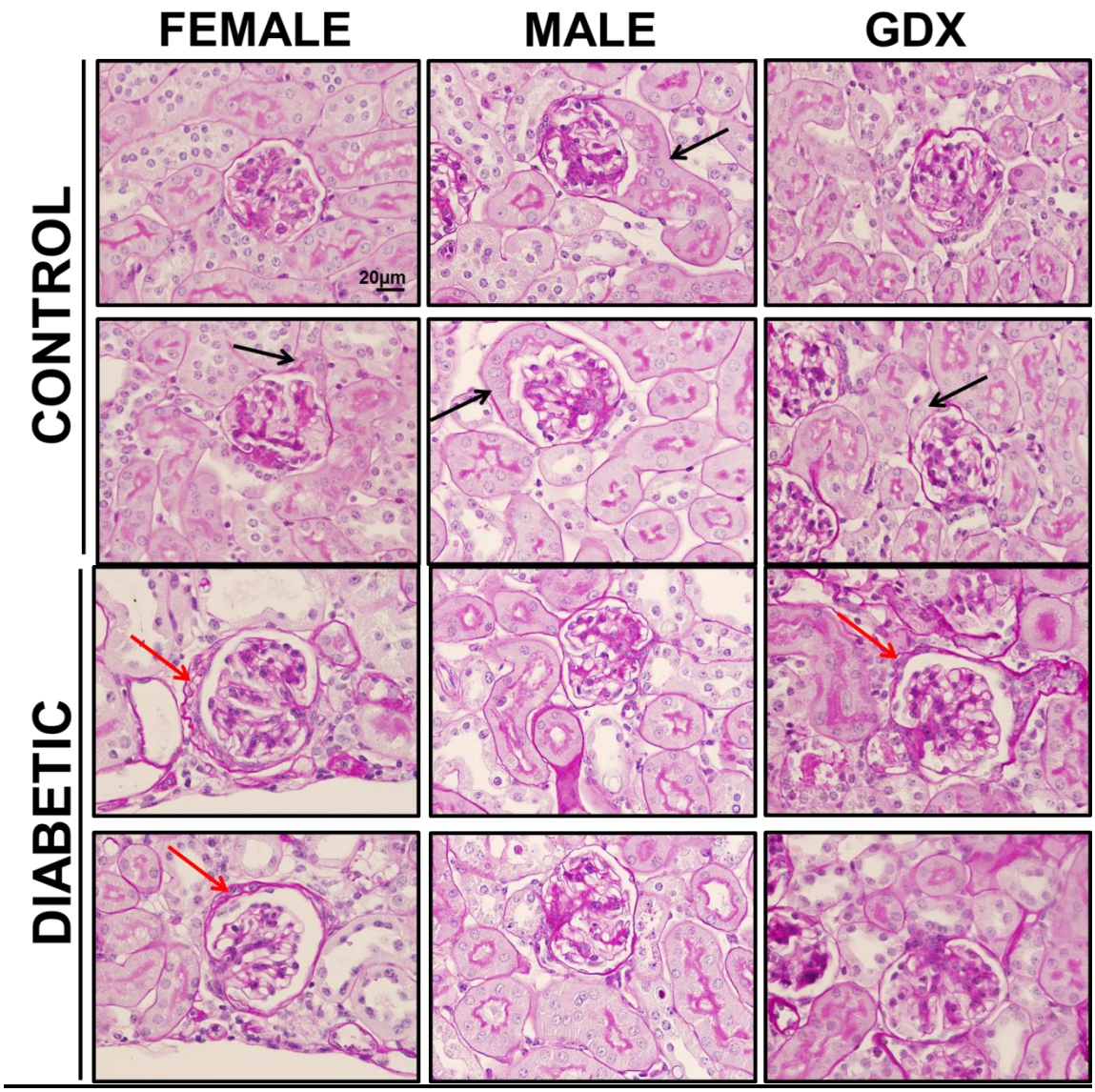

Figure 44. Evaluation of morphologic changes in the glomerular capsule. Microphotographs of PAS-stained kidney sections depicting the effect of sex and diabetes on glomerular capsule epithelialization (black arrows), or thickening (red arrows). Two representative glomeruli were selected for each experimental group. Scale Bar = 20µm. Original magnification x40.

5.A.III. Effect of sex and diabetes on tubular injury

To evaluate the impact of sex hormones in the diabetic tubule, cytoplasmic vacuolization/lipid accumulation was analyzed. In addition, renal expression of several fibrosis markers was studied at mRNA and protein level.

5.A.III.1. Cytoplasmic lipid deposits

Male sex was associated to the presence of PAS negative, lipid material in the cytoplasm of certain tubular cells (Figure 45). Due to the bulky shape of these cells, we

surmise that they are proximal tubule cells. In diabetic males, accumulation of lipid material/vacuoles occurred mainly in the tubular lumen rather than in the cytoplasm of tubular cells. Interestingly, this lipid deposition was almost absent in females and prevented by GDX in both, control and diabetic mice.

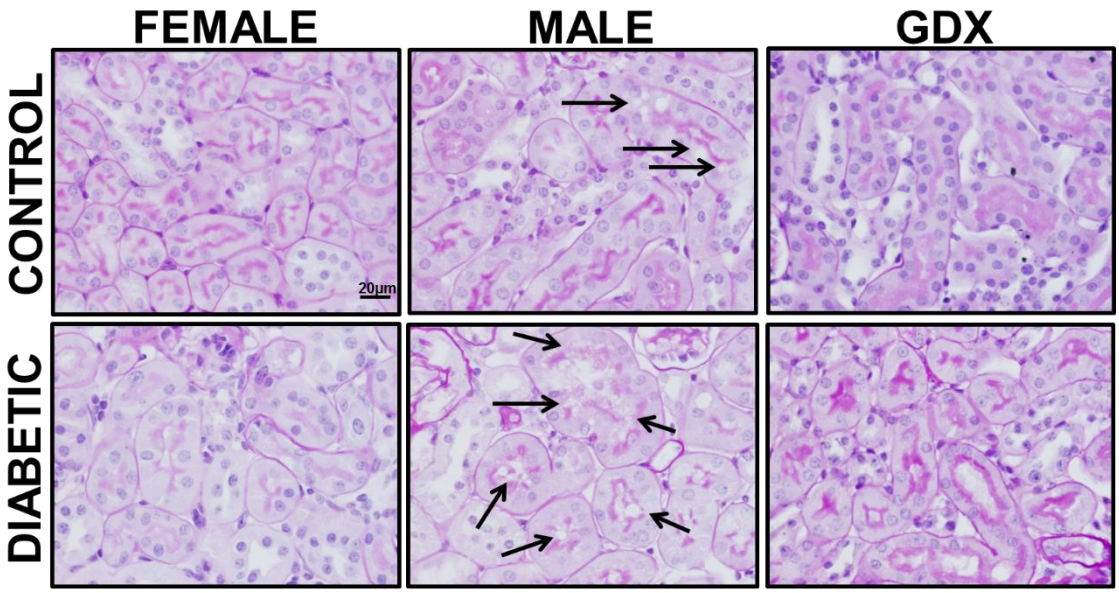

Figure 45. Evaluation of tubular lipid deposition. Microphotographs of PAS-stained kidney sections depicting the effect of sex and diabetes on tubular lipid accumulation. The arrows indicate the presence of lipid deposits and vacuoles. Scale Bar = 20µm. Original magnification x40.

5.A.III.2. Cortical fibrosis

The presence and severity of cortical fibrosis in the studied groups, we first analyzed the gene expression levels of different fibrosis markers: TGF-β1 and CTGF as inductors of fibrotic responses[497]; α-SMA as a marker of myofibroblasts, highly specialized cells with the ability to secrete ECM components and remodel tissue due to their contractile properties[498]; and fibronectin and collagen I and IV chains as extracellular matrix components that are accumulated in fibrotic processes [499].

In our model, diabetes supposed a clear increase in the cortical gene expression of all the analyzed fibrotic markers. Interestingly, this increase was more pronounced in diabetic females and in GDX mice (Figure 46A-F). Indeed, only *Fn1* and *Col1a2* appeared to be significantly up-regulated in diabetic males as compared to their controls (Figure 46D,E). Sex differences in the mRNA levels of these fibrosis markers were also observed under non-diabetic conditions. Specifically, gene expression of *Tgfb1*, *Acta*, *Fn1*, and *Col1a2* and *ColIVa1* was significantly higher in control female mice as compared to males (Figure 46A,C-F). In addition, GDX in control males stimulated the gene expression of all the fibrotic markers analyzed.

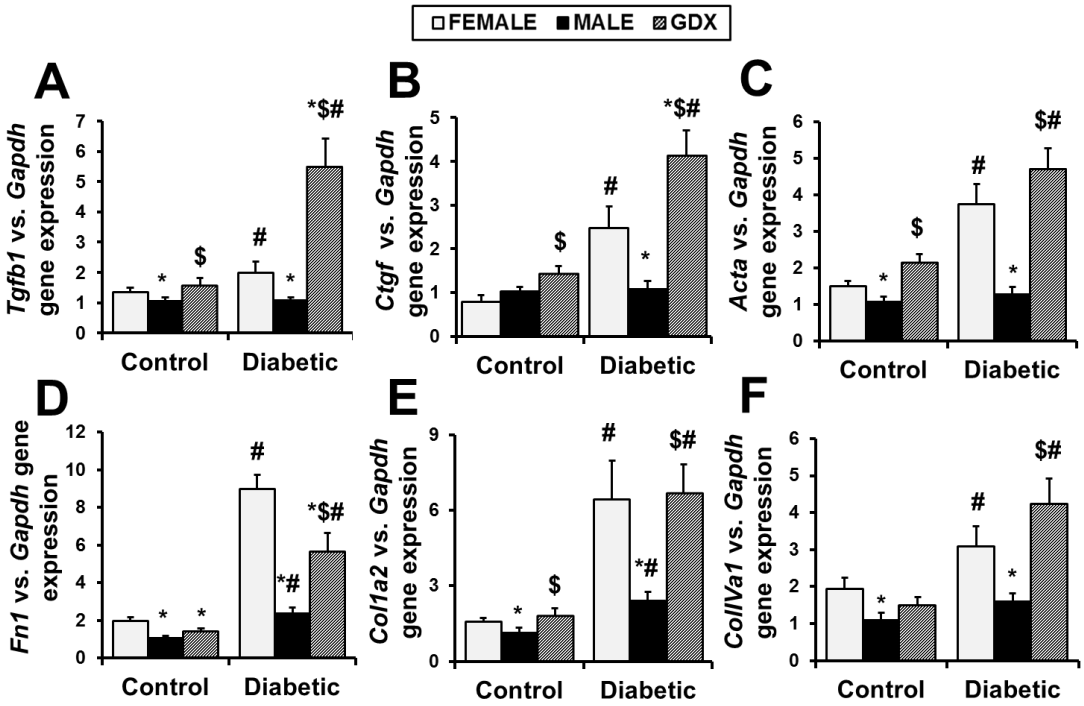

Figure 46. Cortical gene expression of fibrosis markers. mRNA levels were assessed for transforming growth factor-beta (*Tgfb1*, A), connective tissue growth factor (*Ctgf*, B), alpha-smooth muscle actin (*Acta*, C), fibronectin (*Fn1*, D), collagen 1 alpha 2 chain (*Col1a2*, E), and collagen 4 alpha 1 chain (*ColIVa1*, F). Values were normalized to *Gapdh* gene expression. Data are expressed as mean ± SEM. *p<0.05 vs. female; #p<0.05 vs. control; $p<0.05 vs. Non-GDX males.

To assess if the effects of sex and diabetes on renal fibrosis at gene level were also observed at protein level, we next examined cortical α-SMA expression and collagen deposition in the studied groups (Figure 47). Evident fibrosis was observed in the interstitial compartment of diabetic females and males (Figure 47A). Quantification of α-SMA positive area (Figure 47B) and semiquantitative scoring of collagen deposition (Figure 47C) were also performed. In concordance with gene expression data, females showed accentuated α-SMA protein expression and collagen deposition as compared to males. In contrast to the gene expression profiles, protein levels of α-SMA and collagen were not up-regulated by GDX in diabetic males.

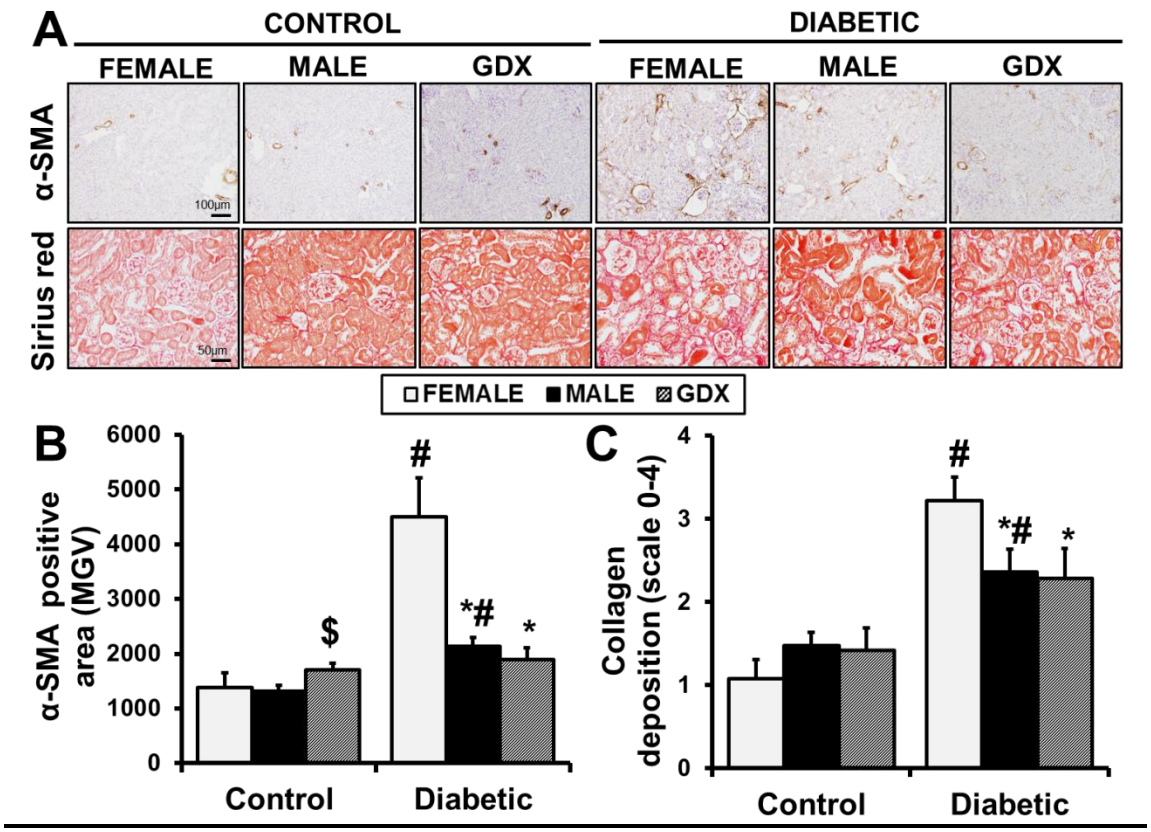

Figure 47. Evaluation of cortical fibrosis at protein level. Representative microphotographs of cortical α-SMA immunostaining and picrosirius red staining for all experimental groups are depicted in panel A. Scale Bar=100μm, Original magnification x10 for α-SMA; Scale Bar=50μm, Original magnification x20 for picrosirius red. On these images, α-SMA expression was quantified using image J software (B). Collagen deposition was measured in a semiquantitative manner (C). Data are expressed as mean±SEM. *p<0.05 vs. female; #p<0.05 vs. control; $p<0.05 vs. Non-GDX males.

5.A.IV. Effect of sex and diabetes on RAS regulation

Our next aim was to correlate the sex divergences on renal injury markers with changes in the expression of RAS components in kidney cortex, urine and circulation.

5.A.IV.1. Gene expression profile of cortical RAS

To obtain a global picture of RAS status in the studied groups, we first analyzed cortical gene expression of the classic initiators of the cascade (AGT and renin), the main regulatory arms of angiotensin peptides metabolism (ACE and ACE2), and enzymes from the alternative, non-classical pathways of ANGII escape (NEP and APN).

Sex by itself exerted a strong influence in the gene expression of all the RAS analyzed components. Control females showed increased mRNA levels of *Agt* (Figure 48A), *Ren* (Figure 48B), and *Nep* (Figure 48E). Interestingly, GDX in control males

significantly stimulated the expression of these three genes to similar levels than the observed in females. *Ace* and *Apn* genes were significantly overexpressed in males and reduced by GDX (Figure 48C,F). In addition, control GDX mice presented a significant increase in *Ace2* gene expression as compared to the non-GDX group.

Diabetes induced a clear increase in cortical *Agt* gene expression in all groups (Figure 48A), suggesting a hyperactivation of renal RAS under hyperglycemic conditions. In diabetic females, this increase was accompanied by significantly reduced *Ren* and *Ace* (Figure 48B,C), as well as augmented *Ace2* mRNA levels in comparison to control females (Figure 48D). In males, diabetes significantly decreased cortical *Ace* and augmented *Ace2* and *Nep* genes (Figure 48C-E). Of mention that diabetes did not modulate *Apn* levels in any of the experimental groups (Figure 48F). The sexual dimorphism on cortical RAS expression observed under physiologic conditions was also reflected in the context of diabetes. In particular, diabetic males showed significantly higher mRNA levels of *Ace*, *Ace2* and *Apn*, as well as diminished *Nep*, as compared to diabetic females. Interestingly, sex differences in the expression of these four genes were not observed when diabetic males were subjected to GDX (Figure 48C-F). In addition, diabetic GDX males presented a clear activation of cortical RAS by means of *Agt* and *Ren* gene expression (Figure 48A-B).

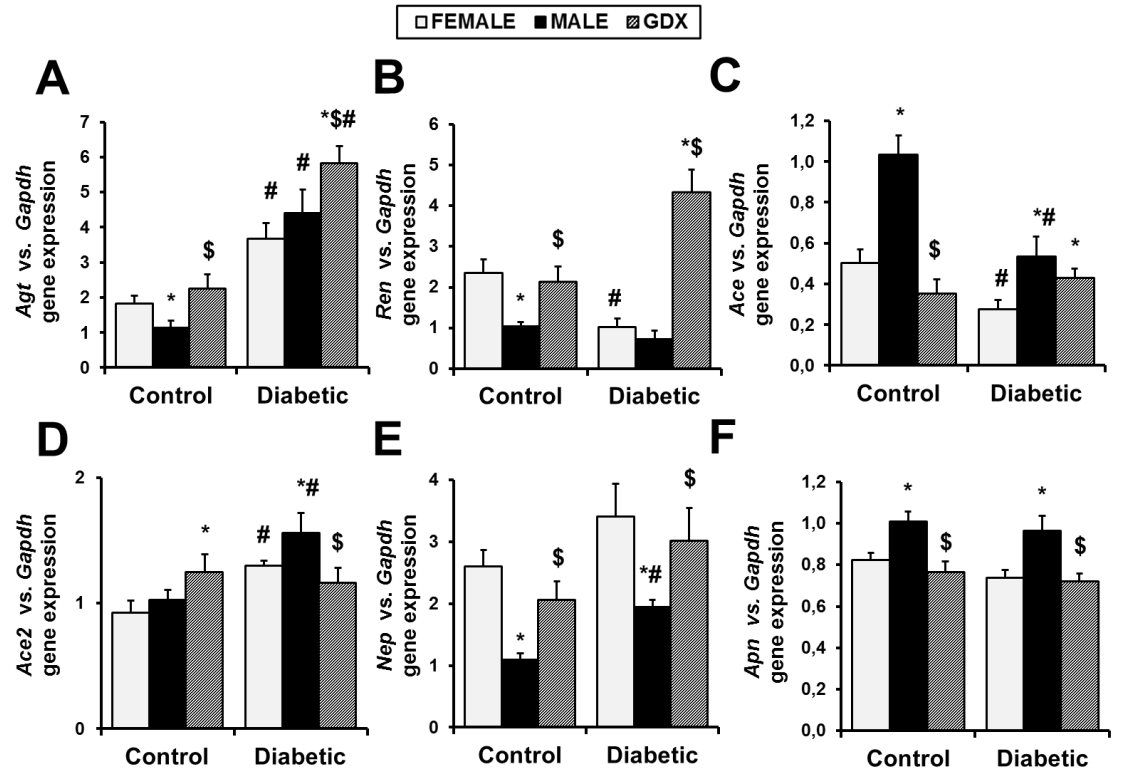

Figure 48. Cortical gene expression of RAS components. mRNA levels were assessed for angiotensinogen (*Agt*, A), renin (*Ren*, B), *Ace* (C), *Ace2* (D), neprilysin (*Nep*, E), and aminopeptidase-N (*Apn*, F). Values were normalized to *Gapdh* gene expression. Data are expressed as mean ± SEM. *p<0.05 vs. female; #p<0.05 vs. control; $p<0.05 vs. Non-GDX males.

As direct regulators of the ANGII/ANG(1-7) balance, it is generally accepted that changes in cortical ACE and ACE2 play a crucial role in the diabetic kidney. Therefore, our next objective was to validate if the sexual dimorphism observed at gene level was also reproduced in experiments evaluating the cortical protein expression and activity of these two enzymes. We also aimed to study if sex-specific ACE and ACE2 regulation in the kidney was associated to sex differences of these enzymes in urine and circulation.

5.A.IV.1. Cortical ACE

In our animal model, sex influenced not only the renal expression of ACE in terms of protein levels, but also the distribution of the enzyme along the renal cortex. After performing immunohistochemistry for ACE in kidney sections, we first observed that control females showed an irregular distribution of the enzyme: whereas a very strong staining was observed in the medulla and the apical site (brush border) of renal tubules from the inner region of the cortex, poor positive signal was detected in the outer cortex (Figure 49A). In control males, ACE also localized in the brush borders of the renal tubules, as previously described. However, the enzyme presented a clear and homogenous pattern across the entire cortex, including the outer area. In turn, ACE positive signal in control GDX mice was very week in both, the outer and the inner area of the cortex. Due to this sex dependence on cortical ACE distribution, we decided to study the effect of sex and diabetes in ACE protein levels and activity in two different portions of renal cortex: the outer cortex and the total cortex (considered as the outer cortex + the transition area).

When analyzing the entire cortex, ACE protein levels were significantly increased in control and diabetic females as compared to males (Figure 49A,B). According to the distribution of ACE in the kidney, this fashion was probably ascribed to overexpression of ACE in the inner cortex (Figure 49A). Oppositely, in the outer cortex, control males showed increased ACE protein expression and activity than females (Figure 49A,C-D). Gonadectomy in control males significantly reduced renal ACE protein levels and activity regardless of the analyzed area (Figure 49A-D).

In general, and in concordance to gene expression data, diabetes was accompanied by a decrease in cortical ACE. However, the extent of this decrease varied depending on the sex and the cortical area analyzed. In females, diabetes reduced ACE expression in the total cortex, but not in the outer cortex. In males, however, the decrease in cortical ACE associated to diabetes was observed in the whole cortex (Figure 49A-D).

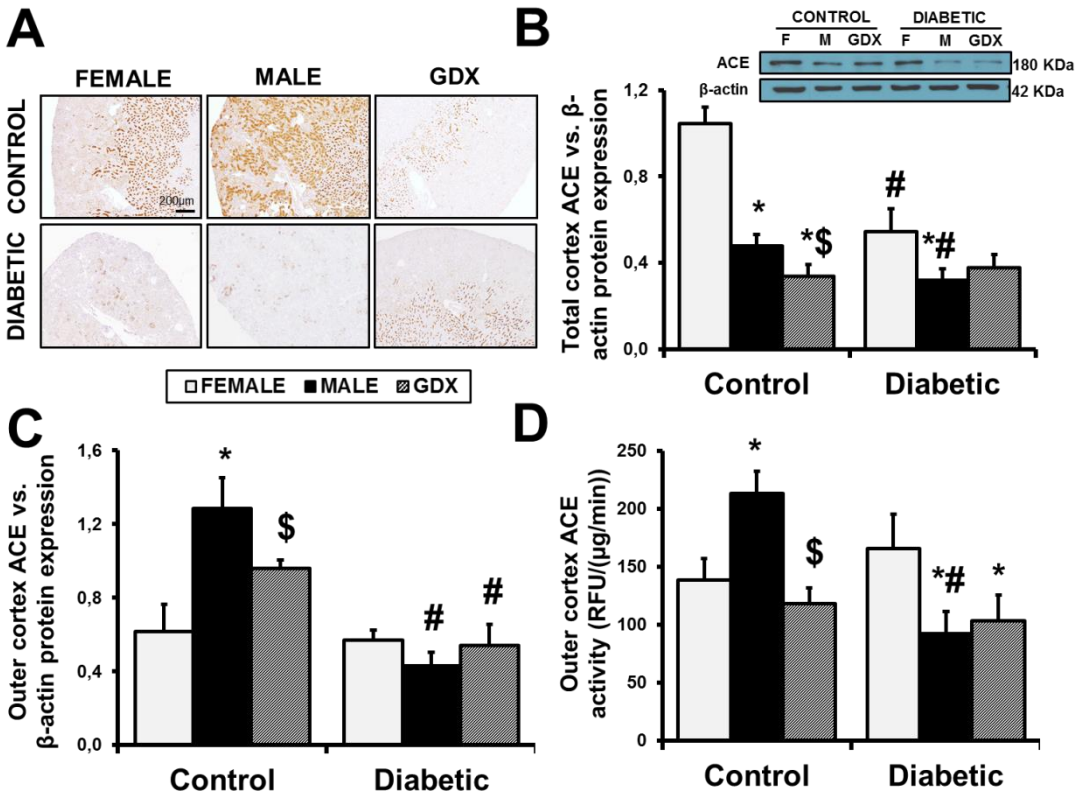

Figure 49. Cortical ACE expression. Panel A shows representative photomicrographs depicting ACE protein localization in the renal cortex from all the experimental groups. Scale Bar = 200µm. Original magnification x4. Panel B: representative immunoblot and densitometries of total cortex ACE protein expression normalized to β-actin. ACE was also analyzed in the outer cortex at the protein (C) and enzymatic activity (D) levels of expression. For these experiments, 6-10 animals were analyzed in each group. Data are expressed as mean ± SEM. *p<0.05 vs. female; #p<0.05 vs. control; $p<0.05 vs. Non-GDX males.

5.A.IV.2. Cortical and urinary ACE2

It is generally accepted that ACE2-mediated ANGII degradation counterbalances ACE-mediated ANGII formation[187]. In addition, ACE and ACE2 have shown to co-localize in the apical site of proximal tubules[183]. For these reasons, we assessed cortical ACE2 in the two cortical areas where ACE was differentially distributed in our groups.

Western Blot experiments for ACE2 expression revealed higher ACE2 protein expression and enzymatic activity in the total cortex of control males as compared to females (Figure 50A,B). This pattern was also observed when analyzing ACE2 activity specifically in the outer cortex (Figure 50C), suggesting that sex-specific regulation of ACE2 expression in this particular area significantly contributed to the changes in ACE2 levels detected in the entire cortex. Gonadectomy in control males significantly increased cortical ACE2 (Figure 50A-C), validating our previous findings at mRNA level.

As observed in the study of gene expression, diabetes significantly augmented cortical ACE2 protein expression and activity in females and males, but not in GDX males (Figure 50A-B). Interestingly, this increase was not observed in the male outer cortex (Figure 50C). Indeed, in the total cortex diabetic males showed significantly higher ACE2 activity than diabetic females, whereas the opposite trend was observed in the outer cortex (Figure 50C).

It has been suggested that urinary ACE2 may be shed from tubular cells in the kidney cortex[500]. Thus, we aimed to explore if sex differences in cortical ACE2 activity were reflected in the activity of this carboxypeptidase in the urine of our experimental groups. Urinary ACE2 activity was significantly increased in all diabetic experimental groups as compared to their controls (Figure 50D). This increase was more pronounced in females. GDX significantly reduced urinary ACE2 activity in diabetic mice.

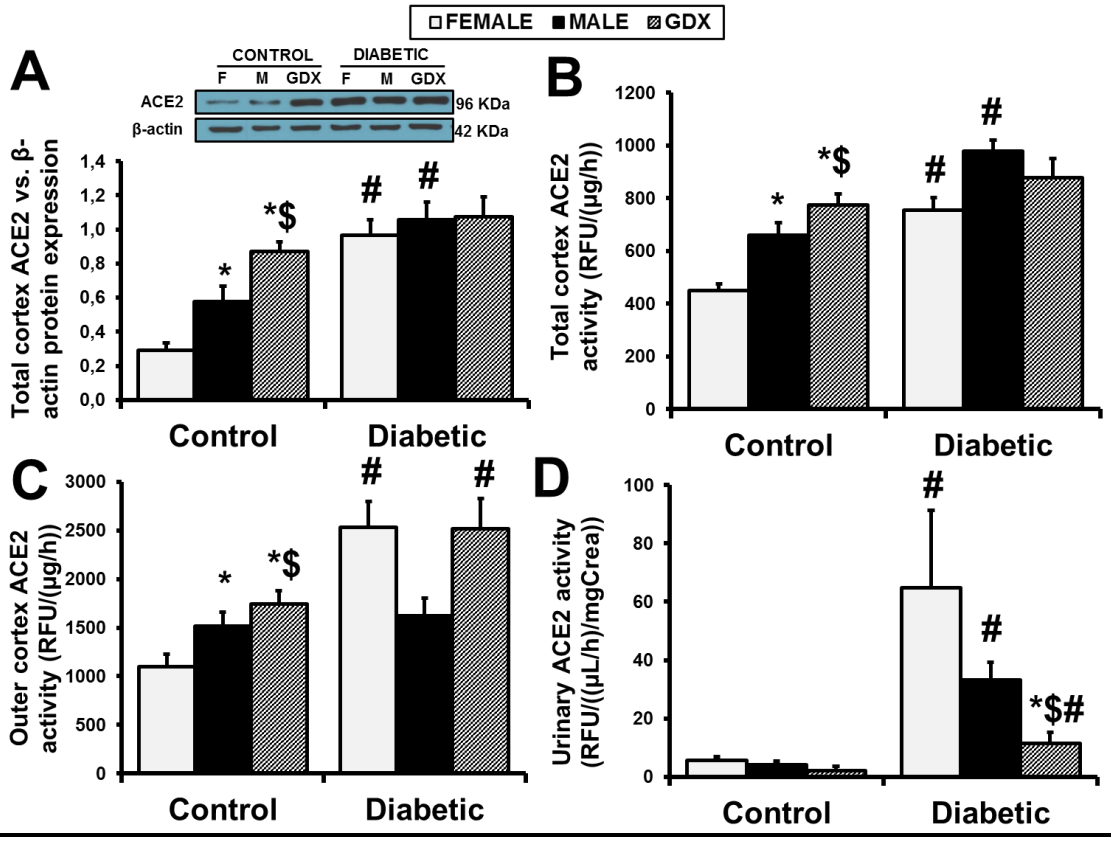

Figure 50. Cortical and urinary ACE2 expression. Panel A: representative immunoblot and densitometries of total cortex ACE2 protein expression normalized to β-actin. ACE2 was also analyzed at the enzymatic activity level in the total cortex (B) and in the outer cortex (C). 6-10 animals per group were analyzed for assessment of cortical ACE2 protein expression and enzymatic activity. 4-8 animals per group were analyzed for urinary ACE2 activity determination. Data are expressed as mean ± SEM. *p<0.05 vs. female; #p<0.05 vs. control; $p<0.05 vs. Non-GDX males.

5.A.IV.3. Circulating ACE and ACE2

Across different tissues, the kidney has been proposed as an important contributor to the levels of active ACE and ACE2 in the serum[177,501]. This contribution may be especially relevant in the context of diabetes[89,496,502]. Our next question was if sex-specific ACE and ACE2 regulation in the kidney cortex was associated to changes in circulating ACE and ACE2 activity according to sex.

As observed in the kidney cortex and mentioned above, serum ACE2 and ACE activities were differentially regulated by sex. Under physiological conditions, males showed a significant raise in the activity of both carboxypeptidases as compared to females. Gonadectomy was accompanied by a significant reduction of both, circulating ACE2 and ACE, in control male mice (Figure 51).

Diabetes was also accompanied by a clear increase in ACE2 and ACE activity in both, female and male mice. This increase was attenuated by GDX. Despite showing similar levels of circulating ACE2 activity (Figure 51A), diabetic males showed significantly higher serum ACE than diabetic females (Figure 51B). Taken together, these findings suggest a role of male sex hormones on promoting systemic RAS hyperactivation, which may be especially relevant in diabetic nephropathy.

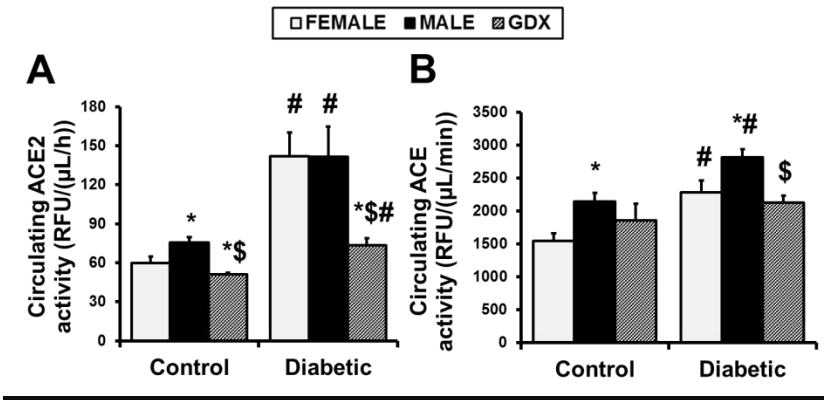

Figure 51. Circulating ACE2 (A) and ACE (B) activity. For these experiments, 8-12 animals were analyzed in each group. Data are expressed as mean ± SEM. *p<0.05 vs. female; #p<0.05 vs. control; $p<0.05 vs. Non-GDX males.

5.A.IV.4. Cortical and circulating ACE2/ACE ratio

It has been suggested that increased ACE2 activity in the serum and the renal cortex may represent a compensatory mechanism to downregulate ACE-mediated circulating ANGII levels and prevent its accumulation in the diabetic kidney[89].

In this study, male sex and diabetes were associated to higher ACE2/ACE protein ratios in the total cortex (Figure 52A). The same pattern was observed when evaluating the outer cortex in terms of protein levels (Figure 52B) and enzymatic activity (Figure 52C). In this area, however, the differences across sexes were not significant. In contrast, diabetic females showed a significantly higher circulating ACE2/ACE than diabetic males, being the only group that presented a significant increase in the ratio as compared to their controls (Figure 52D). Interestingly, GDX in control males dramatically increased ACE2/ACE values in the renal cortex (Figure 52A-C), but did not altered the ratio in serum (Figure 52D).

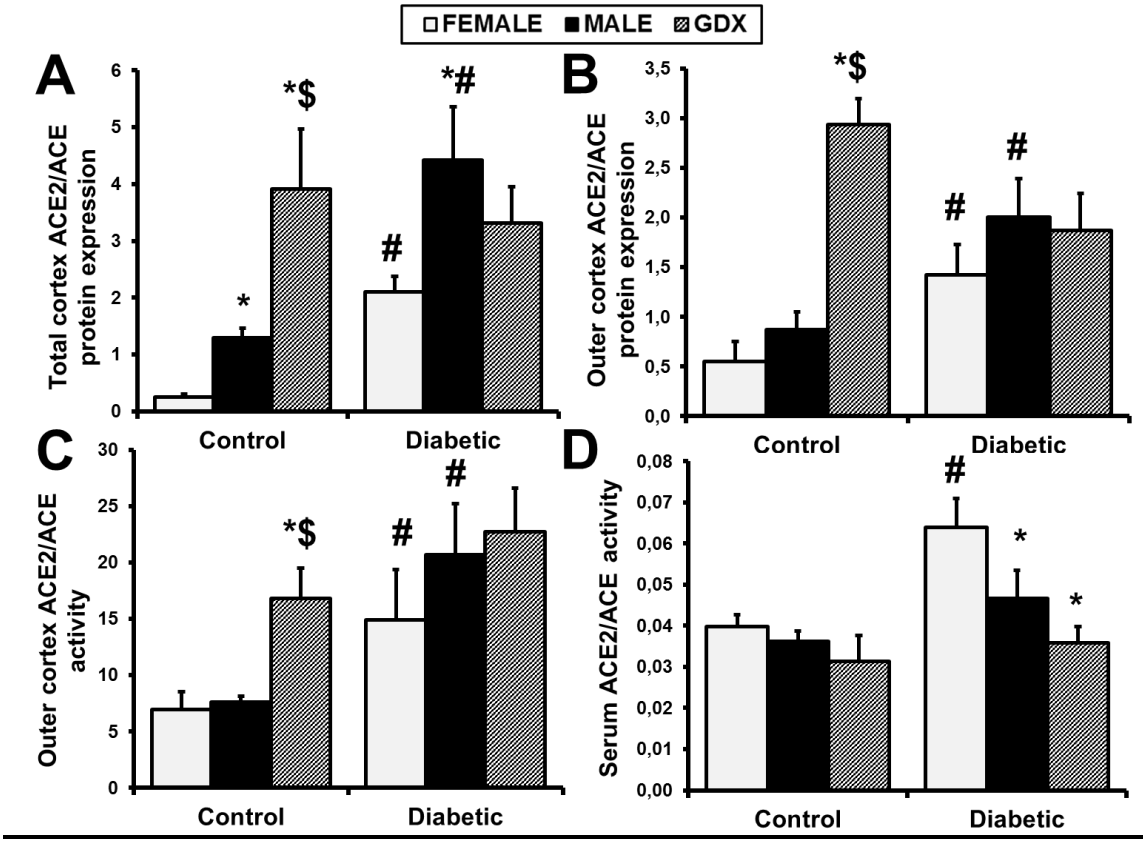

Figure 52. ACE2/ACE ratio in kidney and circulation. ACE2/ACE ratio was determined in terms of protein expression (A and B), outer cortex enzymatic activity (C) and circulating activity (D). For these calculations, values from 8-12 animals were considered in each group. Data are expressed as mean ± SEM. *p<0.05 vs. female; #p<0.05 vs. control; $p<0.05 vs. Non-GDX males.

5.A.V. Effects of sex and diabetes on cortical expression of sex hormone receptors

To evaluate if the effect of sex in diabetic kidney disease and cortical RAS in our animal model were associated to changes in sex hormone signaling, we analyzed the expression of sex hormone receptors in the renal cortex of all experimental groups. In

particular, we assessed cortical mRNA levels of the classic, nuclear ERα and AR, as well as the non-genomic GPER30.

Surprisingly, *Erα* gene expression was significantly higher in control males as compared to females (Figure 53A). In turn, GDX groups showed a tremendous increase in cortical *Ar* gene expression (Figure 53B), suggesting a dysregulation of male sex hormone signaling due to androgen reduction by gonadectomy. Interestingly, the balance between *Erα* and *Ar* gene expression was notably altered in control males as compared to females by means of the *Erα*/*Ar* ratio. This increase was prevented by GDX (Figure 53C).

Diabetes significantly increased cortical estrogen receptors *Erα* and *Gper30* in female and GDX, but not in male mice (Figure 53A,D), whereas decreased AR in all groups (Figure 53B). Despite these alterations, the balance *Erα*/*Ar* was similar between all diabetic groups (Figure 53C). However, *Gper30* gene expression was significantly higher in diabetic female and GDX mice as compared to males (Figure 53D).

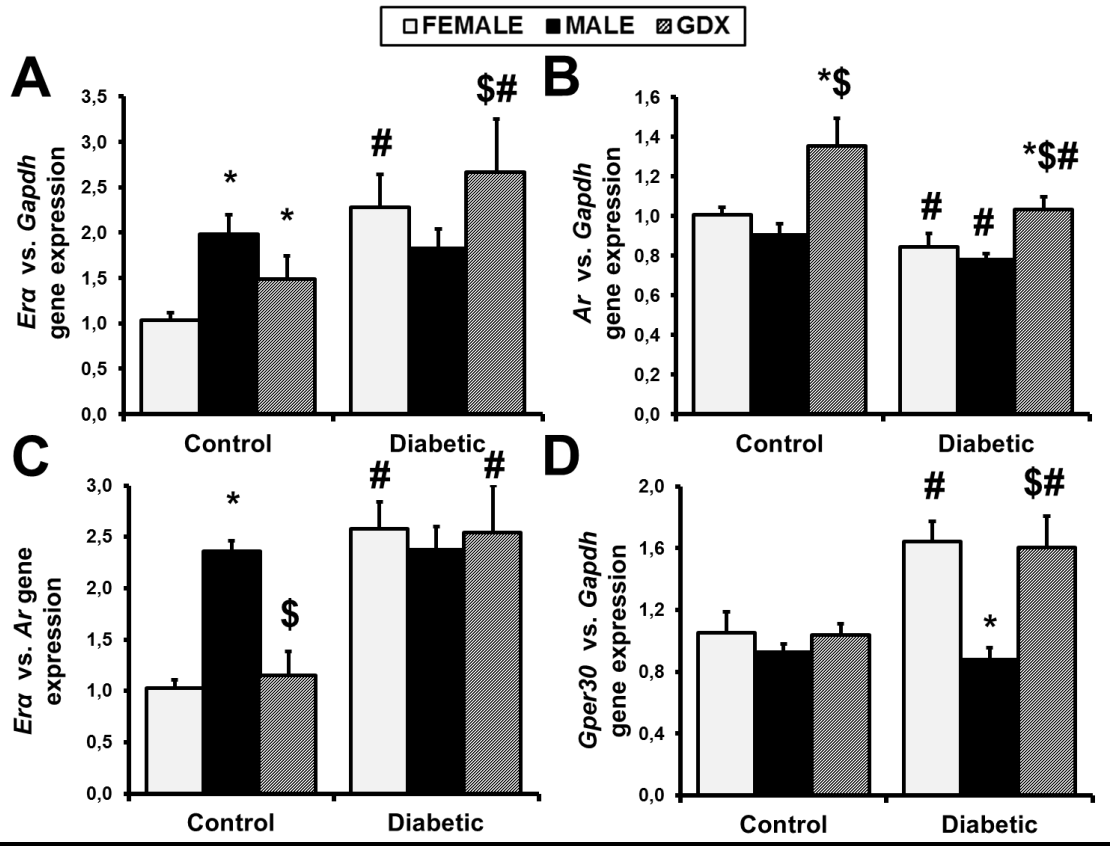

Figure 53. Cortical gene expression of sex hormone receptors. mRNA levels were assessed by RT-qPCR for estrogen receptor alpha (*Erα*, A) and androgen receptor (AR, B). Panel C illustrates *Erα* normalized to *Ar* expression. Cortical gene expression of the G protein-coupled estrogen receptor 30 (*Gper30*) was also assessed (D). Values were normalized to *Gapdh* gene expression. For these experiments, 6-8 animals were analyzed in each group. Data are expressed as mean ± SEM. *p<0.05 vs. female; #p<0.05 vs. control; $p<0.05 vs. Non-GDX males.

5.B. LOSS OF ACE2 ACCENTUATES DIABETIC NEPHROPATHY AND MODULATES RENAL RAS IN TYPE 1 DIABETIC FEMALE MICE

As we demonstrated in the first study, sex differences in diabetic nephropathy are associated to a sex-specific regulation of ACE2 in kidney cortex and circulation. We hypothesized that the dependence on ACE2-mediated ANGII degradation as a renoprotective mechanism to counterbalance or prevent the accumulation of this peptide in diabetes would vary according to sex. In this part of the project, we aimed to evaluate the effects of *Ace2* deletion in the hemodynamics, glomerular function and renal fibrosis of type 1 diabetic females, as well as its relationship with changes in cortical RAS.

5.B.I. Validation of ACE2KO model

We first performed experiments to demonstrate the deletion of the ACE2 sequence codifying the active site of the enzyme. For this purpose, we performed PCR genotyping, kidney protein expression and circulating ACE2 activity in ACE2KO female mice.

As expected, circulating ACE2 activity in ACE2KO females was negligible (Figure 54A). Western Blot analyses showed that the 96KDa band corresponding to the tissue form of ACE2 was present in the kidneys of both, control and diabetic WT, but not ACE2KO females (Figure 54B). Since the antibody employed for ACE2 immunoblotting hybridizes against an epitope containing the active site of the enzyme, the absence of ACE2 band in ACE2KO females indicated that functional ACE2 was not synthesized in their kidneys.

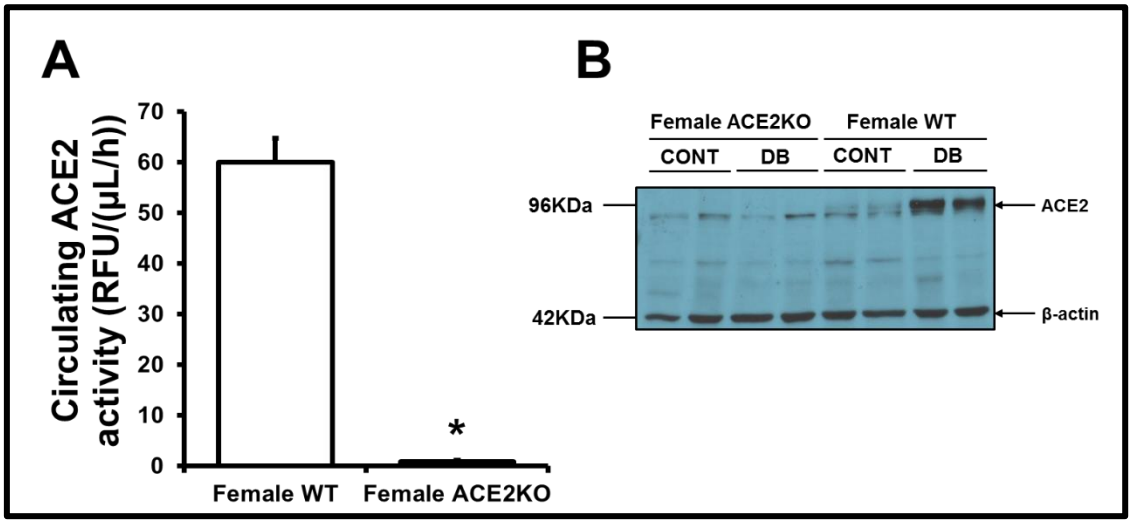

Figure 54. Validation of *Ace2* deletion in female ACE2KO. Lack of functional and active ACE2 protein in ACE2KO female mice was validated in terms of circulating activity (A) and renal protein expression by Western Blot (B). The negligible circulating activity and the absence of the 96KDa band in the first four

lanes of the Western Blot confirmed the lack of functional ACE2 protein in the serum and kidneys of ACE2KO females. Data are presented as mean±SEM. *P<0.05 vs. female WT.

5.B.II. Physiological and functional parameters

STZ administration significantly increased blood glucose levels (Figure 55A) and decreased BW (Figure 55B) in both, WT and ACE2KO females. This trend was already observed at week 2 and maintained throughout all the follow-up. Within the diabetic groups, ACE2KO females showed a more pronounced hyperglycemia than WT females during the first 8 weeks of follow-up (Figure 55A). However, this difference was attenuated at weeks 16 and 18. In addition, control ACE2KO females presented lower BW than the WT during most of the follow-up. In particular, the gain of BW over time in control ACE2KO females started to decrease at week 4.

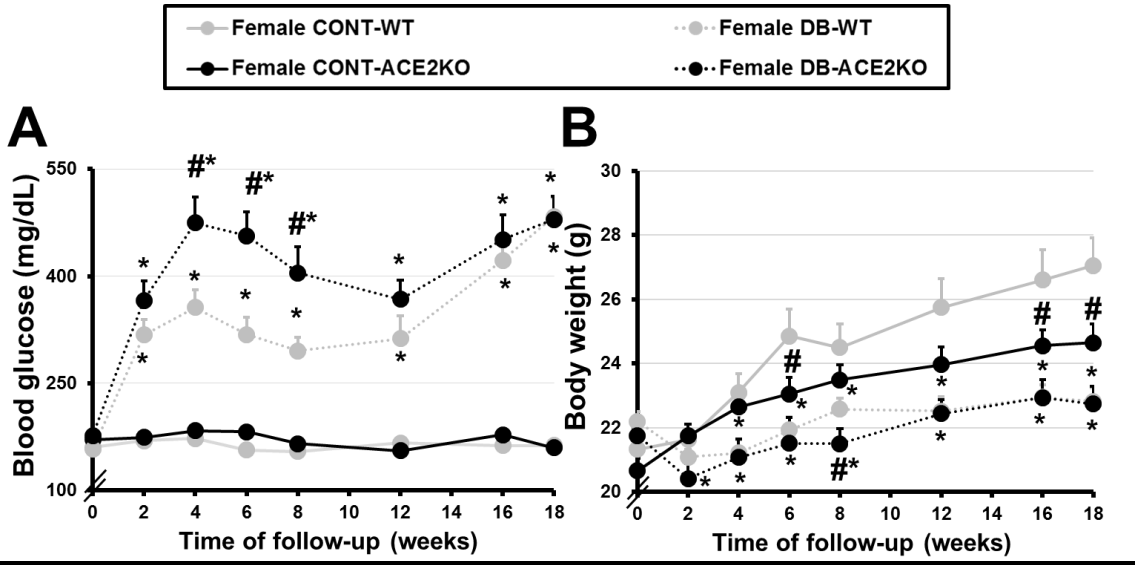

Figure 55. Blood glucose and body weight evolution during the follow-up. Blood glucose levels (A) and body weight (B) were assessed every two weeks and after 3h of fasting in all experimental groups. For these experiments, 8-12 animals were analyzed in each group. Data are expressed as mean±SEM. *p<0.05 vs. CONT; #p<0.05 vs. WT.

The effects of *Ace2* deletion on accentuating hyperglycemia and decreasing BW were also reflected at the end of the study, under non-fasting conditions (Figure 56A,B). Loss of ACE2 was also associated to a significant increase in the KW/BW ratio (Figure 56C) and a modestly higher HW/BW ratio (Figure 56D) in control females. In diabetic females, ACE2 deficiency accentuated renal hypertrophy (Figure 56C) and promoted cardiac hypertrophy (Figure 56D). Diabetes and *Ace2* deletion contributed to an increased SBP and DBP (Figure 56E,F), and decreased heart rate (Figure 56G). Indeed, diabetic ACE2KO females presented the highest values of blood pressure and

the lowest heart rate when compared to the other three groups (Figure 56E-G). Moreover, loss of ACE2 induced a mild increase in GFR in control and diabetic females (Figure 56H) and significantly accentuated albuminuria in diabetic females (Figure 56I).

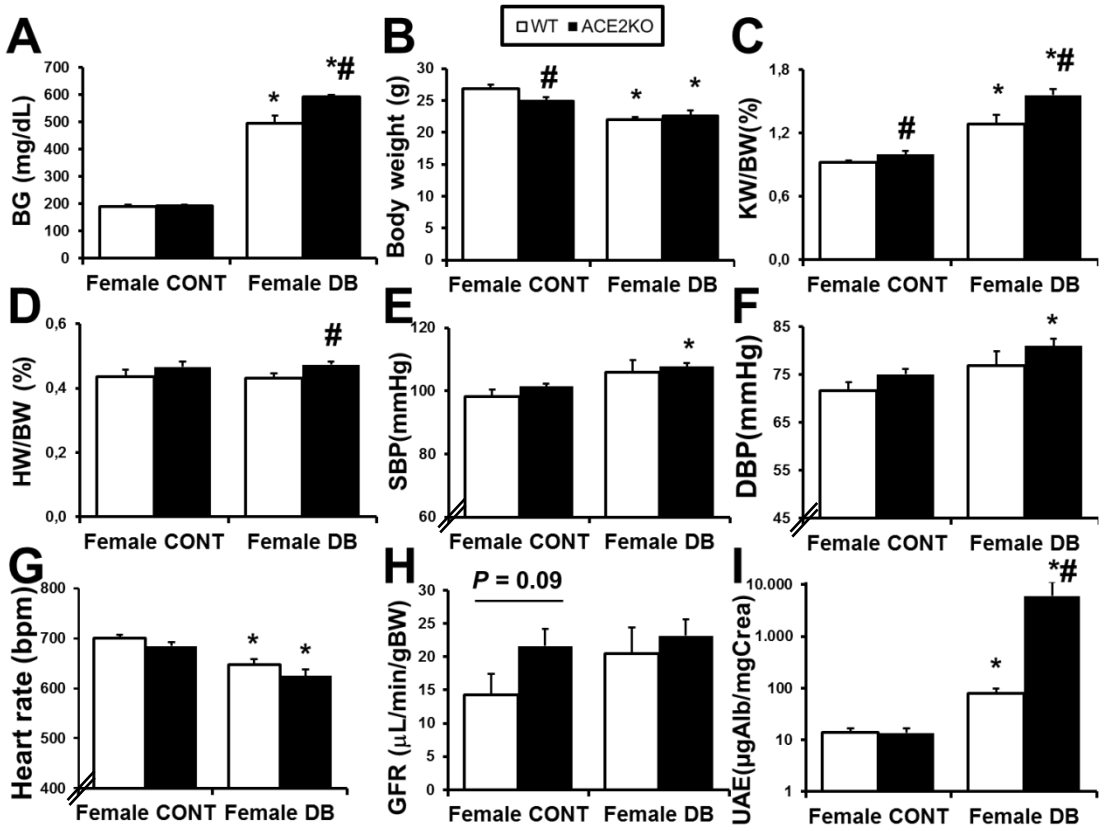

Figure 56. Physiological, hemodynamic, and glomerular functional parameters. Diabetes and *Ace2* deletion effects on blood glucose levels (BG, A), body weight (B), KW/BW (C), HW/BW (D), systolic blood pressure (SBP, E), diastolic blood pressure (DBP, F), heart rate (G), glomerular filtration rate (GFR, H), and urinary albumin excretion (UAE, I) were studied after 19 weeks of diabetes. For these experiments, 8-12 animals were analyzed in each group. Data are expressed as mean±SEM. *p<0.05 vs. CONT; #p<0.05 vs. WT.

5.B.III. Glomerular morphometry

Diabetes was accompanied by an increase in the glomerular tuft area, which was significantly different in the ACE2KO but not in the WT group (Figure 57A-B). Surprisingly, a clear decrease in the mesangial area and the mesangial index was observed in diabetic ACE2KO females as compared to their controls and to the diabetic WT group (Figure 57C-D). We surmised that this unexpected finding was due to an alteration in glomerular structure and morphology in diabetic ACE2KO females. As pointed in Figure 57A, focal dilatations of the loops conformed by the glomerular

capillaries were observed in the diabetic groups. These dilatations were more pronounced in diabetic ACE2KO females as compared to WT.

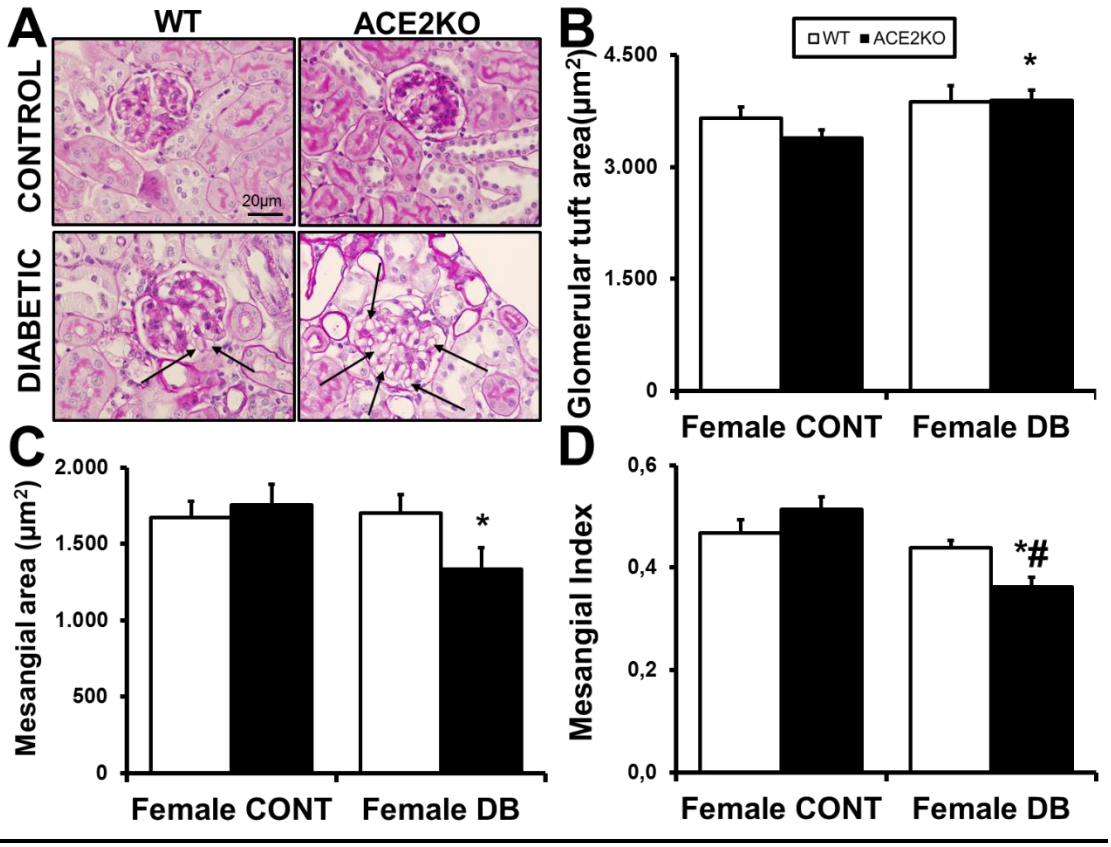

Figure 57. Assessment of glomerular morphometry. Panel A shows representative photomicrographs depicting glomerular morphometric changes in PAS-stained stained sections from all the experimental groups. Black arrows point out dilatations of the glomerular capillaries. Scale Bar=20µm. Original magnification x40. On these images, the effects of diabetes and *Ace2* deletion on glomerular tuft area (B), mesangial area (C) and mesangial index (D) were studied. For these experiments, 8-12 animals were analyzed in each group. Data are expressed as mean±SEM. *p<0.05 vs. CONT; #p<0.05 vs. WT.

5.B.IV. Renal fibrosis and oxidative stress

As expected, diabetes clearly augmented the cortical expression of all the pro-fibrotic markers analyzed, namely TGF-β1, CTGF, collagens I and IV, fibronectin, and α-SMA (Figure 58). Interestingly, loss of ACE2 significantly accentuated the increase in *Tgfb1* but not in *Ctgf* in diabetic females (Figure 58A,B). Accentuated cortical gene expression of *Tgfb1* was accompanied by a more pronounced increase in collagens and fibronectin mRNA levels in diabetic ACE2KO females as compared to the WT group (Figure 58C-E). Of mention that *Ace2* deletion mildly accentuated cortical α-SMA in diabetic females at both, mRNA (Figure 58F) and protein (Figure 58G,H) levels of expression.

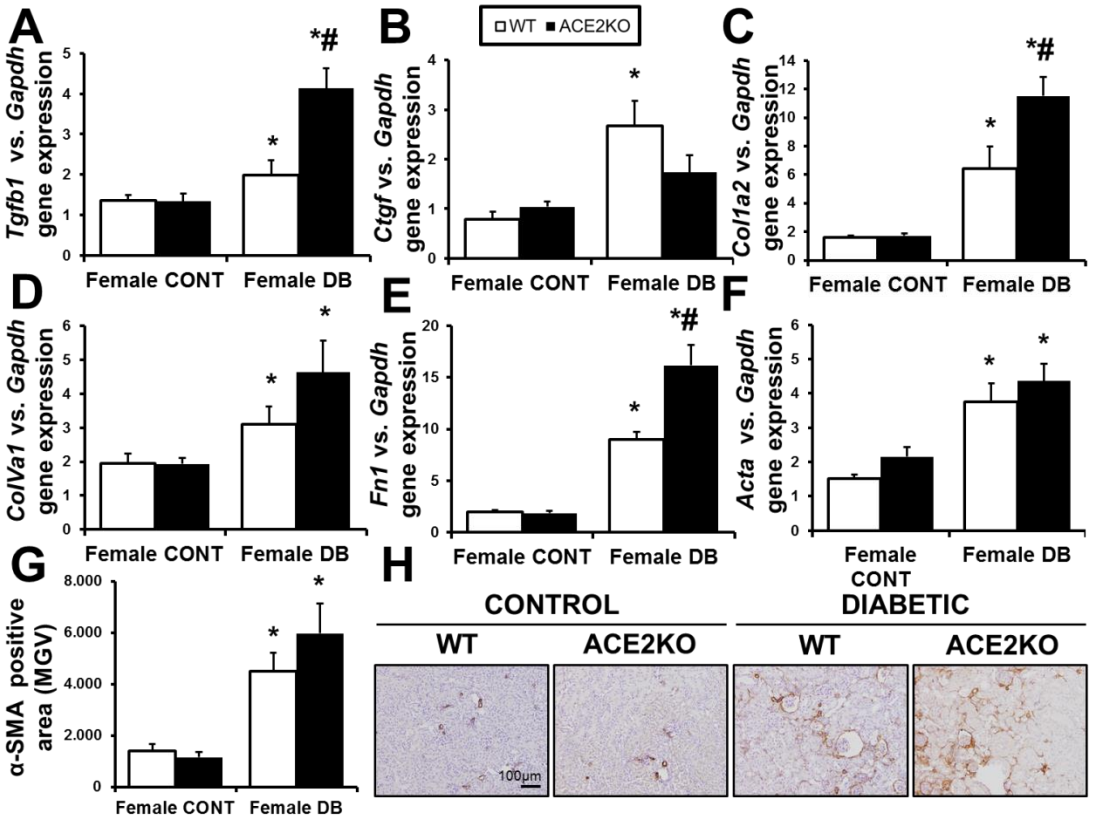

Figure 58. Assessment of renal fibrosis. Cortical mRNA levels of fibrosis markers transforming growth factor-beta (*Tgfb1*, A), connective tissue growth factor (*Ctgf*, B), collagen 1 alpha 2 chain (*col1a2*, C), collagen 4 alpha 1 chain (*collVa1*, D), fibronectin (*Fn1*, E), and alpha-smooth muscle actin (*Acta*, F) were analyzed. Values were normalized to GAPDH gene expression. In addition, protein expression of cortical α-SMA was evaluated by immunostaining and quantified using image J software (G). Representative microphotographs of cortical α-SMA immunostaining are shown in panel H. Scale Bar=100μm, Original magnification x10. For these experiments, 6-10 animals were analyzed in each group. Data are expressed as mean±SEM. *p<0.05 vs. CONT; #p<0.05 vs. WT.

In concordance to the renal fibrosis data, diabetes was accompanied by a tremendous increase in $p47^{phox}$ gene expression (Figure 59A). Oppositely, the mRNA levels of the *Nox2* and *Nox4* subunits were found to be significantly downregulated by diabetes and *Ace2* deletion (Figure 59B,C).

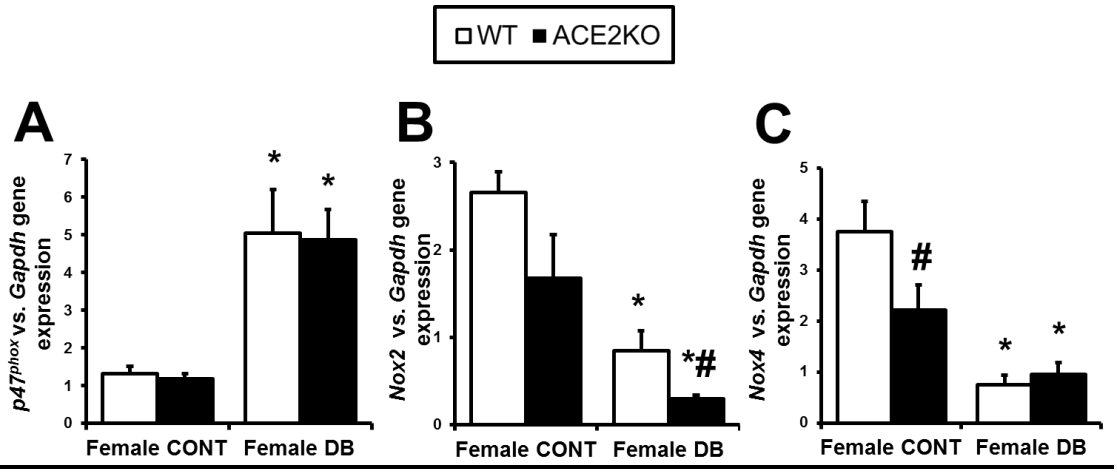

Figure 59. Assessment of renal oxidative stress. Cortical mRNA levels of NADPH oxidase subunits *p47^{phox}* (A), *Nox2* (B), and *Nox4* (C) were analyzed as oxidative stress markers in all the experimental groups. Values were normalized to *Gapdh* gene expression. For these experiments, 6-10 animals were analyzed in each group. Data are expressed as mean±SEM. *p<0.05 vs. CONT; #p<0.05 vs. WT.

5.B.V. RAS components in kidney cortex and serum

Changes in diabetic ACE2KO females regarding glomerular injury and renal fibrosis were associated to alterations in cortical and circulating RAS components. Specifically, *Ace2* deletion modulated the effects of diabetes on cortical RAS activation by significantly increasing *Agt* (Figure 60A) and decreasing *Ren* gene expression (Figure 60B). *Ace* mRNA levels were also reduced to the same extent in both diabetic, WT and ACE2KO female mice (Figure 60C). However, this reduction was not observed at the protein (Figure 60D) and enzymatic activity (Figure 60E) levels. Of mention that Western Blot and ACE activity assays were performed in protein extracts obtained from the outer cortex and not the total cortex of these female mice, probably contributing to these divergences. In the serum, ACE activity was significantly increased in diabetic and in ACE2KO female mice (Figure 60F), suggesting a higher activation of the circulating RAS due to diabetes and *Ace2* deficiency.

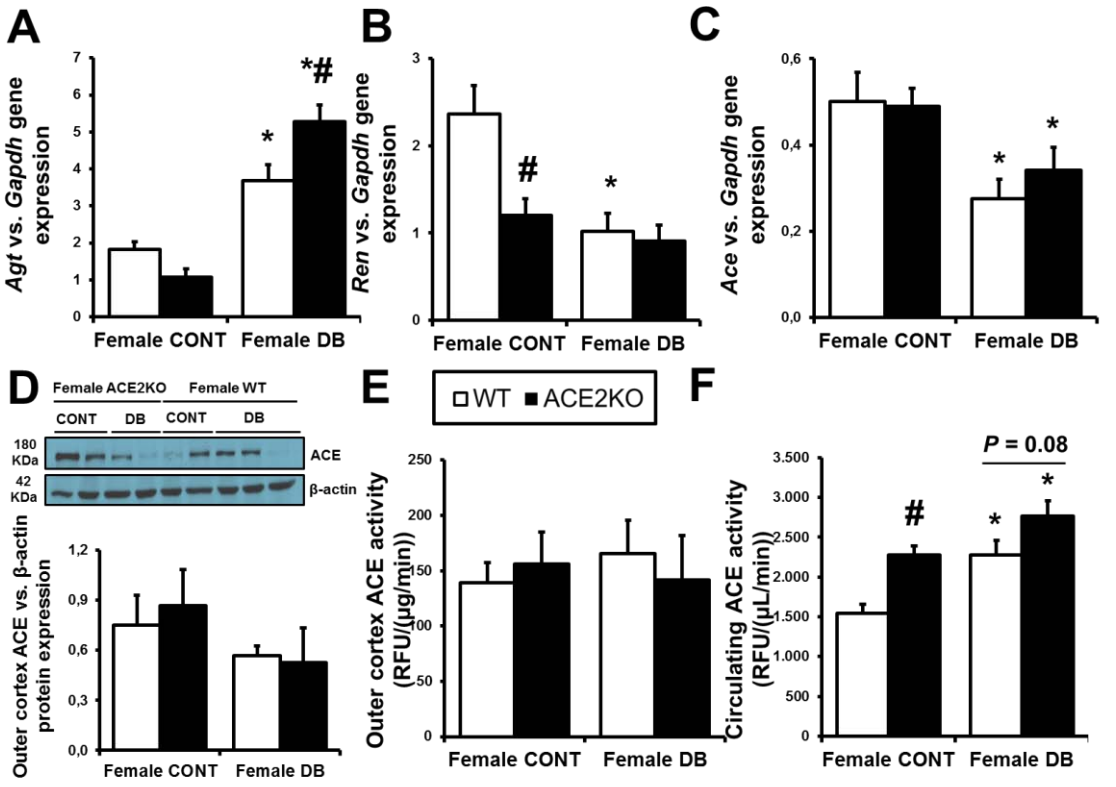

Figure 60. Cortical and circulating expression of ACE and other RAS components. mRNA levels were assessed for angiotensinogen (*Agt*, A), renin (*Ren*, B), and *Ace* (C). Values were normalized to *Gapdh* gene expression. Panel D shows a representative immunoblot and densitometries of ACE protein expression in the outer cortex, normalized to β-actin. ACE activity was also analyzed in the outer cortex (E) and the circulation (F). For these experiments, 6-10 animals were analyzed in each group. Data are expressed as mean±SEM. *p<0.05 vs. CONT; #p<0.05 vs. WT.

5.C. GONADECTOMY PREVENTS THE INCREASE IN BLOOD PRESSURE AND GLOMERULAR INJURY IN *Ace2* KNOCKOUT DIABETIC MALE MICE. EFFECTS ON RENIN-ANGIOTENSIN SYSTEM

5.C.I. Gonadectomy prevents renal hypertrophy, hypertension, hyperfiltration and albuminuria in diabetic ACE2KO male mice

Blood glucose levels were significantly elevated in all STZ-treated groups as compared to their controls (Table 17). Throughout the follow-up, diabetic animals showed lower BW than their controls. In this model, *Ace2* deletion was accompanied by lower BW as compared to WT. In addition, GDX also diminished the BW.

After 19 weeks of study, renal hypertrophy was evaluated by calculating the KW/BW ratio. *Ace2* deletion significantly increased the ratio as compared to the WT animals. In turn, gonadectomy in WT and ACE2KO mice clearly reduced the ratio (Table 17). Diabetes was accompanied by an increased ratio in intact WT and ACE2KO animals,

indicating the presence of renal hypertrophy in these groups due to diabetes. Interestingly, DB-ACE2KO + GDX mice showed significantly lower KW/BW ratio than the DB-WT + GDX group.

Table 17. Physiologic parameters at one month and at the end of the study. Blood glucose (BG) and body weight (BW) at two time-points of the study, after 4 weeks of diabetes induction and after 19 weeks of study, the end-point. At the end of the study, kidney weight (KW) was also recorded in all the experimental groups. 8-12 animals were analyzed in each group. Values are expressed as means±SEM; (n = 8-12 per group). *P<0.05 compared to non-diabetic controls. †P<0.05 compared to WT. §P<0.05 compared to non-GDX.

	CONT-WT	CONT-ACE2KO	CONT-ACE2KO + GDX	DB-WT	DB-WT + GDX	DB-ACE2KO	DB-ACE2KO + GDX
BG(mg/dL) 4wks	191.88 ± 5.31	192.26 ± 4.05	182.67±7.04	442.25±31.29*	303.91±27.36§	493.43±28.02*	268.93±21.53*§
BG(mg/dL) 19wks	207.29 ± 5.49	194.00 ± 6.66	208.50±10.05	538.33±25.35*	294.30±21.59§	545.57±22.25*	242.14±10.11*†§
BW(g) 4 wks	31.44 ± 0.54	27.31 ± 0.60†	25.62±0.80	28.18±0.61*	24.24±0.23§	25.95±0.48†	24.60±0.49
BW(g) 19 wks	36.55 ± 0.89	29.98 ± 0.75†	26.47±1.24§	27.35±0.73*	23.92±0.43§	25.09±0.67*†	24.74±0.73
KW(g) 19 wks	0.37 ± 0.01	0.33 ± 0.01†	0.25±0.01§	0.35±0.02	0.22±0.02§	0.35±0.01	0.20±0.01*§
KW/BW(%) 19wks	0.98 ± 0.02	1.12 ± 0.03†	0.95±0.07§	1.28±0.07*	0.93±0.08§	1.43±0.05*	0.79±0.02*†§

Ace2 deletion significantly increased SBP and DBP in intact diabetic mice (Figure 61A and B). This increase was not observed in DB-ACE2KO + GDX animals. GFR was increased in DB-WT mice as compared to their controls (Figure 61C). *Ace2* deletion accentuated hyperfiltration by increasing GFR in controls. Gonadectomy significantly reduced GFR in diabetic WT and ACE2KO mice. Diabetes significantly increased UAE in WT and ACE2KO mice (Figure 61D). Surgical castration significantly decreased UAE in diabetic WT and ACE2KO mice. Among these groups, DB-ACE2KO + GDX mice presented significantly lower UAE than their respective DB-WT + GDX mice.

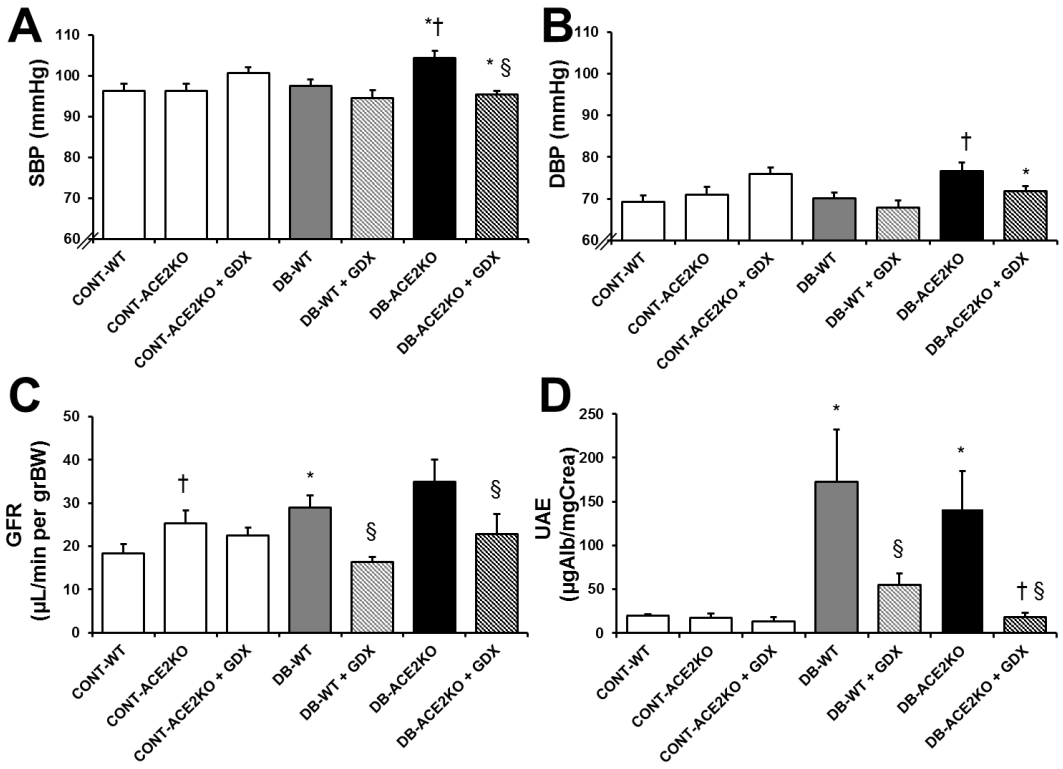

Figure 61. Influence of diabetes, *Ace2* deletion and gonadectomy on hemodynamics and glomerular function. SBP and DBP (8-12 animals per group), glomerular filtration rate and urinary albumin excretion (UAE, 8-12 animals per group) were evaluated in all the experimental groups.Data are expressed as means±SEM. *P<0.05 compared to non-diabetic controls. †P<0.05 compared to WT. §P<0.05 compared to non-GDX.

5.C.II. Gonadectomy prevents glomerular hypertrophy and mesangial matrix expansion in diabetic ACE2KO male mice

Glomerular tuft area was significantly increased in DB-WT and DB-ACE2KO as compared to controls (Figure 62A and C). In concordance to the low renal weight observed in these groups, glomerular area was decreased in gonadectomized WT and ACE2KO diabetic mice. Interestingly, this reduction was only significant in the ACE2KO. DB-WT and DB-ACE2KO mice showed an elevated mesangial index in comparison to the non-diabetic groups (Figure 62B and C). In ACE2KO mice, the mesangial index was significantly higher as compared to WT. Gonadectomy prevented the increase in the mesangial index in both, diabetic WT and ACE2KO mice. Interestingly, DB-ACE2KO + GDX mice showed a significantly higher mesangial index than their respective DB-WT + GDX mice.

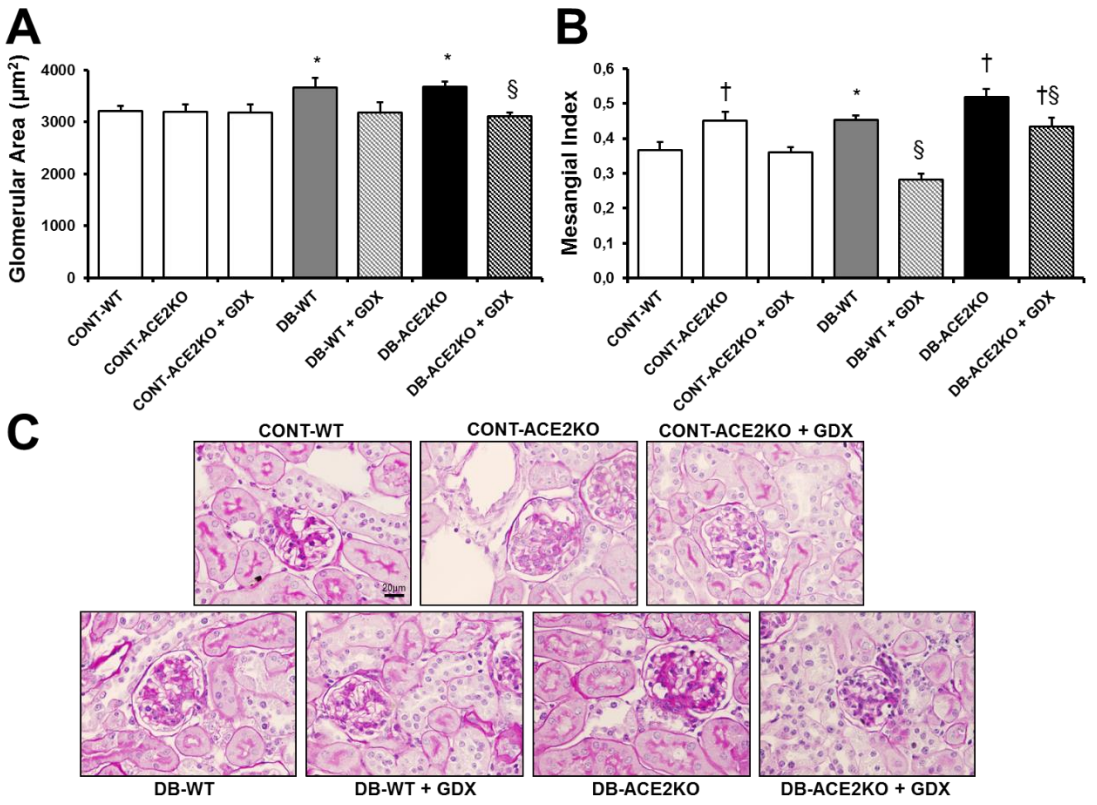

Figure 62. Influence of diabetes, *Ace2* deletion and gonadectomy on glomerular structural alterations. Periodic Acid-Schiff (PAS) staining was performed on 3µm kidney sections from all the experimental groups. Glomerular tuft area (A) and mesangial index (B) were calculated by ImageJ software. Representative PAS sections from all the experimental groups are shown in panel C. For these experiments, 7-10 animals were analyzed in each group. Data are expressed as means±SEM. *P<0.05 compared to non-diabetic controls. †P<0.05 compared to WT. §P<0.05 compared to non-GDX. Scale Bar=20µm. Original magnification x40.

5.C.III. Gonadectomy prevents podocyte loss and glomerular hypercellularity in diabetic ACE2KO male mice

The proportion of cells that were identified as podocytes in glomerulus was significantly decreased in the diabetic groups as compared to controls (Figure 63A and B). This decrease was significantly accentuated in DB-ACE2KO mice as compared to DB-WT. DB-ACE2KO mice also showed a significantly higher number of cells per glomeruli as compared to the DB-WT (Figure 63C). In contrast, gonadectomized ACE2KO diabetic mice showed decreased cell number and increased podocytes within glomeruli. These changes were not observed in the DB-WT + GDX group.

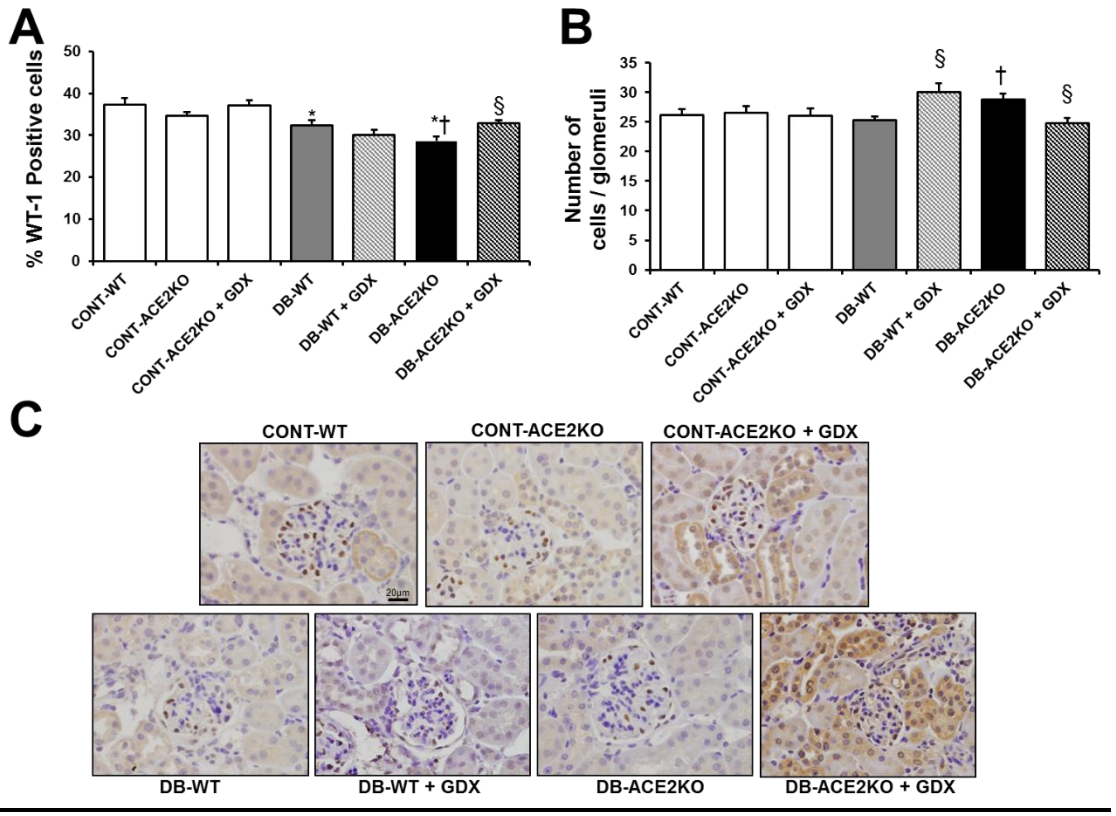

Figure 63. Influence of diabetes, *Ace2* deletion and gonadectomy on podocyte loss and glomerular cellularity. Podocyte number is represented as the % of brown positive cells after WT-1 immunostaining (A). Total cell number was also assessed in the same photomicrographs (B). Representative photomicrographs depicting glomerular WT-1 staining from all the experimental groups are shown in panel C. For these experiments, 6-10 animals were analyzed in each group. Data are expressed as means±SEM.*P<0.05 compared to non-diabetic controls. Scale Bar=20µm. Original magnification x40.

5.C.IV. Gonadectomy attenuates renal fibrosis in diabetic ACE2KO male mice

Interstitial fibrosis was evaluated by two different approaches. To test the progression of fibrogenesis, the presence of interstitial myofibroblast in renal cortex was evaluated by α-SMA immunostaining. This actin isoform predominates within vascular smooth-muscle cells and plays an important role in fibrogenesis. As expected, α-SMA staining was detected in the media of renal arteries and arterioles and diabetes significantly increased its interstitial expression in WT and ACE2KO mice as compared to their non-diabetic controls (Figure 64).

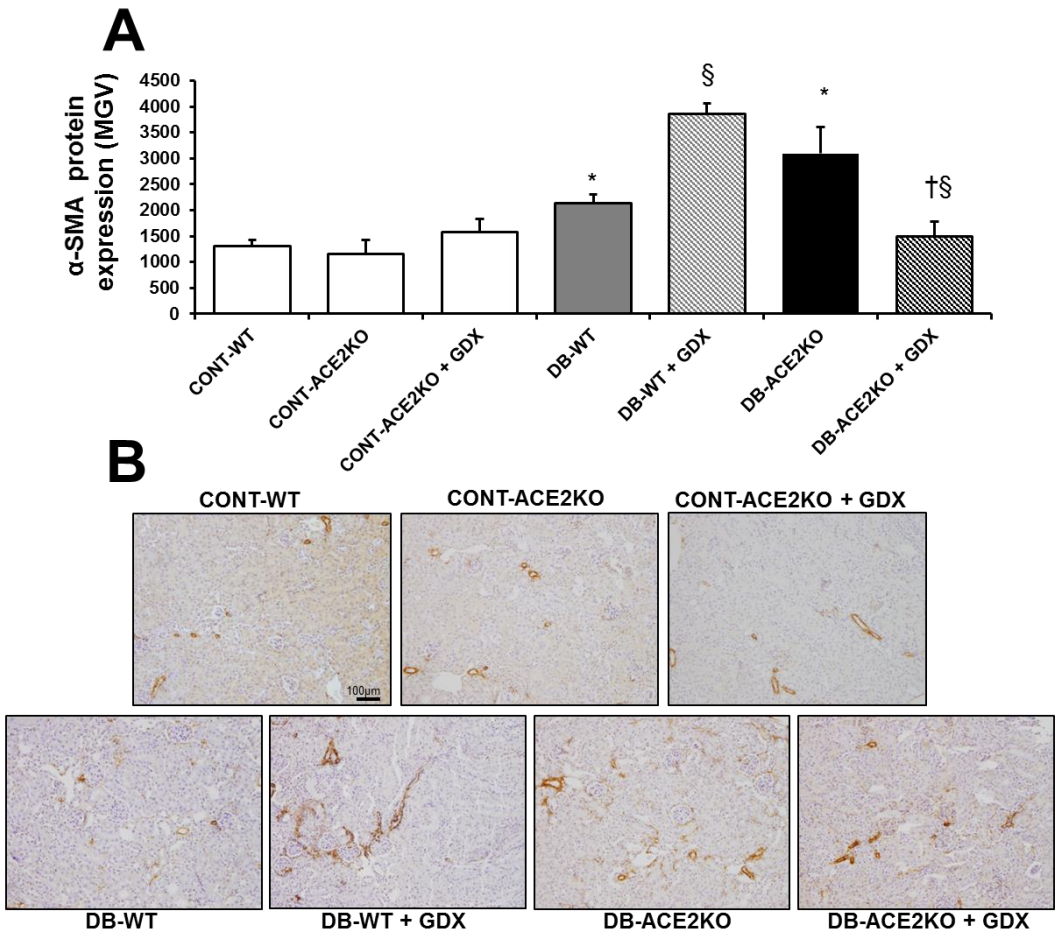

Figure 64. Influence of diabetes, *Ace2* deletion and gonadectomy on cortical α-SMA expression. The degree of brown staining as α-SMA-positive areas was quantified by ImageJ software and represented as Mean Grey Value (A). Panel B shows representative sections for tubulointerstitial α-SMA immunostaining from all the experimental groups. Scale Bar=100µm. Original magnification x10. For these experiments, 6-9 animals were analyzed in each group. Data are expressed as mean±SEM. *P<0.05 compared to non-diabetic controls. †P<0.05 compared to WT. §P<0.05 compared to non-GDX.

The second approach was the evaluation of Sirius Red staining as collagen type I, and III fibril marker. The technique revealed increased collagen deposition in diabetic mice as compared to controls (Figure 65). Interestingly, collagen accumulation was enhanced in DB-ACE2KO mice as compared to DB-WT. Surgical castration significantly reduced both, α-SMA staining and collagen deposition, in ACE2KO diabetic mice. In contrast, DB-WT + GDX mice exhibited a significant increase in α-SMA expression and collagen deposition, being these markers of fibrosis significantly higher in comparison to the DB-ACE2KO + GDX group (Figure 64 and 65).

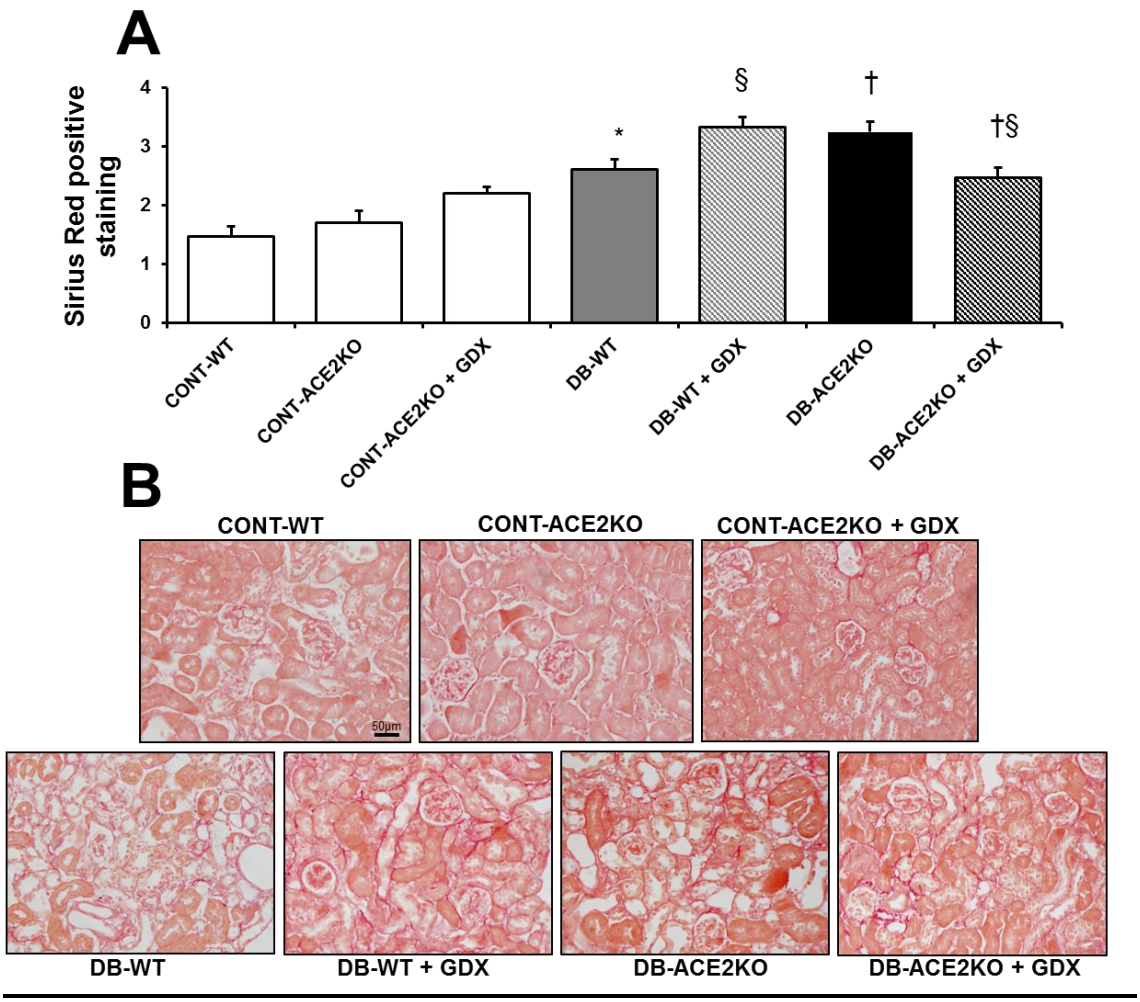

Figure 65. Influence of diabetes, *Ace2* deletion and gonadectomy on collagen deposition. Cortical collagen was analyzed in a semiquantitative manner (scale 0-4) on Sirius Red-stained tissue sections (A). Panel B shows representative photomicrographs for Sirius Red-positive staining (intense red) from all the experimental groups. Scale Bar=50µm. Original magnification x20. For these experiments, 6-8 animals were analyzed in each group. Data are expressed as mean±SEM. *P<0.05 compared to non-diabetic controls. †P<0.05 compared to WT. §P<0.05 compared to non-GDX.

5.C.V. Gonadectomy reduces AKT activation in diabetic ACE2KO male mice

To determine whether the status of Akt Ser473 phosphorylation in diabetes was related to *Ace2* deletion and the effect of surgical castration, western blot analyses were performed. Akt phosphorylation (pAkt) was increased in WT diabetic mice as compared to their controls (Figure 66A-B). In addition, *Ace2* deletion was accompanied by an increase of pAkt and the phospo/Akt ratio in both, control and diabetic mice. Gonadectomy clearly decreased pAkt and the phospo/Akt ratio in these groups. Gonadectomy did not modify pAkt and phospo/Akt ratio in WT diabetic mice (Figure 66A-D).

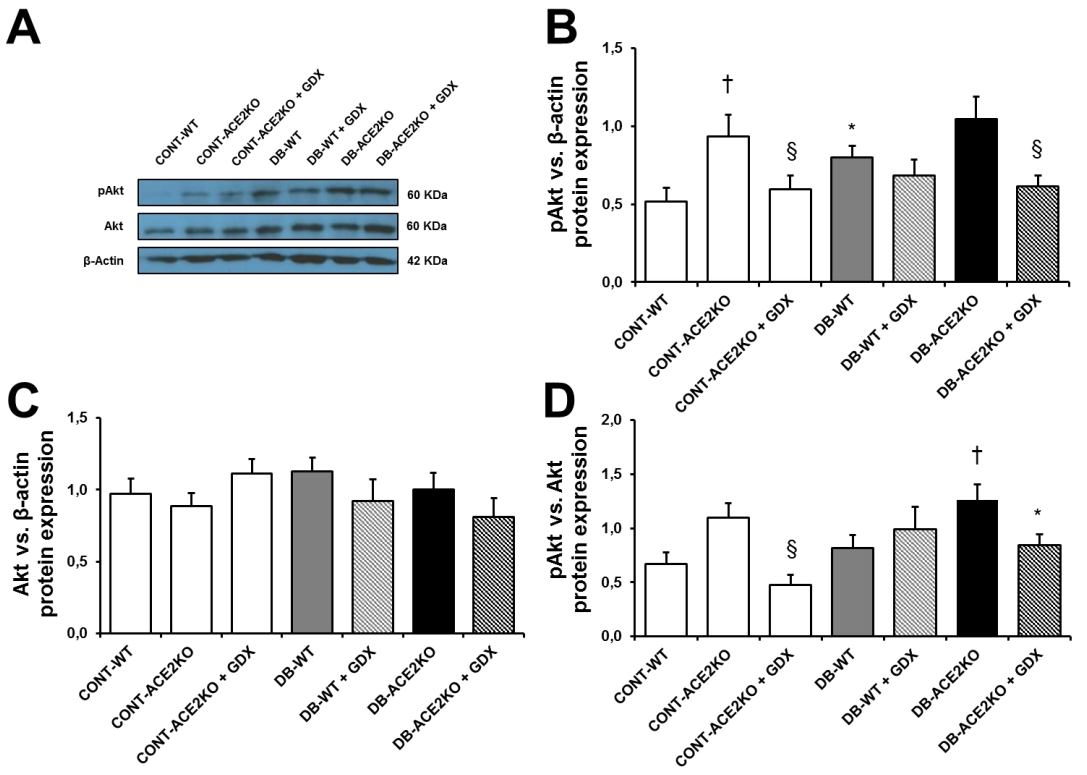

Figure 66. Influence of diabetes, *Ace2* deletion and gonadectomy on phosphorylated and total Akt in kidney cortex. Panel A: Representative immunoblot depicting cortical pAkt, Akt and β-actin in kidneys from all the experimental groups. Densitometry analysis of each band was performed using Image J. Intensities for pAkt and Akt were normalized to β-actin (panels B and C), and pAkt/Akt ratio was also calculated (Panel D). For these experiments, 6-8 animals were analyzed in each group. Data are expressed as mean±SEM. *P<0.05 compared to non-diabetic controls. †P<0.05 compared to WT. §P<0.05 compared to non-GDX.

5.C.VI. Diabetes, loss of ACE2 and gonadectomy alter circulating and renal ACE in male mice

Serum ACE (sACE) activity was significantly increased in WT and ACE2KO diabetic mice as compared to controls (Figure 67A). sACE was also enhanced in ACE2KO-CONT as compared to WT-CONT. Gonadectomized mice markedly displayed low sACE.

Renal ACE (rACE) was significantly decreased in diabetic mice in terms of enzymatic activity (Figure 67B) and protein levels (Figure 67C) in comparison to controls. *Ace2* deletion was accompanied by lower rACE enzymatic activity and protein expression. As shown in Figure 67D, the reduction of rACE levels by *Ace2* deletion or diabetes was observed in the renal cortex by immunohistochemistry.

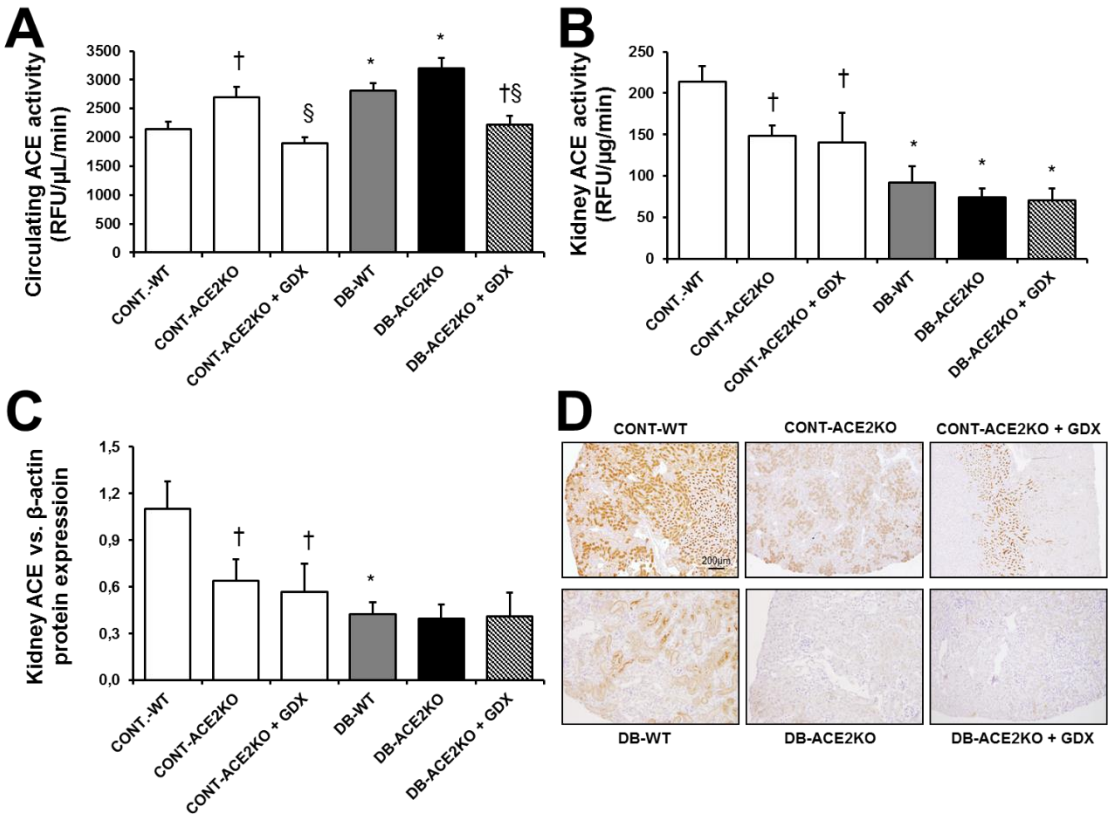

Figure 67. Influence of diabetes, *Ace2* deletion and gonadectomy on ACE expression in serum and kidney cortex. ACE activity in serum (A) and kidney cortex (B) from all the experimental groups. Panel C shows representative photomicrographs depicting ACE protein localization in the renal cortex from all the experimental groups. Scale Bar = 200µm. Original magnification x4. Panel D: immunoblot of cortical ACE protein expression normalized to β-actin from all the experimental groups. For these experiments, 6-10 animals were analyzed in each group. Data are expressed as mean±SEM. *P<0.05 compared to non-diabetic controls. †P<0.05 compared to WT. §P<0.05 compared to non-GDX.

5.C.VII. Diabetes, loss of ACE2 and gonadectomy alter cortical RAS expression in male mice

Gene expression of RAS components was studied in our model. Diabetes was accompanied by higher cortical *Agt* gene expression in all experimental groups (Figure 68A). *Mas1* mRNA levels were also augmented, whereas *Ace* gene expression was decreased in both, DB-WT and DB-ACE2KO mice, as compared to their controls (Figure 68C,I). Interestingly, only ACE2KO diabetic mice showed a significant decrease in *Ren* and *At1r* expression, as well as higher *Ctsg* mRNA levels (Figure 68D,H). In turn, neprilysin (*Nep*) gene expression was augmented in DB-WT mice (Figure 68G). Gonadectomized animals depicted a hyperactivated RAS by means of gene expression analysis. In control gonadectomized ACE2KO, cortical gene expression of *Agt*, *Ren* and *Nep* was significantly increased as compared to CONT-ACE2KO mice (Figure 68A,B,G). In contrast, renal *ace*, aminopeptidase N and *Mas1* mRNA levels were

significantly decreased in this group (C,F,I). In diabetic mice, gonadectomy significantly enhanced *Ren*, *Nep* and *At1r* cortical mRNA levels (Figure 68B,G,H), whereas diminished *Apn* and *Mas1* gene expression, in both WT and ACE2KO animals (Figure 68F,I). Among the diabetic gonadectomized groups, *Mas1* mRNA levels were significantly increased in DB-WT + GDX as compared to ACE2KO-DB + GDX mice (Figure 68I). Interestingly, gonadectomy dramatically increased *Agt* gene expression in diabetic WT but not ACE2KO (Figure 68A). In addition, gonadectomy induced a significant increase in *Ctsg* only in ACE2KO mice (Figure 68D).

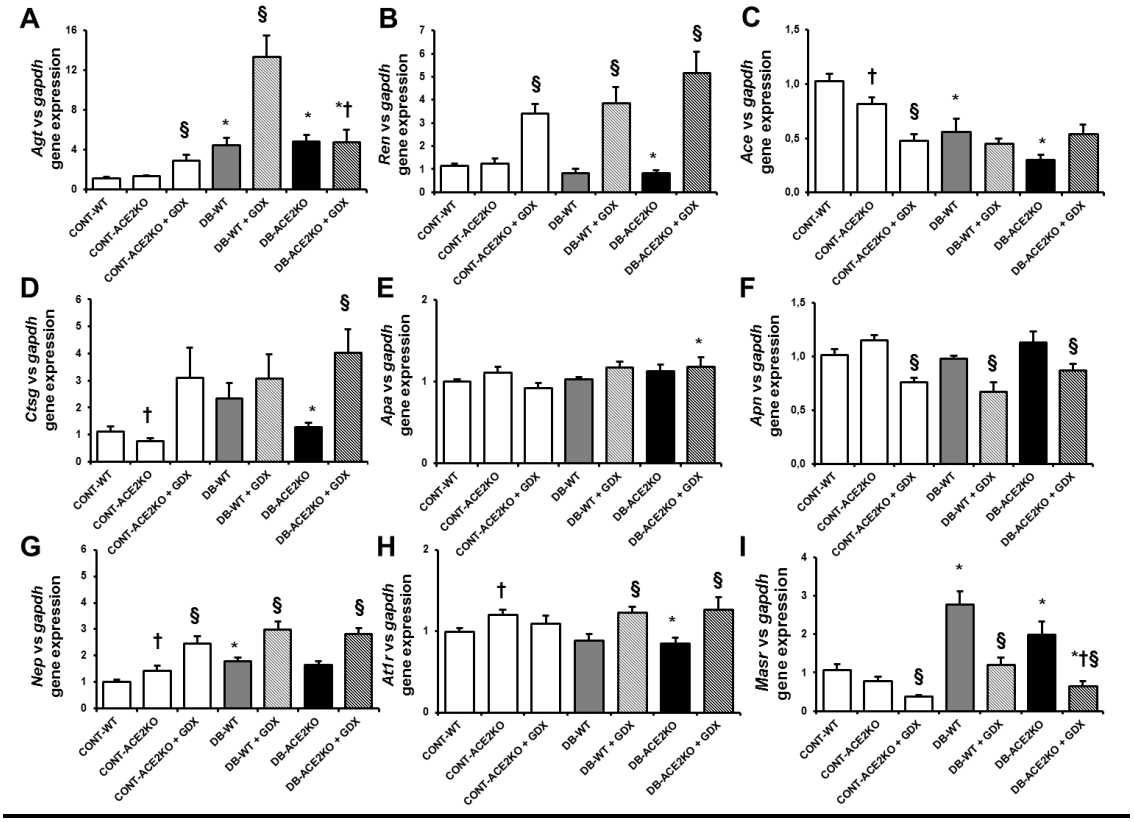

Figure 68. Cortical gene expression of RAS components. mRNA levels were assessed for angiotensinogen (*Agt*, A), renin (*Ren*, B), ACE (C), cathepsin G (C*tsg*, D), aminopeptidase-A (*Apa*, E), aminopeptidase-N (*Apn*, F), neprilysin (*Nep*, G), AT1R (*At1r*, H) and Mas receptor (*Masr*, I) were determined by real-time quantitative PCR and normalized to GAPDH in all the experimental groups. For these experiments, 6-10 animals were analyzed in each group. Data are expressed as mean±SEM. *P<0.05 compared to non-diabetic controls. †P<0.05 compared to WT. §P<0.05 compared to non-GDX.

5.C.VIII. Principal component analysis

In this study, we simultaneously evaluated the effect of *Ace2* deletion, diabetes and gonadectomy in several hallmarks of diabetic nephropathy in the glomeruli and the tubulointerstitial compartment, as well as its relationship with changes in renal RAS. To have a better understanding of the predominant effects of each of these three factors

on renal injury and renal RAS expression, we undertook PCA of all experimental groups. Distribution of variances for all the analyzed renal parameters showed that the effect of diabetes was more pronounced in ACE2KO mice as compared to WT. In diabetic and gonadectomized mice, a different effect was observed between the WT and the ACE2KO groups (Figure 69A). Interestingly, additional PCA revealed a similar distribution when considering only the tubulointerstitial fibrosis markers as determinants of sample variation (Figure 69B). In contrast, independent analysis for the hemodynamic parameters and glomerular injury markers indicated a predominant effect of diabetes over gonadectomy in both, WT and ACE2KO mice (Figure 69C). When evaluating the distribution of our study groups according to RAS components gene expression, PCA reflected that both, gonadectomy and diabetes alone exerted a clear effect on changing the levels of these genes. This effect was notably accentuated when these factors were combined in diabetic and gonadectomized animals, and even more pronounced in mice expressing ACE2 (Figure 69D).

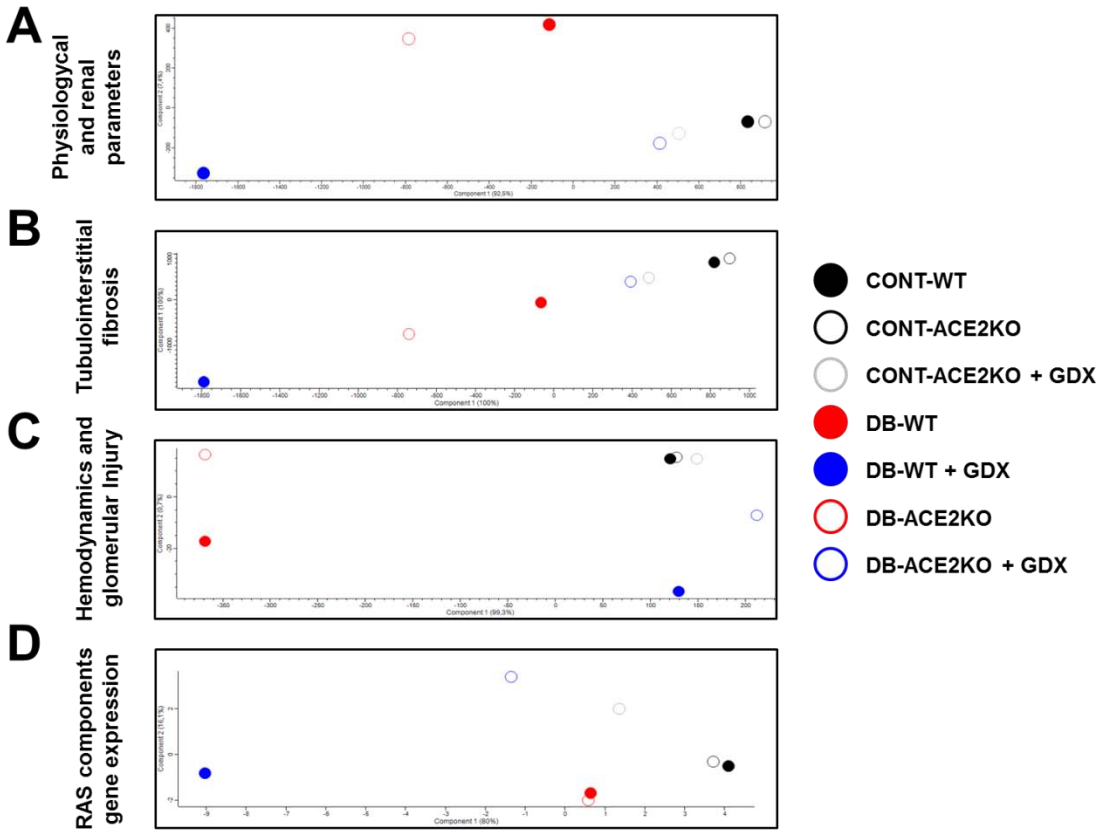

Figure 69. Principal component analysis (PCA) plot of the experimental groups. PCA was performed using Perseus software for different groups of variables to evaluate the predominant effects of *Ace2* deletion, diabetes and gonadectomy in the physiological and renal parameters, tubulointerstitial fibrosis, hemodynamics and glomerular injury markers, and RAS components gene expression. Panel A depicts PCA for all the assessed physiological and renal parameters, namely blood glucose, body weight, KW/BW, SBP, UAE, GFR, glomerular area, mesangial index, WT-1 positive cells, total cell number, Sirius Red score, and α-SMA protein expression. PCA was also performed independently for the hemodynamic and glomerular parameters, namely SBP, UAE, GFR, glomerular area, mesangial index, WT-1 positive cells,

and total cell number (B), as for the markers of tubulointerstitial fibrosis, namely Sirius Red score and α-SMA protein expression (C). In addition, predominant effects of *Ace2* deletion, diabetes and gonadectomy on the expression of the nine analyzed RAS genes were assessed (D).

5.D. SEXUAL DIMORPHISM IN THE DIABETIC KIDNEY IN RESPONSE TO ACE2 DOWNREGULATION AND ANGII-INFUSION.

5.D.I. Sexual dimorphism and role of ACE2 on ANGII-induced renal and cardiac hypertrophy and hypertension in diabetic mice

The means of blood glucose and body, kidney and heart weights in each experimental group were determined at the end of follow-up and are summarized in Table 19. With these values, KW/BW and HW/BW ratios were calculated.

STZ administration was associated with a significant increase in blood glucose levels in all the experimental groups. As observed in study 1 (19 weeks of diabetes), diabetic WT males showed a significantly accentuated hyperglycemia, as compared to the diabetic WT females, after 12 weeks of diabetes. These sex differences were not statistically significant in the diabetic ACE2KO groups, as ACE2KO-DB females presented slightly higher blood glucose values than WT-DB females. Interestingly, ANGII infusion significantly decreased blood glucose in WT control males, but did not alter glucose levels in any of the diabetic groups (Table 19). Classic physiological differences attributed to sex were observed, as all male mice had an increase in body and kidney weights as compared to the corresponding female group. Again, in our model of type 1 diabetes, hyperglycemia was accompanied by a significant decrease in BW and an augment in KW/BW in all diabetic groups. *Ace2* deletion also induced a decrease in the final BW, which was significant in males but not in females. In contrast, loss of ACE2 significantly accentuated renal hypertrophy in diabetic females, but not in males (Table 18).

In our model, heart weight was another parameter affected by sex, diabetes, ANGII and loss of ACE2. In WT mice, heart weight was significantly higher in males as compared to females. In turn, the diabetic groups showed lower values of heart weight than their controls, and ANGII promoted cardiac hypertrophy in terms of increased HW/BW ratio in all experimental groups. In males, this increase was significant in control but not in diabetic groups, regardless of the presence or absence of ACE2. In females, however, significant cardiac hypertrophy associated to ANGII administration was observed in the ACE2KO but not in the WT groups.

Table 18. Physiological parameters at the end of the study. Blood glucose (BG), body weight, kidney weight, and heart weight were measured after 12 weeks of diabetes and 28 days of ANGII infusion. 8-12 animals were monitored in each group. F: females; M: males. Data are expressed as mean ± SEM. $ P<0.05 vs. SHAM, *P<0.05 vs. non-diabetic controls (CONT), †P<0.05 vs. WT, #P<0.05 vs. females.

Study group	BG (mg/dL)	Body weight (g)	Kidney weight (g)	Heart weight (g)	KW/BW (%)	HW/BW (%)
F-WT-CONT + SHAM	172.00 ± 7.61	25.87 ± 0.66	0.27 ± 0.01	0.13 ± 0.01	1.04 ± 0.05	0.49 ± 0.03
F-WT-CONT + ANGII	175.17 ± 7.05	25.13 ± 0.92	0.24 ± 0.01$	0.13 ± 0.01	0.95 ± 0.03	0.54 ± 0.02
F-WT-DB+ SHAM	306.55 ± 31.74*	21.24 ± 0.43*	0.24 ± 0.02	0.10 ± 0.01*	1.13 ± 0.08	0.46 ± 0.02
F-WT-DB + ANGII	389.36 ± 44.05*	20.83 ± 0.27*	0.23 ± 0.01	0.10 ± 0.01*	1.09 ± 0.07	0.49 ± 0.03
F-ACE2KO-CONT + SHAM	177.00 ± 11.77	24.40 ± 0.57	0.23 ± 0.01	0.12 ± 0.01	0.93 ± 0.06	0.50±0.02
F-ACE2KO-CONT + ANGII	157.30 ± 8.07	23.28 ± 0.46	0.23 ± 0.01	0.15 ± 0.01$	1.00 ± 0.04	0.65 ± 0.03$†
F-ACE2KO-DB+ SHAM	354.30 ± 46.83*	20.24 ± 0.65*	0.27 ± 0.02	0.10 ± 0.01*	1.34 ± 0.10*†	0.50 ± 0.03
F-ACE2KO-DB + ANGII	436.78 ± 51.50*	19.82 ± 0.77*	0.26 ± 0.01	0.12 ± 0.01*†	1.31 ± 0.04*†	0.60 ± 0.02$†
M-WT-CONT + SHAM	199.67 ± 9.93	33.33 ± 1.02#	0.36 ± 0.02#	0.17 ± 0.01#	1.09 ± 0.05	0.50 ± 0.04
M-WT-CONT + ANGII	158.11 ± 7.97$	31.79 ± 1.06#	0.35 ± 0.02#	0.19 ± 0.01#	1.10 ± 0.07	0.61 ± 0.02$
M-WT-DB+ SHAM	492.13 ± 41.44*#	27.62 ± 0.66*#	0.35 ± 0.02#	0.13 ± 0.01*#	1.27 ± 0.07*	0.47 ± 0.04
M-WT-DB + ANGII	554.33 ± 16.76*#	26.17 ± 0.78*#	0.34 ± 0.03#	0.14 ± 0.01*#	1.31 ± 0.12#	0.55 ± 0.04
M-ACE2KO-CONT + SHAM	175.50 ± 9.72	28.06 ± 0.62†#	0.28 ± 0.02†#	0.13 ± 0.01†	1.00 ± 0.07	0.45 ± 0.04
M-ACE2KO-CONT + ANGII	165.75 ± 11.19	27.79 ± 0.58†#	0.31 ± 0.02†#	0.17 ± 0.01$†	1.10 ± 0.04	0.60 ± 0.03$
M-ACE2KO-DB+ SHAM	494.25 ± 48.16*	24.72 ± 0.99*†#	0.32 ± 0.02	0.12 ± 0.01#	1.40 ± 0.10*	0.50 ± 0.02
M-ACE2KO-DB + ANGII	570.13 ± 20.21*	23.10 ± 0.83*†#	0.30 ± 0.01#	0.13 ± 0.00*	1.29 ± 0.04*	0.57 ± 0.02

ANGII increased SBP and DBP in all diabetic, ACE2KO and male groups (Figure 70A,B). This observation is indicative of successful systemic ANGII delivery in our mice, and gives consistency to our method of subcutaneous minipump implantation. This effect has been previously reported in mice receiving the same dose of ANGII[503], and was expectable due to the vasoconstrictor effects of the peptide[220]. In females, the ANGII-associated increase in blood pressure was significantly accentuated by diabetes and loss of ACE2. Indeed, control and diabetic ACE2KO females presented significantly higher values of SBP and DBP than the WT groups. In males, ANGII induced hypertension to a similar extent in both, control and diabetic, WT and ACE2KO mice. ACE2KO-DB + ANGII males showed significantly attenuated hypertension as compared to females (Figure 70A,B).

Regarding heart rate, this parameter was significantly decreased by diabetes in female in the absence of ACE2. In males, the decrease in heart rate was also promoted by ANGII administration, but only in the context of diabetes or ACE2 deficiency (Figure 70C).

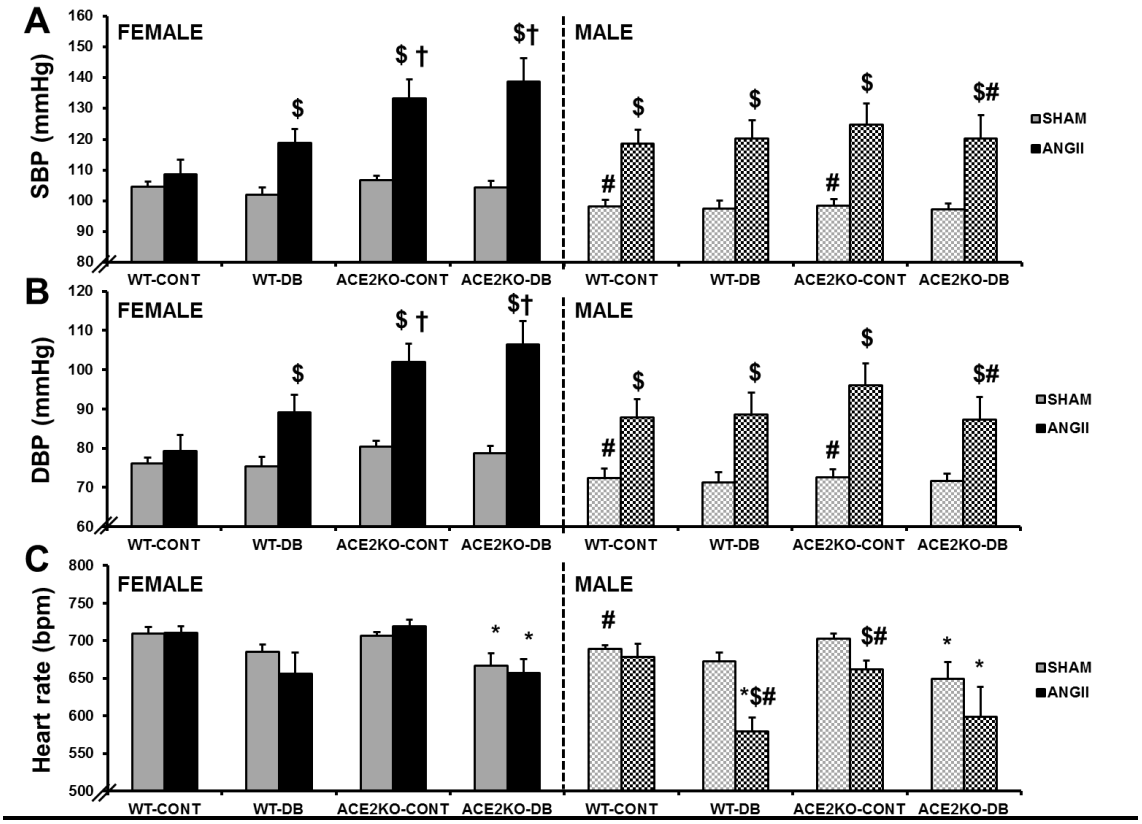

Figure 70. Blood pressure and heart rate at the end of the study. Sex differences on the effect of *Ace2* deletion on systolic (A) and diastolic (B) blood pressure and heart rate (C) were studied after 12 weeks of diabetes and 28 days of ANGII infusion. For these experiments, 8-12 animals were included in each group. Data are expressed as mean ± SEM. $ P<0.05 vs. SHAM, *P<0.05 vs. non-diabetic controls (CONT), †P<0.05 vs. WT, #P<0.05 vs. females.

It is important to clarify that female and male, control and diabetic, WT and ACE2KO mice were randomly distributed into subgroups receiving ANGII minipump or SHAM surgery. As shown in Table 19, no differences in blood glucose, BW, SBP, DBP or heart rate were found between ANGII-receiving mice and their corresponding SHAM groups before the surgery. This observation strengthens the robustness of our experimental design, confirming that the ANGII-related differences in blood glucose, BW, blood pressure and heart rate observed at the end of the study were mediated by the exogenous ANGII administrated.

Table 19. Physiological parameters at baseline. Blood glucose (BG), body weight (BW), systolic and diastolic blood pressure (SBP and DBP) and heart rate were measured at baseline (i.e, before ANGII infusion, after 8 weeks of diabetes). 8-12 animals were monitored in each group. Data are expressed as mean ± SEM. $ P<0.05 vs. SHAM, *P<0.05 vs. non-diabetic controls (CONT), †P<0.05 vs. WT, #P<0.05 vs. females.

Study group	BG(mg/dL)	BW (g)	SBP (mmHg)	DBP (mmHg)	Heart rate (bpm)
F-WT-CONT + SHAM	167.90 ± 6.61	24.83 ± 0.70	102.74 ± 1.71	74.23 ± 1.92	706.30 ± 5.64
F-WT-CONT + ANGII	163.17 ± 3.76	24.48 ± 0.92	103.33 ± 1.74	76.44 ± 1.27	710.90 ± 7.17
F-WT-DB+ SHAM	267.82 ± 36.13*	21.19 ± 0.40*	99.66 ± 2.24	71.89 ± 1.84	674.02 ± 5.64*
F-WT-DB + ANGII	278.73 ± 20.97*	20.75 ± 0.30*	101.00 ± 2.21	74.37 ± 2.34	683.33 ± 11.50*
F-ACE2KO-CONT + SHAM	166.13 ± 11.17	23.89 ± 0.37	104.04 ± 1.29	77.05 ± 1.96	703.52 ± 11.33
F-ACE2KO-CONT + ANGII	156.13 ± 11.17	23.36 ± 0.68	105.36 ± 0.91	78.62 ± 1.67	700.68 ± 9.19
F-ACE2KO-DB+ SHAM	301.00 ± 25.71*	20.74 ± 0.45*	107.29 ± 2.22†	80.32 ± 1.98†	673.86 ± 13.16
F-ACE2KO-DB + ANGII	329.50 ± 184.13*	21.23 ± 0.48*	104.28 ± 2.20	76.02 ± 2.68	672.82 ± 6.37*
M-WT-CONT + SHAM	184.13 ± 7.61#	32.13 ± 1.36#	100.38 ± 0.51	73.73 ± 0.96	692.21 ± 9.62
M-WT-CONT + ANGII	177.13 ± 9.47	33.78 ± 0.79#	99.00 ± 1.92	71.97 ± 1.80	687.44 ± 11.00#
M-WT-DB+ SHAM	380.38 ± 39.44*#	27.65 ± 0.65*#	97.49 ± 3.74	71.94 ± 3.26	680.83 ± 9.21
M-WT-DB + ANGII	411.08 ± 27.66*#	28.36 ± 0.62*#	102.66 ± 1.73	76.13 ± 2.06	651.00 ± 12.79
M-ACE2KO-CONT + SHAM	185.57 ± 9.04	27.37 ± 0.71†#	101.94 ± 0.81	76.01 ± 0.79	702.35 ± 9.24
M-ACE2KO-CONT + ANGII	183.29 ± 8.05	27.24 ± 0.42†#	99.90 ± 2.24	74.53 ± 2.10	692.53 ± 6.58
M-ACE2KO-DB+ SHAM	407.33 ± 42.93*	24.81 ± 1.22#	97.97 ± 1.82#	71.27 ± 1.88#	639.43 ± 23.35
M-ACE2KO-DB + ANGII	456.38 ± 28.47*#	25.95 ± 0.34*†#	98.50 ± 1.63	72.61 ± 1.71	639.43 ± 12.35*

5.D.II. Sexual dimorphism and role of ACE2 on ANGII-induced albuminuria and GFR decrease in diabetic mice

ANGII and diabetes promoted an increase in UAE in all the experimental groups (Figure 71A). In females, loss of ACE2 significantly accentuated the ANGII-induced increase in UAE in both, control and diabetic mice. In males, the effect of ANGII was comparable between WT and ACE2KO groups. Sex differences in UAE in the context of diabetes were influenced by the presence or absence of functional ACE2. In WT mice, diabetic males showed significantly higher UAE values than females. However, these differences disappeared in the context of ACE2 deficiency.

ANGII-induced albuminuria was accompanied by a decrease in GFR in all the experimental groups, except for the diabetic males (Figure 71B). In females, GFR was significantly decreased in the WT but not in the ACE2KO groups. *Ace2* deletion was also accompanied by lower GFR values in control females, and in control and diabetic males.

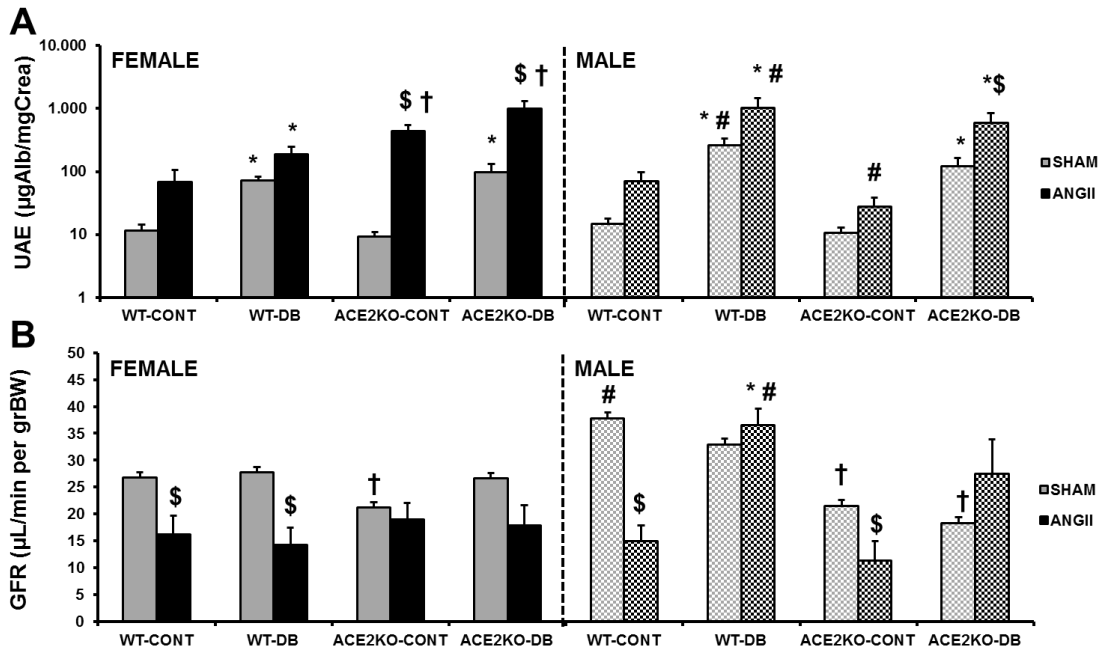

Figure 71. Renal functional parameters. Sex differences in the effect of *Ace2* deletion on urinary albumin excretion (UAE, A) and glomerular filtration rate (GFR, B) were studied after 12 weeks of diabetes and 28 days of ANGII infusion. For these experiments, 5-12 animals were included in each group. Data are expressed as mean ± SEM. $ P<0.05 vs. SHAM, *P<0.05 vs. non-diabetic controls (CONT), †P<0.05 vs. WT, #P<0.05 vs. females.

5.D.III. Histopathological renal alterations induced by diabetes and ANGII-induced hypertension are sex-dependent

5.D.III.1. Tubular injury

Representative images of these alterations, namely dilatation of distal tubules, nuclear glycogen accumulation, and acute tubular necrosis (ATN) are depicted in Figure 72A. Each lesion of interest was considered to be present in a particular individual if observed in at least one tubule. The frequency of animals per group showing these alterations was calculated.

Dilatation of distal tubules was characterized by loss of the brush borders and expansion of the tubular lumen (Figure 72A). As shown in Figure 72B, ANGII promoted these dilatations in female groups. This effect was more pronounced in ACE2KO diabetic females.

Nuclear glycogen accumulation was characterized by the presence of PAS positive deposits inside the nuclei of the tubular cells (Figure 72A). According to the literature and our findings from study 1, diabetes was associated to a clear increase of this alteration in all groups (Figure 72C). Interestingly, in the present study we observed that *Ace2* deletion and ANGII infusion also contributed to the presence of nuclear

glycogenation, and in a sex-dependent manner. In females, positive PAS nuclei were observed even in non-diabetic groups receiving ANGII. In males, ANGII infusion modestly increased the frequency of WT mice with glycogen accumulation. This frequency was accentuated by *Ace2* deletion in the context of diabetes (Figure 72C).

ATN is a medical condition involving the death of tubular epithelial cells that form the renal tubules of the kidneys[504]. Processes related to ATN were described in tubules containing cells with white cytoplasm, which was usually accompanied by a loss of morphology and structural integrity (Figure 72A). ANGII administration increased the frequency of mice showing this alteration (Figure 72D). In females, diabetes was associated to signs of acute tubular injury, but in less than 50% of the animals analyzed. This frequency was increased up to 60% in the diabetic and ANGII-infused groups. In males, a higher number of diabetic WT, rather than diabetic ACE2KO mice, presented this injury.

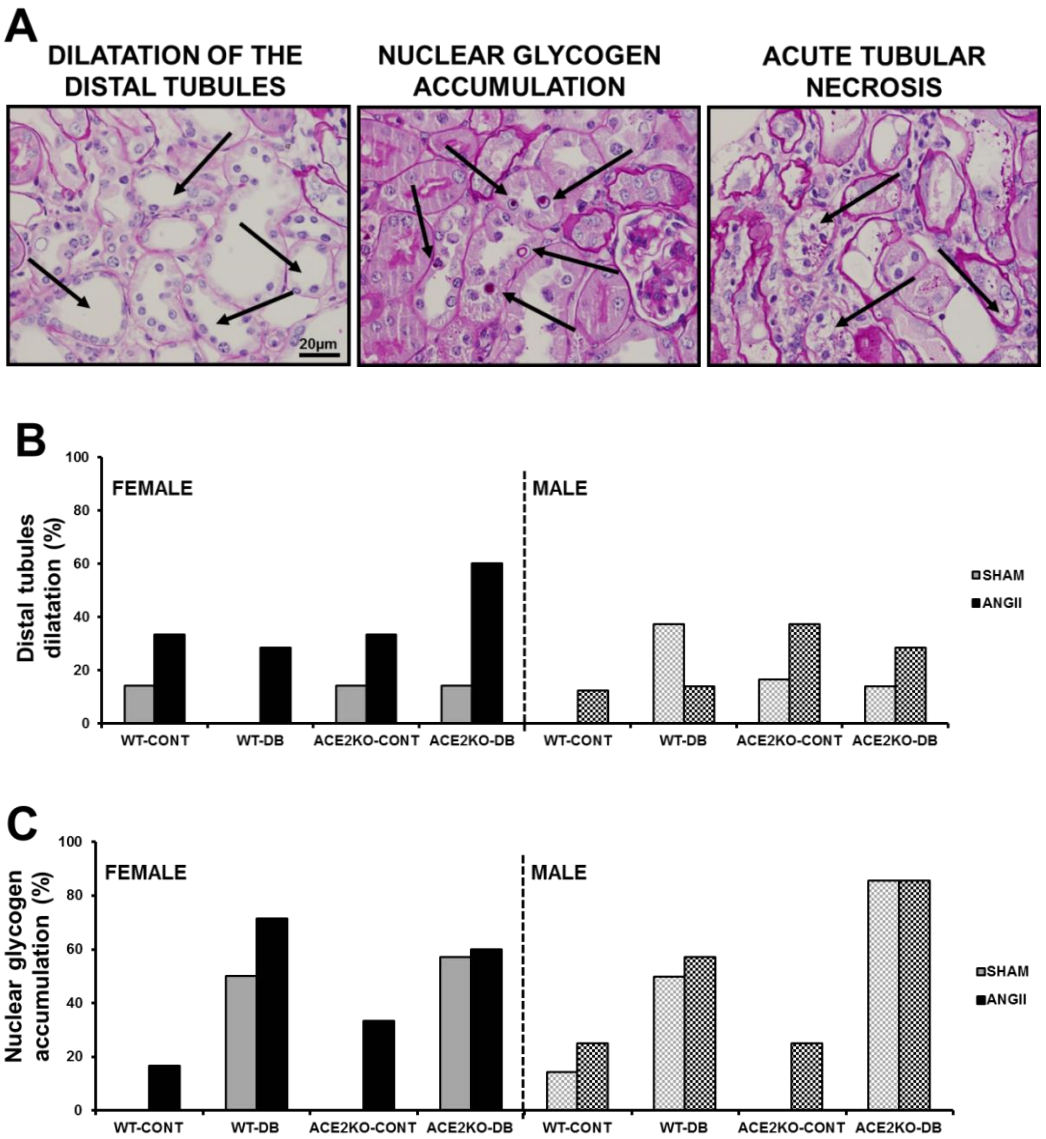

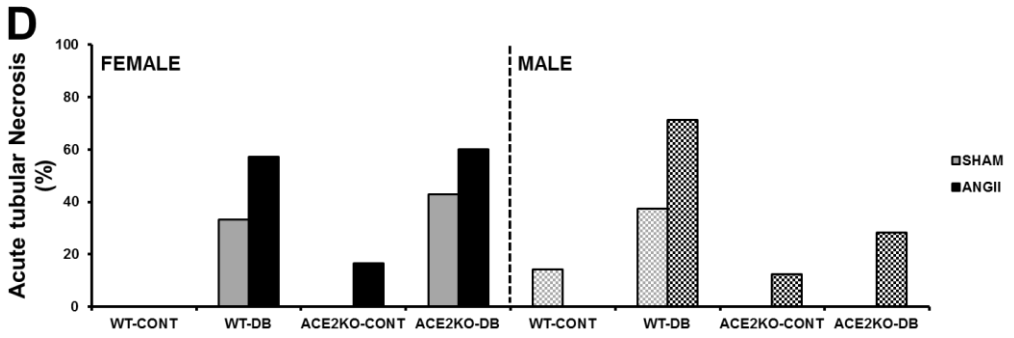

Figure 72. Evaluation of tubular lesions. Representative images of distal tubules dilatation, nuclear glycogen accumulation and acute tubular necrosis are depicted in panel A. Scale Bar = 20μm. Original magnification x40. Bar graphs show the percentage of animals per group showing tubular dilatation (B), nuclear glycogen deposition (C) and acute tubular injury (D). 5-8 animals per group were evaluated. . Semi-quantifications are expressed in percentages.

5.D.III.2. Glomerular morphology and injury

Our next aim was to evaluate if the glomerular features that differed between sexes after 19 weeks of follow-up (30 weeks of age) were also observed in the present study. In particular, we aimed to demonstrate if the influence of sex and diabetes on the epithelialization and the hyperplasic thickening of the Bowman's capsule were relevant at 12 weeks of follow-up (23 weeks of age), and if this effect was altered by loss of ACE2 and ANGII infusion. In each sample, a positive score was given if the feature of interest was present in more than 50% of the glomeruli (epithelialization) or in at least 1 glomerulus (hyperplasic thickening). The frequency of animals per group showing these structures was calculated.

As previously observed in study 1, male sex was strongly associated to the epithelialization of the Bowman's capsule (Figure 73A,C). Twelve weeks of diabetes induced either a complete loss or a significant reduction of this epithelialization in the glomeruli from the majority of the kidneys evaluated. Interestingly, ANGII infusion also decreased the frequency of mice with this feature in control ACE2KO, but not in control WT males. In contrast, the hyperplasic thickening of the glomerular capsule associated to diabetes was exclusively observed in females (Figure 73B,C). This alteration was detected in a lower number of diabetic ACE2KO females, as compared to the frequency observed in the diabetic WT group.

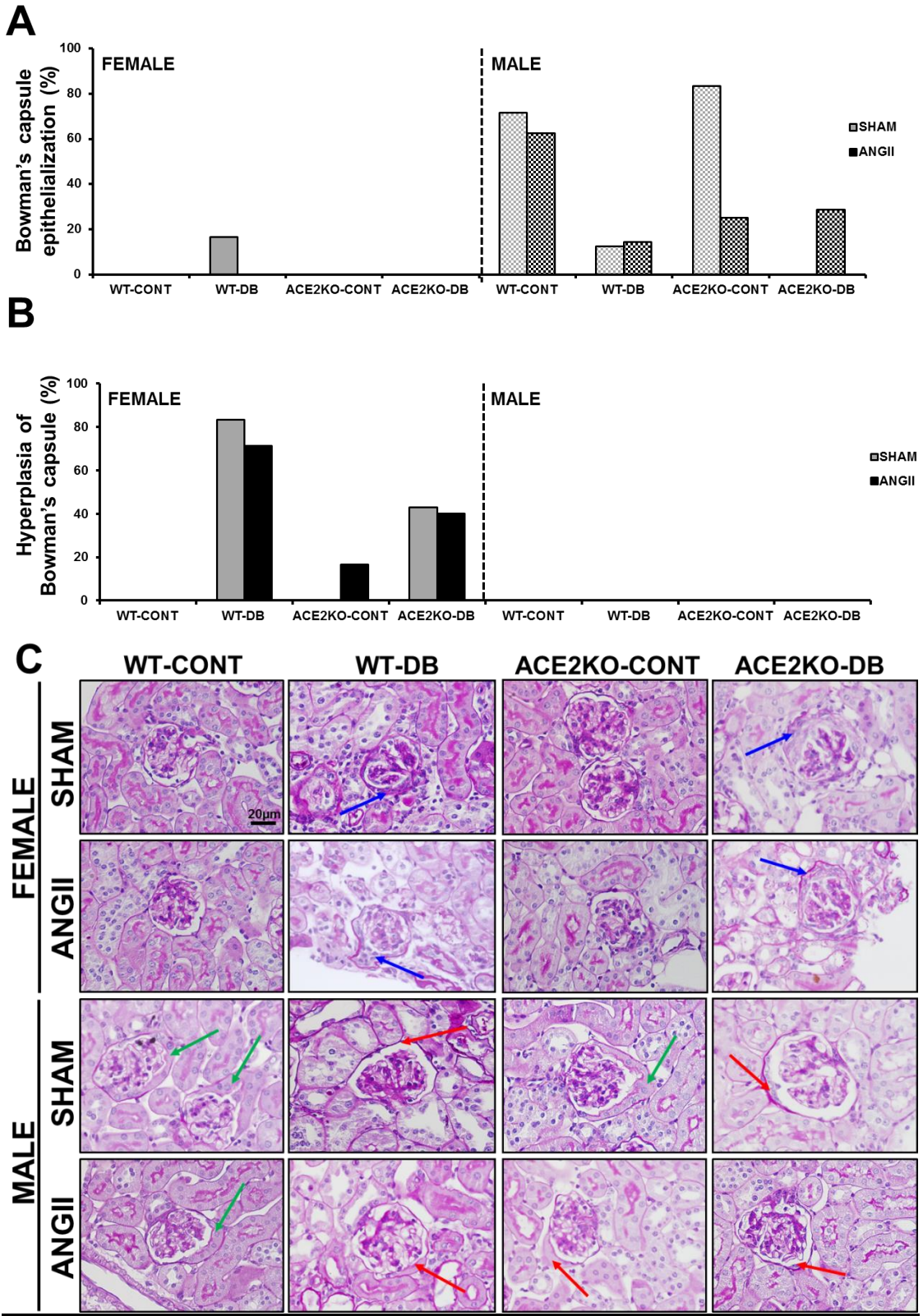

Figure 73. Evaluation of changes in the glomerular capsule. Bar graphs show the percentage of animals per group showing epithelialization (A) or hyperplasia (B) of the Bowman's capsule. Semi-quantifications are expressed in percentages. 5-8 animals per group were evaluated. Representative images of these features are shown in panel C. Blue arrows point at the hyperplasic thickening of the capsule observed in diabetic females. Green arrows indicate Bowman's capsule epithelialization in control males. Red arrows show complete or partial loss of this epithelialization in diabetic and/or ANGII-infused males. Scale Bar = 20µm. Original magnification x40.

5.D.IV. Sexual dimorphism and role of ACE2 on ANGII-induced glomerular hypertrophy and mesangial expansion in diabetic mice

ANGII and diabetes induced morphometric changes in the glomeruli by increasing glomerular area (GA) and glomerular tuft area (GTA) (Figure 74A,B,E). Glomerular morphometric analysis by computerized image analysis revealed a sexual dimorphism on these alterations. In females, *Ace2* deletion significantly increased GA and GTA in healthy mice, as well as modestly accentuated these alterations in diabetic and ANGII-infused mice. In males, the increase in GA and GTA associated to diabetes was only evident in ANGII-infused, but not in SHAM-operated mice. ANGII significantly increased GTA and GA in diabetic ACE2KO but not WT males. Interestingly, glomeruli from WT-CONT + SHAM males were found to be significantly bigger than the ones from WT-CONT + SHAM females, in terms of GA (figure XA,E), indicating a sexual dimorphism in the morphology of the healthy murine glomeruli.

Changes in GA and GTA were accompanied by changes in the mesangial area specifically in males, but not in females (Figure 74C,E). In concordance with glomerular size data, expansion of mesangial area due to diabetes was only significant in ANGII-infused males. In this sense, ANGII significantly augmented mesangial area in diabetic ACE2KO but not WT males.

After performing an exhaustive qualitative analysis of the PAS-stained sections, we noticed that, in some of the diabetic groups, the edge of the glomerular tuft was closer to the capsule, as compared to the controls (Figure 74E). In addition, morphometric analysis revealed that not only GTA, but also GA, was altered by ANGII and diabetes (Figure 74A,B). For these reasons, we decided to numerically evaluate changes in Bowman space area (BA) that may result on functional alterations. As shown in Figure 74D, BA was significantly reduced in female and male WT-DB mice as compared to their controls. ANGII was also associated to lower values of BA, but only in control males. In turn, *Ace2* deletion significantly decreased BA in control females, without inducing any changes in males. Of mention that, in concordance with the effect of sex on GA, BA was significantly higher in healthy males as compared to females.

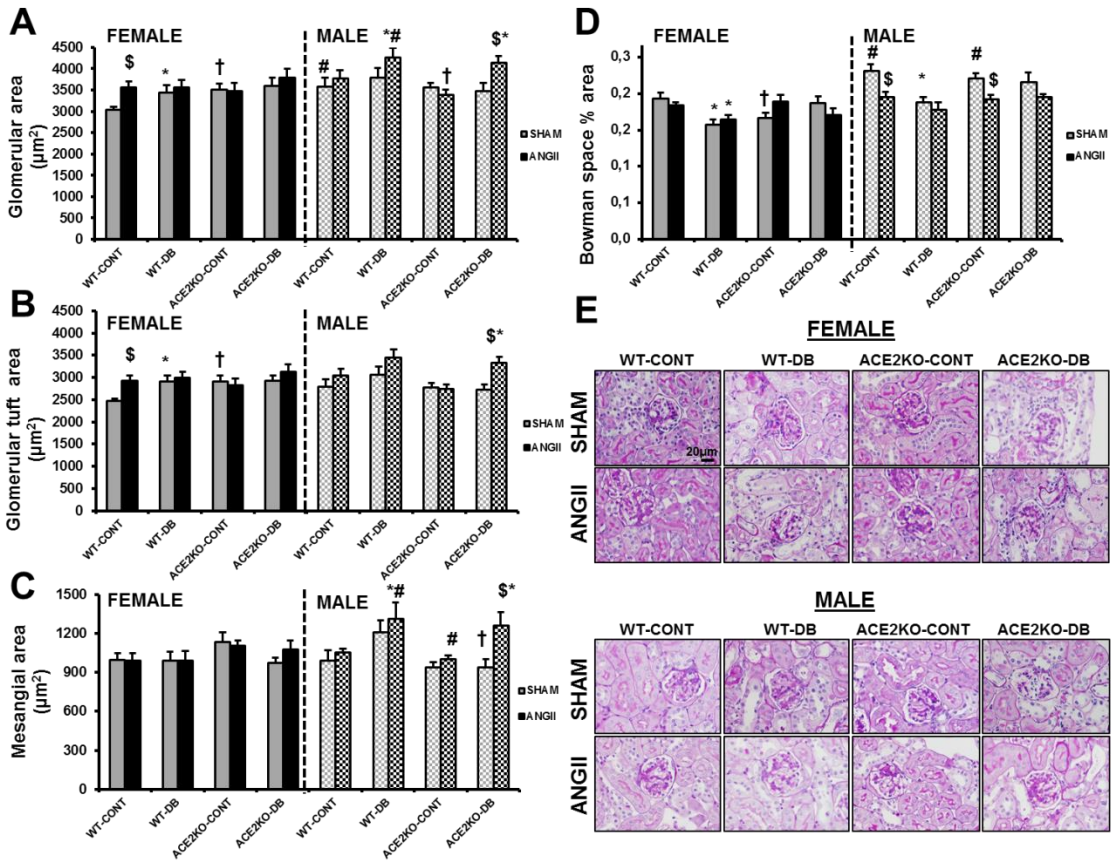

Figure 74. Assessment of glomerular morphometry. Sex differences on the effect of *Ace2* deletion on glomerular area (A), glomerular tuft area (B), mesangial area (C), and Bowman space area (D) were studied after 12 weeks of diabetes and 28 days of ANGII infusion. Panel E shows representative photomicrographs depicting glomerular morphometric changes in PAS-stained stained sections from all the experimental groups. Scale Bar=20µm. Original magnification x40. For these experiments, 6-9 animals were included in each group. Data are expressed as mean±SEM. $ P<0.05 vs. SHAM, *P<0.05 vs. non-diabetic controls (CONT), †P<0.05 vs. WT, #P<0.05 vs. females.

5.D.V. Sexual dimorphism and role of ACE2 on ANGII-induced podocyte loss in diabetic mice

The effects of diabetes, ANGII, and *Ace2* deletion on podocyte number (%POD) differed according to sex (Figure 75A,C). In WT females, diabetes and ANGII infusion significantly decreased %POD. Surprisingly, ANGII promoted a significant increase in the %POD in control ACE2KO females. In WT males, diabetes only caused a slight diminution in %POD. ANGII infusion tended to decrease %POD in all male groups (Figure 75A,C). No differences between groups were observed in the total cell number (Figure 75B).

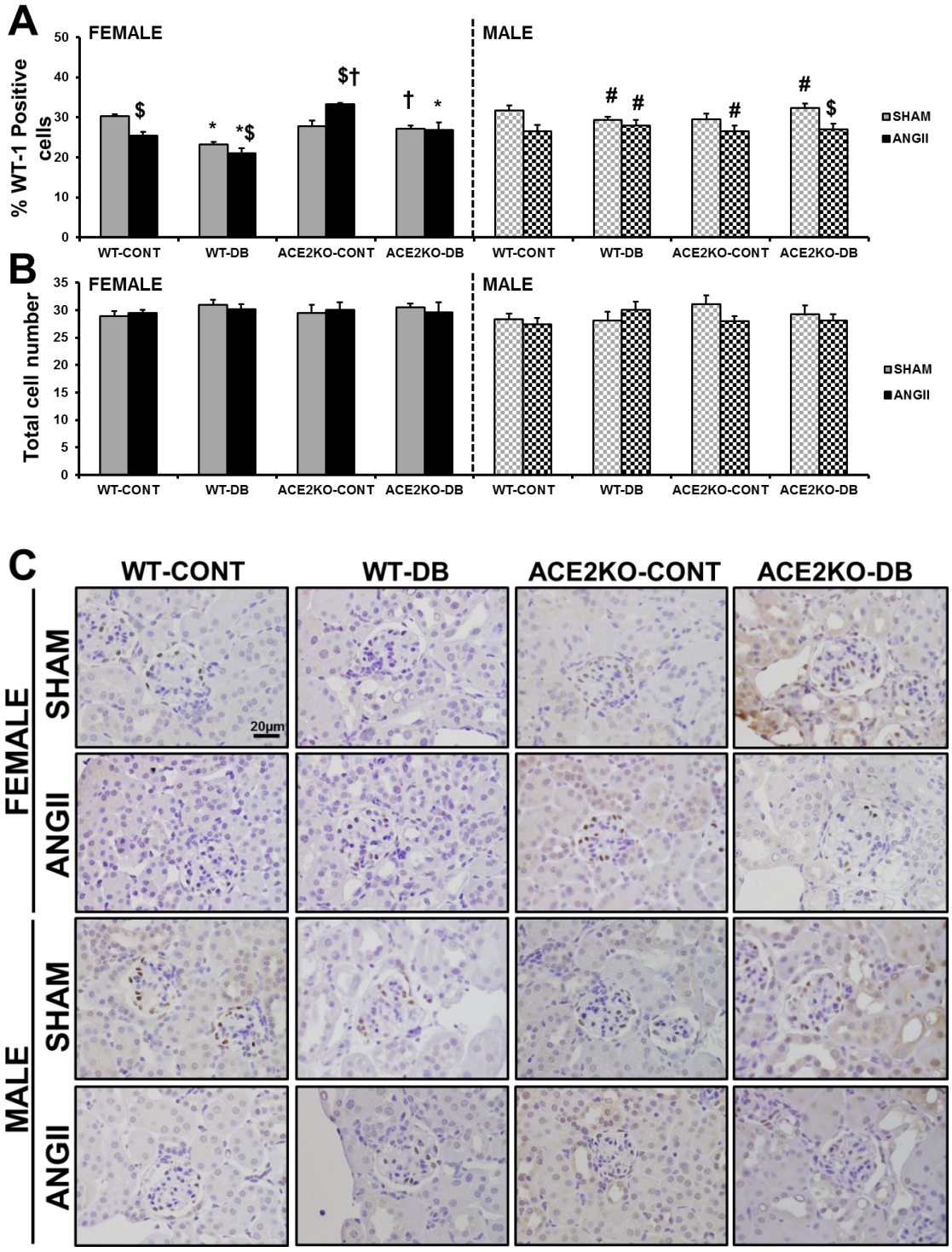

Figure 75. Assessment of podocyte number and glomerular cellularity. Podocyte number is represented as the % of brown positive cells after WT-1 immunostaining (A). Total cell number was also assessed in the same photomicrographs (B). Representative photomicrographs depicting glomerular WT-1 staining from all the experimental groups are shown in panel C. Scale Bar=20µm. Original magnification x40. For these experiments, 6-10 animals were analyzed in each group. Data are expressed as mean±SEM. $ P<0.05 vs. SHAM, *P<0.05 vs. non-diabetic controls (CONT), †P<0.05 vs. WT, #P<0.05 vs. females.

5.D.VI. Sexual dimorphism and role of ACE2 on ANGII-induced renal fibrosis and inflammation in diabetic mice

ANGII and high glucose increase TGF-β1 signaling in the kidney[505–507]. TGF-β1 triggers the activation of several molecular pathways that contribute to the development of fibrosis and inflammation in diabetic nephropathy progression[508,509]. We aimed to elucidate if sex modulated the activation of these pro-fibrotic and pro-inflammatory processes in the context of diabetes and ANGII-induced hypertension[150,341].

We analyzed the gene expression of *Tgfb1*, collagen I alpha 2 chain (*col1a*2, as a marker of fibrosis), and monocyte chemoattractant protein 1 (*mcp1*, as a marker of inflammation), in the renal cortex of our experimental groups.

In general terms, hyperglycemia was accompanied by a significant increase in cortical *Tgfb1* and *Col1a*2 gene expression (Figure 76A,B). Interestingly, this increase was not observed in the ACE2KO groups receiving ANGII. Female sex was also associated to higher mRNA levels of these markers. A similar pattern was observed when evaluating the effects of diabetes, ANGII infusion and loss of ACE2 on *Tgfb1* and *Col1a*2 gene expression in each sex. However, some divergences between females and males were found. In females, ANGII significantly accentuated the increase in cortical *Tgfb1* gene expression in diabetic WT but not ACE2KO mice. In males, ANGII not only up-regulated *Tgfb1* in the renal cortex of the WT groups, but also significantly downregulated *Tgfb1* and *Col1α*2 gene expression in diabetic ACE2KO mice. Diabetes and ANGII also stimulated the expression of the *Mcp1* gene in the renal cortex (Figure 76C). In this case, sex and loss of ACE2 did not modulate these effects.

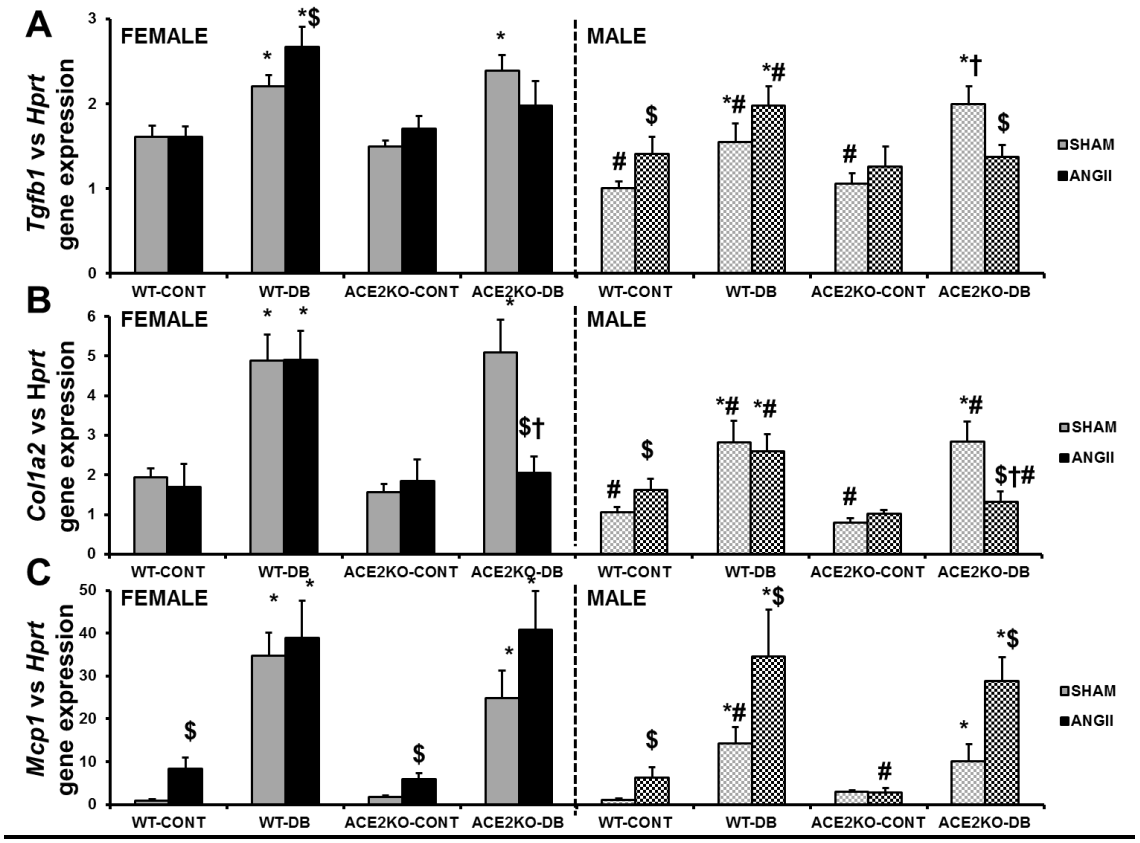

Figure 76. Cortical gene expression of fibrotic and inflammatory markers. mRNA levels were assessed for transforming growth factor beta (*Tgfb1*, A), collagen I alpha 2 chain (*Col1a2*, B), and monocyte chemoattractant protein (*Mcp1*, C). Values were normalized to *Hprt* gene expression. For these experiments, 5-9 animals were analyzed in each group. Data are expressed as mean±SEM. $ P<0.05 vs. SHAM, *P<0.05 vs. non-diabetic controls (CONT), †P<0.05 vs. WT, #P<0.05 vs. females.

5.D.VII. Sexual dimorphism and role of ACE2 on cortical and circulating RAS expression in diabetic and ANGII-infused mice

Our next aim was to correlate the sex divergences on renal injury markers with changes in the expression of RAS components in kidney cortex and circulation. In the first 2 studies, we demonstrated a clear effect of sex, diabetes and *Ace2* deletion on the cortical expression and distribution of ACE2 and ACE and their circulating activities. Due to the direct contribution of these enzymes in ANGII metabolism, we speculate that specific regulation of ACE2 and ACE conferred different susceptibility to develop certain lesions of diabetic nephropathy in each sex. In the present part of the thesis, we explored if this sex-specific ACE2 and ACE regulation was also reflected in the context of ANGII-induced hypertension.

5.D.VII.1. ANGII modulates the effects of diabetes on circulating and cortical ACE2 in a sex-dependent manner

Male sex was associated to higher ACE2 levels in both, serum and kidney cortex (Figure 77A-C). However, this sex effect was only significant in the renal cortex of control ANGII-infused mice (Figure 77B,C). Twelve weeks of diabetes were accompanied by a significant increase in ACE2 activity in the serum and the total cortex of all groups receiving STZ (Figure 77A,B). In diabetic females, ANGII infusion increased active ACE2 in the serum and decreased ACE2 activity in the outer cortex, but not in a significant fashion. Conversely, in diabetic males ANGII administration significantly decreased circulating ACE2 and augmented ACE2 activity in the outer cortex (Figure 77A,C). The effects of sex, diabetes and ANGII infusion on ACE2 activity in different areas of the cortex correlated with the pattern of ACE2 protein expression and distribution observed by immunohistochemistry (Figure 77D,E).

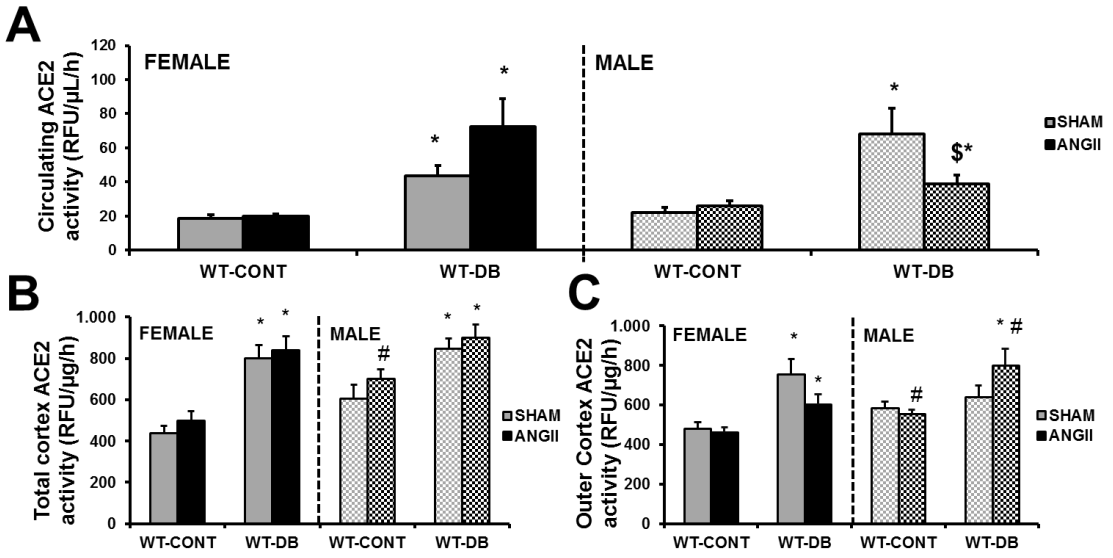

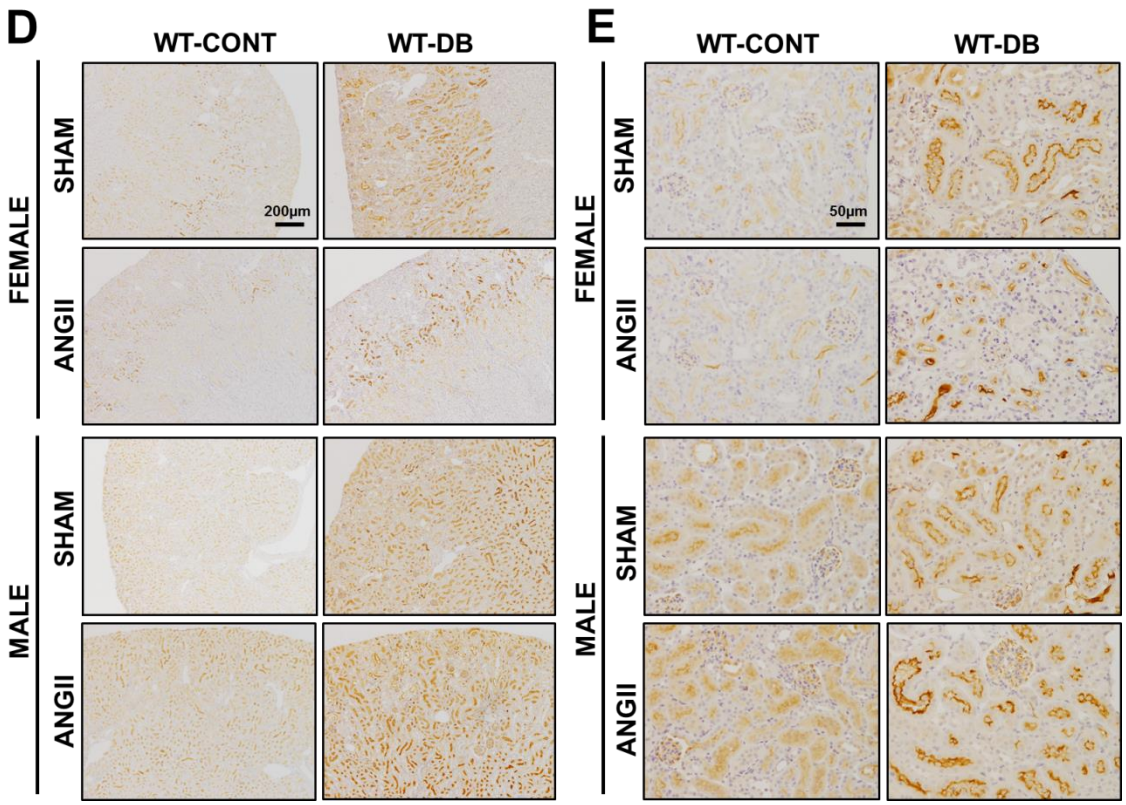

Figure 77. Circulating and cortical ACE2. ACE2 activity was assessed in the serum (A), the total cortex (B) and the outer cortex (C) of all WT groups. Data are expressed as mean±SEM. Panel D shows representative photomicrographs depicting ACE2 protein localization in the entire renal cortex. Scale Bar= 200µm. Original magnification x4. Panel E is composed by zoomed-in images that represent differences between groups on ACE2 expression specifically in the outer cortex. Scale Bar=50µm. Original magnification x20.

5.D.VII.2. ANGII modulates the effects of diabetes and *Ace2* deletion on circulating and cortical ACE in a sex-dependent manner

Circulating ACE activity in our animal model was strongly regulated by sex. Firstly, male sex was clearly associated to higher levels of serum ACE activity in all experimental groups (Figure 78A). In addition, a sexual dimorphism regarding the effects of diabetes, ANGII infusion and loss of ACE2 was observed. In females, diabetes and loss of ACE2 significantly increased circulating ACE, while ANGII infusion promoted a slight decrease of this parameter. In males, regulation of circulating ACE followed a particular pattern: whereas ANGII, diabetes, or *Ace2* deletion alone induced a significant increase, combination of these factors gradually decreased ACE activity in serum, to the point that diabetic ACE2KO mice receiving ANGII showed the lowest values of circulating ACE across all male studied groups.

In the renal cortex, the effects of male sex and diabetes on ACE activity mirrored the pattern observed in circulation, as both factors were associated to lower levels of ACE (Figure 78B,C). Sex divergences on cortical ACE activity, however, differed between

the two areas analyzed. When analyzing the total cortex, all male groups showed significantly lower ACE activity than females (Figure 78B). This decrease was less clear in the outer cortex, where only diabetic ACE2KO males presented a significant diminution as compared to their female groups (Figure 78C). The pattern of ACE distribution along the renal cortex provided visual evidence to support these differences. As pointed in Figure 78D, in control females, the presence of focal areas with strong positive staining coming from the transition area into the outer cortex may explain their higher levels of ACE activity as compared to the diabetic and the male groups.

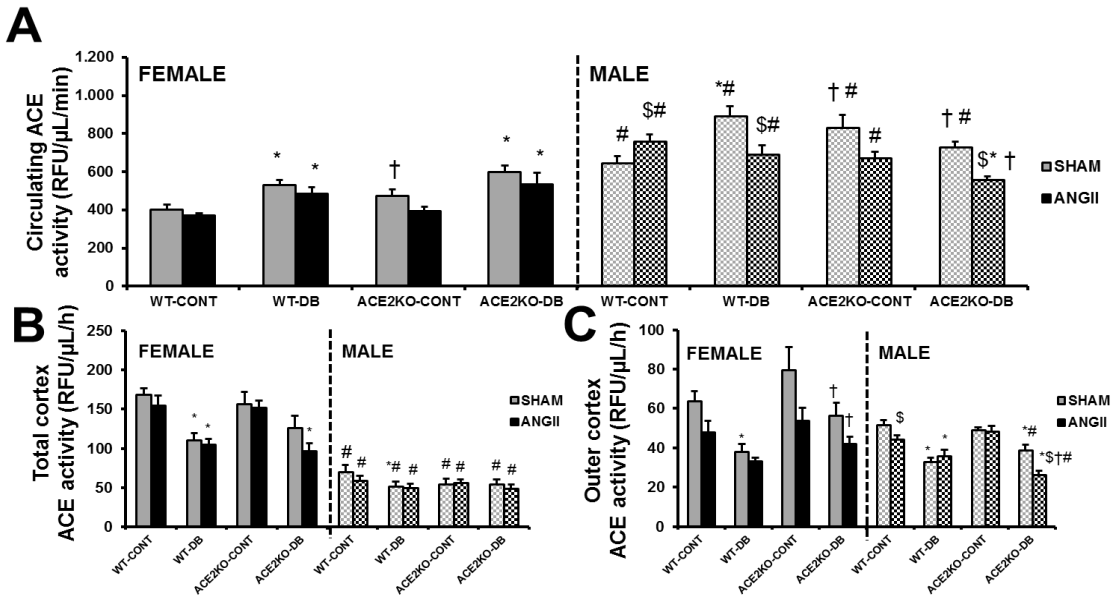

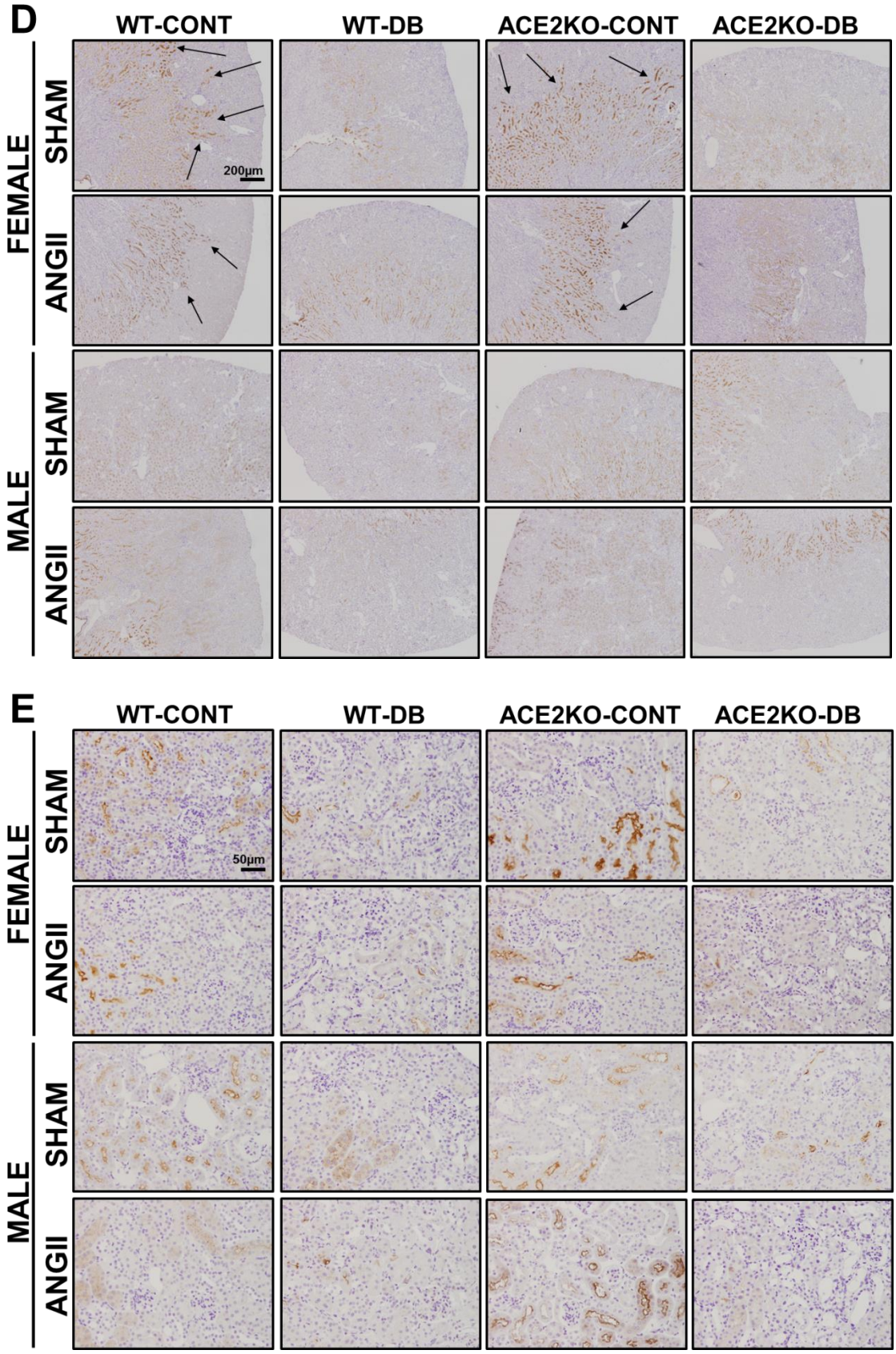

Figure 78. Circulating and cortical ACE. ACE activity was assessed in the serum (A), the total cortex (B) and the outer cortex (C) of all experimental groups. Data are expressed as mean±SEM. Panel D shows representative photomicrographs depicting ACE protein localization in the entire renal cortex. Black arrows indicate focal areas of strong positive staining in control females. Scale Bar=200µm. Original magnification

x4. Panel E is composed by zoomed-in images that represent differences between groups on ACE expression specifically in the outer cortex. Scale Bar=50μm. Original magnification x20.

Interestingly, loss of ACE2 and ANGII administration significantly altered cortical ACE in a sex-dependent manner, but only when analyzing the outer part of the cortex. Together with diabetes, the absence of ACE2 and the administration of ANGII promoted a significant decrease in ACE activity and protein expression in this area, and specifically in males. Combination of these factors in ACE2KO-DB + ANGII males was associated to the lowest values and positive staining of ACE activity among all the studied groups (Figure 78C,E). We next aimed to elucidate if this decrease was also reflected at the mRNA level, and if it was associated with oscillations in other RAS components such as renin, which has been previously shown to be downregulated by ANGII[152,510,511].

5.D.VII.3. ANGII downregulates the classic AGT-RENIN-ACE axis of cortical RAS in a sex- and ACE2-dependent manner in diabetic mice

We surmised that infusion of exogenous ANGII in our experimental groups would alter the status of RAS in the renal cortex in response to increased concentrations of this peptide. Real-time qPCRs were performed for *Agt*, *Ren*, *Ace* and *At1r* to evaluate the status of the classic “pro-ANGII” axis in the kidney cortex. In the same samples, *Nep* and *Apa* mRNA levels were also determined as critical components of the alternative ANGII escape mechanisms.

Female sex was associated to higher mRNA levels of *Agt* in all the experimental groups (Figure 79A). This increase in respect to male mice was significant in all control groups. In turn, diabetes, ANGII and loss of ACE2 stimulated the expression of cortical *Agt* at gene level and in a sex-dependent manner. In females, progressive accumulation of these pathological factors was accompanied by a gradual increase in *Agt* gene expression. In males, ANGII infusion significantly augmented *Agt* mRNA levels in control ACE2KO mice and accentuated the diabetes-induced increase in *Agt* in the diabetic ACE2KO. These changes were not observed in WT mice (Figure 79A).

In parallel with *Agt*, females showed a significant elevation in *Ren* gene expression as compared to males, which was only significant in the control and sham-operated groups (Figure 79B). As expected, ANGII infusion was associated to a clear decrease in renin gene expression in all groups. These downregulation was modulated by sex, diabetes and loss of ACE2. In females, ACE2KO-CONT + SHAM mice presented significantly lower *Ren* expression than the WT-CONT + SHAM. In males, diabetes and

Ace2 deletion accentuated the effects of ANGII on diminishing cortical levels of *Ren*. Indeed, ACE2KO-DB + ANGII male mice had the lowest values of *Ren* gene expression among all the studied groups (Figure 79B).

Diabetes decreased the mRNA levels of cortical *Ace* and *At1r* in all groups (Figure 79C,D). Administration of ANGII was also associated to lower gene levels of *Ace*, especially in non-diabetic animals. Within the diabetic groups, the ANGII-mediated negative regulation of Ace was more pronounced in ACE2KO males. This group presented the lowest values of cortical *Ace* gene expression among all the studied groups (Figure 79C). Of mention that sex, ANGII and loss of ACE2 did not significantly alter *At1r* gene expression in the renal cortex (Figure 79D).

Hyperglycemia was also associated to a decrease in cortical *Nep* and *Apa* gene expression (Figure 79E,F). In turn, all female groups showed higher *Nep* mRNA levels than males. Furthermore, ANGII infusion significantly increased *Nep* in diabetic WT females (Figure 79E), and promoted a mild increase in *Apa* gene expression in all groups (Figure 79F).

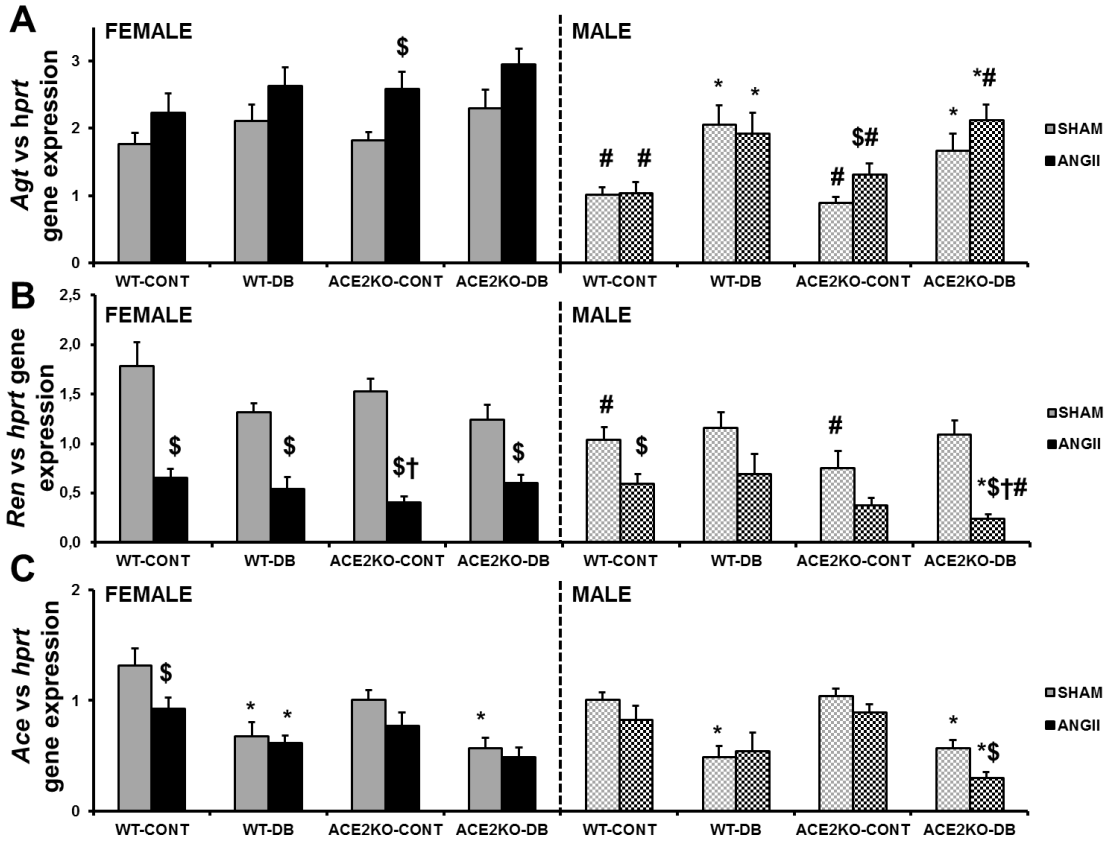

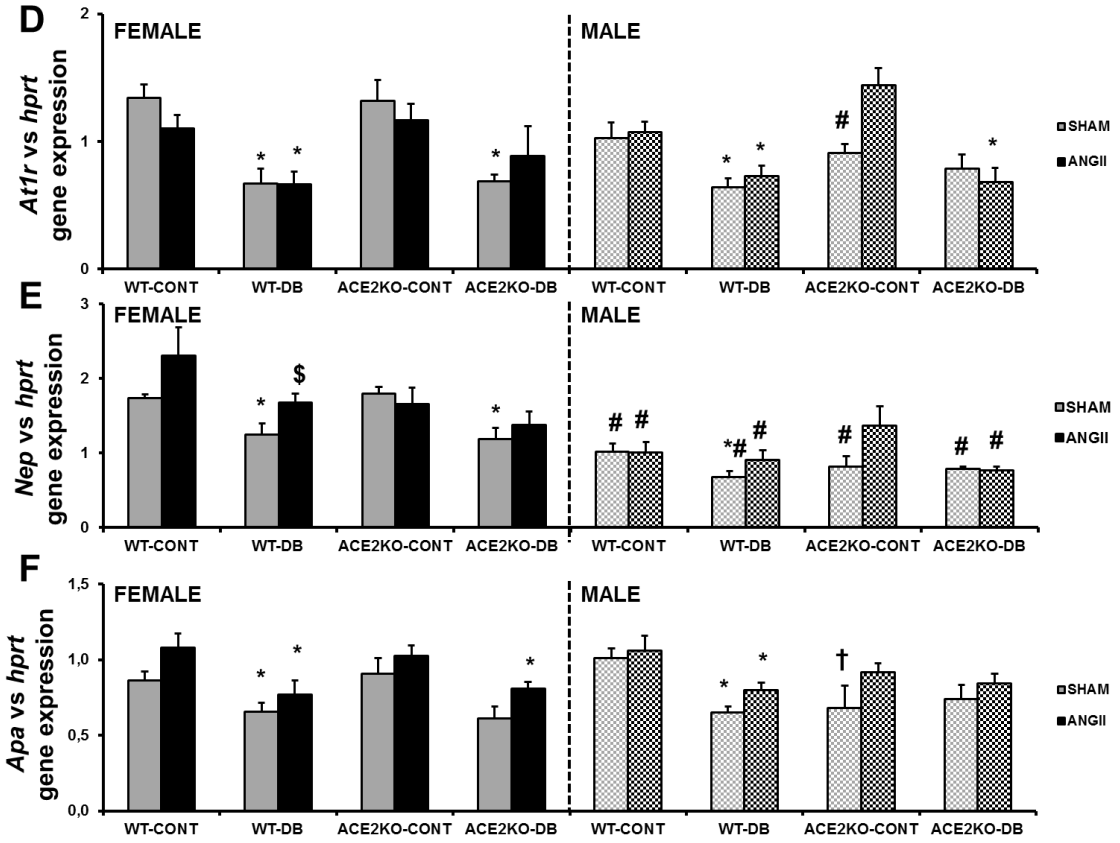

Figure 79. Cortical gene expression of RAS components at the end of the study. mRNA levels were assessed for angiotensinogen (*Agt,* A), renin (*Ren*, B), *Ace* (C), *At1r* (D), neprilysin (*Nep*, E), and aminopeptidase-A (*Apa*, F), Values were normalized to *Hprt* gene expression. For these experiments, 5-9 animals were analyzed in each group. Data are expressed as mean±SEM. $ P<0.05 vs. SHAM, *P<0.05 vs. non-diabetic controls (CONT), †P<0.05 vs. WT, #P<0.05 vs. females.

5.D.VIII. Principal component analysis

To have a global view of the predominant effects of sex, *Ace2* deletion, diabetes and ANGII infusion on renal injury and RAS status, we undertook PCA of all experimental groups. Distribution of variances for the hemodynamics and glomerular injury markers showed a predominant effect of ANGII infusion, but with some differences across sexes. In females, the effect of ANGII infusion was more pronounced in the ACE2KO groups, especially in the ACE2KO-DB + ANGII females. In males, the predominant effect of ANGII was observed specifically in the diabetic groups, and it was not accentuated in the ACE2KO-DB+ANGII males as compared to the WT-DB + ANGII (Figure 80A). Conversely, independent analysis for the markers of fibrosis and inflammation indicated a predominant effect of diabetes over ANGII infusion in both, female and male mice. Within the diabetic groups, ACE2KO-DB + ANGII females showed the most notable separation from control groups (Figure 80B). In addition, predominant effect of sex was observed when evaluating the distribution of our study

groups according to ACE activity (Figure 80C) and cortical RAS components expression (Figure 80D). Among female groups, diabetes and ANGII exerted predominant effects on these variables (Figure 80C,D). Within the male groups, the greatest separation of ACE activity and cortical RAS values was observed when the three studied pathological conditions, namely loss of ACE2, diabetes and ANGII infusion, were combined in the ACE2KO-DB + ANGII (Figure 80C,D).

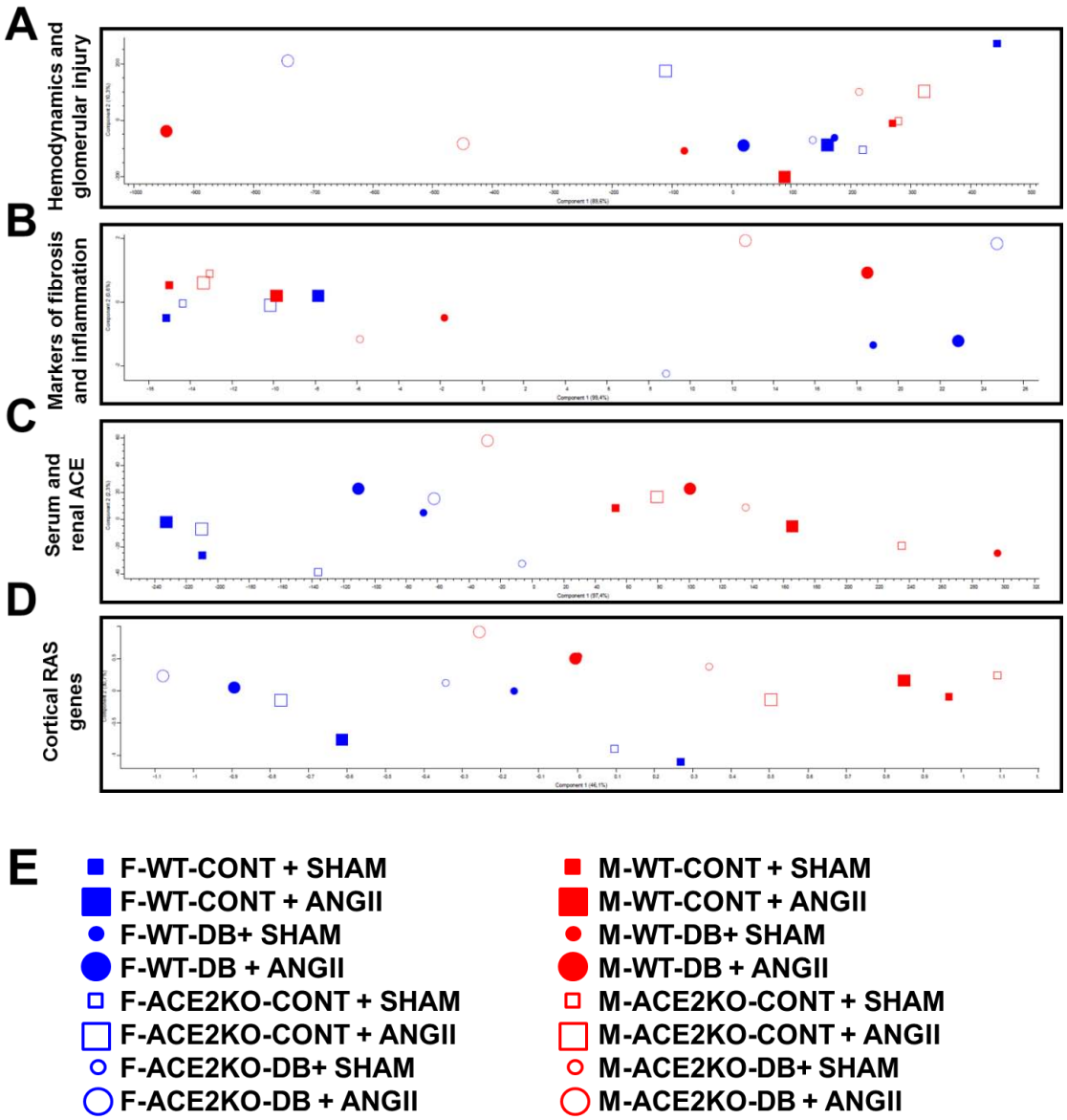

Figure 80. Principal component analysis (PCA) plot of the experimental groups. PCA was performed using Perseus software for different groups of variables to evaluate the predominant effects of sex, *Ace2* deletion, diabetes and ANGII infusion in the variables of study. Panel A depicts PCA for the most relevant hemodynamic and glomerular parameters, namely SBP, UAE, GFR, glomerular tuft area, and % of WT-1 positive cells. PCA was also performed for the markers of cortical fibrosis and inflammation, namely *Tgfb1*, *Col1a2* and *Mcp1* genes (B). In addition, predominant effects of sex, *Ace2* deletion, diabetes and ANGII infusion on the activity of ACE in serum and kidney (C) and the expression of the six analyzed RAS genes were evaluated (D). The legend of the symbols corresponding to each experimental group is depicted in panel E. Briefly: blue color = female(F); red color = male(M); filled = WT; empty = ACE2KO; square = control, circle = diabetic; small size = SHAM; large size = ANGII.

5.E. SILAC-BASED PROTEOMICS OF PRIMARY HUMAN KIDNEY CELLS REVEALS A NOVEL LINK BETWEEN MALE SEX HORMONES AND IMPAIRED ENERGY METABOLISM IN DIABETIC KIDNEY DISEASE.

5.E.I. Sex hormone stimulation of PTEC

PTEC at the 4th and 5th passage were split into T25 flasks, deprived of serum for 18h and treated with ethanol (CONT), DHT, or EST for 8h. Experiments 1 and 2 were performed at passage 4, while experiments 3 and 4 were performed at passage 5. We determined in each passage levels of phosphorylated AKT and ERK after 10min stimulation with DHT or EST. Western blot analysis showed that both sex hormones led to phosphorylation of ERK (Figure 81A,B) and AKT (Figure 81A,C) in comparison with the control cells.

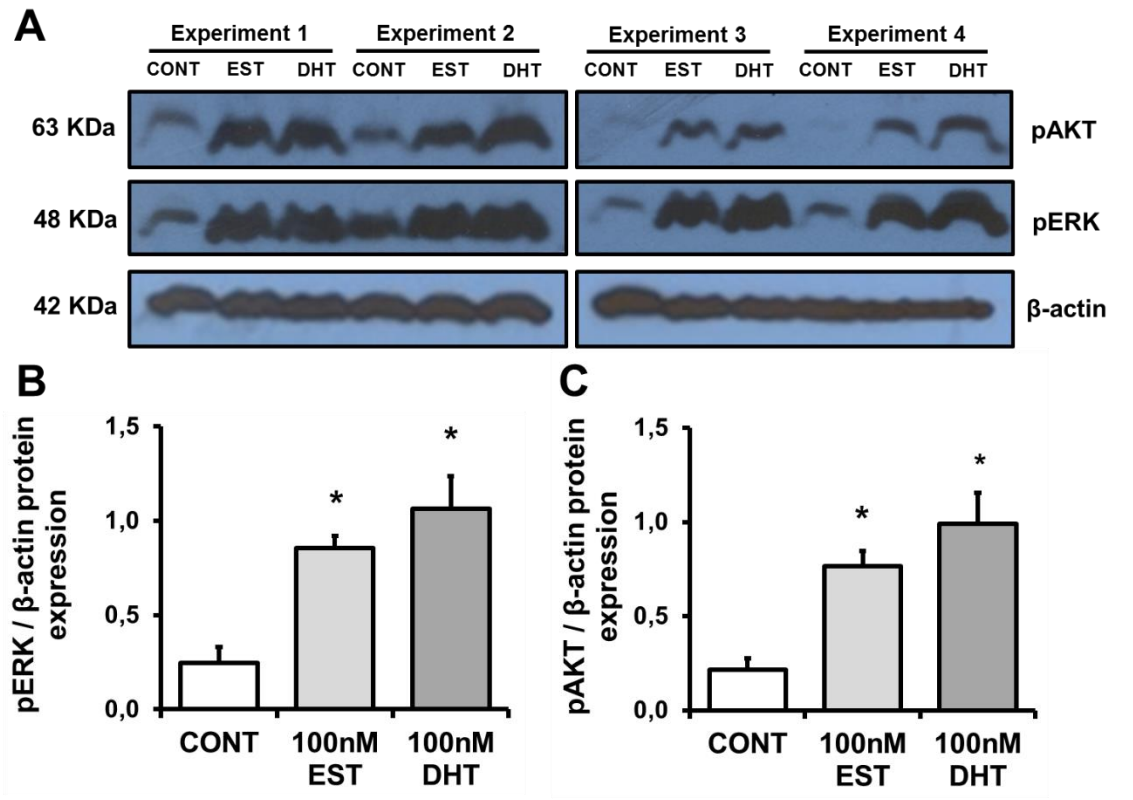

Figure 81. Control experiments. Panel A shows a representative Western blot demonstrating phosphorylation of AKT and ERK after stimulation with EST and DHT, but not in cells exposed to ethanol alone (CONT). Densitometry analysis of each band was performed using Image J software. Intensities for pERK (B) and pAKT (C) were calculated and normalized to β-actin. Data are expressed as mean±SEM. *P<0.05 compared to control cells.

This control experiment demonstrated that DHT and EST engaged the androgen and estrogen receptor, respectively, leading to predictable signaling events in the cells. Although phosphorylation of AKT and ERK are one of many downstream events

initiated by sex hormones, this was an important confirmation that PTEC exhibited a biological response to DHT and EST.

5.E.II. Spike-in SILAC quantitative analysis of sex hormone-treated PTEC proteome

5.E.II.1. Labeling efficiency of HK-2 cells

For accurate, in-depth characterization of the proteomes in these different conditions we employed the advantages of spike-in SILAC[478,479]. We thus heavy-labeled immortalized proximal tubular cell line (HK-2), and used it in spike-in experiments for relative quantification. We first evaluated the efficiency of labeling of HK-2 cells. Although even 5 doublings demonstrated excellent labeling efficiency, we selected 8 doublings, which showed the highest labeling efficiency (99.66%) (Table 20).

Table 20. Summary of labeling efficiency results in SILAC-labeled HK-2 at different time points.

Cell population doublings	Aminoacid	Labeling efficiency (%)
>5 Doublings (10 days)	Arg+6	99,24
	Lys+8	99,44
	Average	99,34
>6 Doublings (12 days)	Arg+6	99,15
	Lys+8	99,58
	Average	99,37
>8 Doublings (16 days)	Arg+6	99,89
	Lys+8	99,43
	Average	99,66
>10 Doublings (21 days)	Arg+6	98,84
	Lys+8	99,42
	Average	99,13

5.E.II.2. Identified and quantified proteins

Proteins from “heavy” HK-2 cells were spiked into the lysate of each of the samples from treated cells, acting as an internal heavy standard to quantify the light proteome of PTEC under each experimental condition. Mixed proteomes were then analyzed by online liquid chromatography mass spectrometry (LC-MS/MS). EST-treated PTEC in experiment 1 ultimately showed poor protein recovery after peptide fractionation, and was thus eliminated from analysis.

MS analysis identified 5111 proteins. Of those, 5043 were accurately quantified in at least one sample, and 3958 were accurately quantified in at least one replicate of each condition (Figure 82A). Log2 transformed ratios and their distributions were evaluated. Histograms showed normal distributions for all three ratios (Figure 82B-D). However,

histograms for DHT/CONT and EST/CONT were modestly shifted to the right (Figure 82B,C), even after normalization.

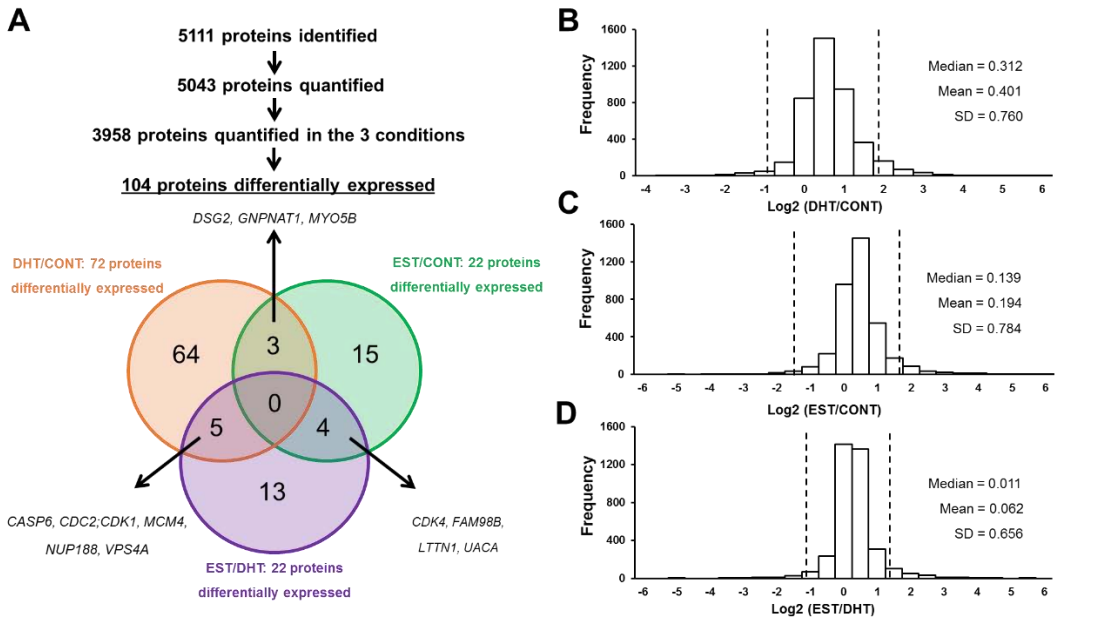

Figure 82. Identified, quantified and differentially expressed proteins in our spike-in SILAC approach. The scheme illustrates the number of identified and quantified proteins, followed by a Venn diagram representing the number and overlap of significantly regulated proteins according to significance A for DHT/CONT, EST/CONT and EST/DHT ratio values (A). Histograms depicting the distributions of Log2 transformed DHT/CONT (B), EST/CONT (C) and EST/DHT (D) ratios are shown. Vertical lines represent 1.96·SD.

5.E.II.3. Technical and biological reproducibility

Spearman's rank correlations were calculated between H/L normalized ratios of two different samples, considering all possible combinations among the 11 samples. As shown in Table 21, correlation coefficients between biological replicates from the same passage were higher than the coefficients between biological replicates from different passages. This observation was true not only in treated but also in control cells, indicating an intrinsic variability of the PTEC proteome across passages. Similar findings had been reported previously[479].

Table 21. Spearman's rank correlations between H/L normalized ratios of two different samples. Values for biological replicates within the same passage are depicted in green, while orange cells indicate the correlation coefficient between samples from different passages.

H/L normalized ratios	CONT_1	CONT_2	CONT_3	CONT_4	DHT_1	DHT_2	DHT_3	DHT_4	EST_2	EST_3	EST_4
CONT_1											
CONT_2	0,861										
CONT_3	0,553	0,526									
CONT_4	0,572	0,537	0,878								
DHT_1	0,832	0,777	0,607	0,632							
DHT_2	0,815	0,772	0,638	0,638	0,867						
DHT_3	0,483	0,475	0,846	0,853	0,547	0,564					
DHT_4	0,452	0,437	0,850	0,859	0,502	0,529	0,871				
EST_2	0,849	0,820	0,568	0,593	0,858	0,812	0,506	0,466			
EST_3	0,489	0,472	0,840	0,856	0,558	0,545	0,870	0,861	0,501		
EST_4	0,466	0,455	0,864	0,851	0,521	0,548	0,863	0,893	0,480	0,865	

5.E.II.4. Differentially expressed proteins

We decided to only consider those proteins that were differentially regulated in both passages, or that at least, did not change in the opposite direction in different passages. Based on significance A, a total of 104 proteins were differentially expressed between 2 conditions (Figure 82A, Table 22).

Table 22. Summarized median DHT/CONT, EST/CONT and EST/DHT ratios for the 104 proteins that are differentially expressed in at least one of the comparisons.

Gene names	DHT/CONT			EST/CONT			EST/DHT		
	Median	SEM	Significantly regulated	Median	SEM	Significantly regulated	Median	SEM	Significantly regulated
AHCTF1	1,026	0,271	NO	2,000	0,538	NO	2,215	0,756	YES (Upregulated)
ALDH1B1	7,439	0,072	YES (Upregulated)	0,852	0,214	NO	0,996	0,297	NO
ALDH4A1	6,806	2,960	YES (Upregulated)	1,575	0,444	NO	0,381	0,331	NO
ARHGAP4	0,834	0,501	NO	3,166	NaN	NO	9,212	6,840	YES (Upregulated)
ATP1B3	1,095	0,128	NO	1,334	0,210	NO	1,823	0,327	YES (Upregulated)
BCKDHA	5,963	3,364	YES (Upregulated)	1,705	2,316	NO	0,817	0,105	NO
C14orf159	8,330	3,011	YES (Upregulated)	0,981	0,049	NO	1,138	0,035	NO
C19orf25	5,837	1,241	YES (Upregulated)	0,495	NaN	NO	0,848	NaN	NO
CAD	3,704	3,848	YES (Upregulated)	1,100	14,303	NO	1,011	0,523	NO
CALR	7,818	1,205	YES (Upregulated)	0,981	0,576	NO	0,997	0,252	NO
CASP6	5,212	1,577	YES (Upregulated)	1,232	0,428	NO	0,256	0,050	YES (Downregulated)
CDC2;CDK1	20,344	10,175	YES (Upregulated)	1,386	1,118	NO	0,187	0,757	YES (Downregulated)
CDC37	1,953	0,520	NO	2,027	1,051	YES (Upregulated)	1,202	0,392	NO
CDC73	2,510	0,947	NO	3,039	NaN	NO	2,065	0,120	YES (Upregulated)
CDK4	1,664	0,095	NO	4,016	2,809	YES (Upregulated)	2,101	1,989	YES (Upregulated)
CDK5RAP3	8,448	0,470	YES (Upregulated)	0,947	0,021	NO	0,567	0,461	NO
CDKN2AIP	6,325	0,988	YES (Upregulated)	NaN	NaN	NO	0,839	NaN	NO
CRNKL1	0,756	0,362	NO	2,182	0,474	NO	3,394	0,895	YES (Upregulated)
CTSB	16,341	3,667	YES (Upregulated)	1,062	1,245	NO	1,501	0,673	NO
CTSC	8,085	2,518	YES (Upregulated)	0,943	0,410	NO	1,301	0,379	NO
CTSZ	8,807	0,076	YES (Upregulated)	0,952	0,080	NO	0,986	0,297	NO
CYP3A5	19,781	3,384	YES (Upregulated)	0,481	NaN	NO	0,029	NaN	NO
DDAH2	1,171	1,905	NO	7,923	2,302	YES (Upregulated)	1,238	2,374	NO
DPP7	9,013	3,814	YES (Upregulated)	1,012	0,244	NO	1,167	0,516	NO
DSG2	3,466	1,034	YES (Upregulated)	2,618	0,891	YES (Upregulated)	0,776	0,074	NO
DUSP23	1,232	0,625	NO	2,664	0,351	YES (Upregulated)	1,457	0,500	NO
ECHS1	6,356	0,933	YES (Upregulated)	0,973	0,079	NO	1,050	0,324	NO
EDIL3	1,488	1,519	NO	2,216	0,611	YES (Upregulated)	0,874	0,615	NO
F11R	1,955	0,596	NO	1,914	0,279	NO	1,167	1,352	NO
FAM98B	2,897	0,806	NO	10,421	8,163	YES (Upregulated)	4,965	0,486	YES (Upregulated)
FAU	0,636	0,123	NO	0,859	0,532	NO	2,238	0,332	YES (Upregulated)
FKBP4	15,092	8,408	YES (Upregulated)	0,706	1,665	NO	0,894	0,258	NO
GATAD2B	1,928	0,342	NO	2,380	0,192	YES (Upregulated)	1,346	0,474	NO
GGH	6,630	0,150	YES (Upregulated)	0,875	0,182	NO	1,142	0,158	NO
GLDC	1,483	0,505	NO	2,482	0,567	YES (Upregulated)	1,746	0,212	NO
GLS	6,892	1,572	YES (Upregulated)	0,854	0,362	NO	1,113	0,009	NO
GLUD1;GLUD2	9,265	1,726	YES (Upregulated)	0,957	0,351	NO	1,054	0,321	NO
GNA13	17,180	4,978	YES (Upregulated)	9,777	9,754	NO	1,065	0,061	NO
GNPNAT1	5,626	1,631	YES (Upregulated)	2,171	0,001	YES (Upregulated)	0,421	0,122	NO
GPI	12,068	9,117	YES (Upregulated)	1,242	3,165	NO	1,019	0,250	NO
HADHA	8,027	1,105	YES (Upregulated)	0,882	0,683	NO	1,073	0,254	NO
HADHB	7,514	1,955	YES (Upregulated)	0,990	0,981	NO	1,027	0,218	NO
HELLS	0,133	NaN	NO	0,255	NaN	NO	1,901	0,018	YES (Upregulated)
HEXB	7,279	2,790	YES (Upregulated)	0,475	0,225	NO	0,523	0,112	NO
HPCAL1;HPCA;NCALD	6,180	0,548	YES (Upregulated)	0,848	0,831	NO	0,895	0,164	NO
HSPA14	2,183	2,053	YES (Upregulated)	2,030	0,477	NO	1,017	0,280	NO
HYOU1	11,009	0,051	YES (Upregulated)	0,790	0,057	NO	1,020	0,025	NO
IDH3G;hCG_2004980	0,598	0,049	NO	1,513	0,202	NO	2,521	0,132	YES (Upregulated)
IMPAD1	1,135	0,136	NO	1,768	0,124	NO	1,910	0,161	YES (Upregulated)
KHSRP	13,118	3,911	YES (Upregulated)	0,794	1,575	NO	0,893	0,205	NO
LEMD3	0,429	0,094	NO	1,080	0,178	NO	2,602	0,720	YES (Upregulated)
LETM1	6,306	0,888	YES (Upregulated)	0,974	0,618	NO	1,143	0,259	NO
LTN1	0,789	0,147	NO	2,683	0,257	YES (Upregulated)	3,494	0,415	YES (Upregulated)
LYAR	1,308	1,701	YES (Upregulated)	0,866	0,712	NO	0,973	0,233	NO
MAN2B1	4,416	2,410	YES (Upregulated)	1,669	0,359	NO	0,577	0,302	NO
MCM4	8,936	13,031	YES (Upregulated)	0,203	0,610	NO	0,150	0,041	YES (Downregulated)
MDH2	9,249	2,752	YES (Upregulated)	0,792	0,351	NO	1,008	0,296	NO
MRPL40	2,273	0,496	YES (Upregulated)	3,368	NaN	NO	0,800	NaN	NO
MSH6	1,443	0,338	NO	2,255	3,419	YES (Upregulated)	1,224	1,457	NO
MYEF2	6,874	0,127	YES (Upregulated)	0,705	NaN	NO	0,943	NaN	NO
MYO5B	2,852	0,321	YES (Upregulated)	3,176	0,705	YES (Upregulated)	2,493	2,910	NO
NASP	3,023	1,839	YES (Upregulated)	0,922	0,729	NO	0,971	0,701	NO
NUCB1	8,733	4,209	YES (Upregulated)	0,948	1,403	NO	0,517	0,339	NO
NUDT15	0,881	NaN	NO	2,576	0,008	YES (Upregulated)	NaN	NaN	NO
NUP188	2,734	1,835	YES (Upregulated)	0,767	0,062	NO	0,185	0,073	YES (Downregulated)
PALLD	5,965	3,219	YES (Upregulated)	2,502	5,275	NO	1,139	0,099	NO
PARK7	11,700	5,605	YES (Upregulated)	1,168	0,158	NO	1,072	0,345	NO
PCBD1	6,425	3,355	YES (Upregulated)	1,104	0,199	NO	0,487	0,259	NO
PDHB	8,464	2,035	YES (Upregulated)	0,782	1,070	NO	0,837	0,223	NO
PIN1	1,455	0,431	NO	2,345	0,941	YES (Upregulated)	1,323	0,439	NO
PLBD2	7,145	4,383	YES (Upregulated)	1,271	1,318	NO	1,117	0,271	NO
PPIL3	3,224	2,113	YES (Upregulated)	1,783	1,372	NO	0,715	0,459	NO
PPM1G	15,859	1,541	YES (Upregulated)	3,151	1,825	NO	0,860	0,513	NO
PSAP	9,220	3,803	YES (Upregulated)	1,091	0,865	NO	0,968	0,270	NO
PTBP1	10,770	4,759	YES (Upregulated)	0,947	2,358	NO	0,994	0,168	NO
QPRT	3,164	2,123	YES (Upregulated)	1,187	0,490	NO	0,967	0,254	NO
RABGGTA	2,152	1,583	YES (Upregulated)	1,495	0,121	NO	0,939	0,188	NO
RHEB	42,329	40,063	YES (Upregulated)	2,055	0,572	NO	0,472	0,435	NO
RIPK1	6,101	4,253	YES (Upregulated)	1,347	0,465	NO	0,883	0,104	NO
RPA2	0,350	NaN	NO	1,902	0,777	YES (Upregulated)	0,282	NaN	NO
RPS6	0,676	0,160	NO	1,900	NaN	NO	2,290	0,468	YES (Upregulated)
RPUSD2	3,334	1,153	YES (Upregulated)	3,419	NaN	NO	1,568	NaN	NO
SDF4	8,346	0,535	YES (Upregulated)	0,996	0,556	NO	1,309	0,364	NO
SFN	2,435	0,263	NO	2,558	0,180	YES (Upregulated)	0,926	0,130	NO
SLC4A1AP	2,952	0,878	YES (Upregulated)	1,078	0,047	NO	0,699	0,331	NO
SOD2	6,109	1,587	YES (Upregulated)	1,145	1,153	NO	0,588	0,231	NO
SRSF10	10,303	8,225	YES (Upregulated)	5,309	4,715	NO	7,268	2,388	NO
SRSF2;SRSF8	6,395	3,138	YES (Upregulated)	1,507	6,084	NO	1,327	0,262	NO
SUCLG2	7,160	0,323	YES (Upregulated)	0,926	0,626	NO	1,020	0,286	NO
TALDO1	7,875	3,891	YES (Upregulated)	1,025	0,292	NO	0,955	0,288	NO
TKT	3,950	2,514	YES (Upregulated)	1,156	0,338	NO	1,028	0,289	NO
TMPO	1,956	1,434	NO	1,637	0,177	NO	2,094	0,669	YES (Upregulated)
TMSB15B;TMSB15A	0,585	2,257	NO	5,868	2,490	YES (Upregulated)	1,883	0,485	NO
TMSB4X	15,253	9,388	YES (Upregulated)	1,263	0,124	NO	1,053	0,358	NO
TNRC11;MED12	7,550	1,477	YES (Upregulated)	NaN	NaN	NO	NaN	NaN	NO
TNS1	0,874	1,030	NO	1,429	0,346	NO	3,222	0,300	YES (Upregulated)
TOP2A	5,088	2,515	YES (Upregulated)	3,521	2,395	NO	0,608	0,170	NO
TRIO	1,265	1,483	NO	3,080	2,610	YES (Upregulated)	2,087	4,268	NO
TUBB6	3,253	3,862	YES (Upregulated)	0,959	0,179	NO	0,541	0,209	NO
UACA	2,560	5,024	NO	2,852	0,217	YES (Upregulated)	2,319	0,107	YES (Upregulated)
UHRF1	1,279	0,522	NO	0,187	0,029	YES (Downregulated)	0,621	0,409	NO
UNG	2,747	0,528	YES (Upregulated)	2,405	NaN	NO	0,734	NaN	NO
VPS4A	4,048	0,848	YES (Upregulated)	1,041	0,125	NO	0,303	0,022	YES (Downregulated)
WDR5	2,186	2,707	YES (Upregulated)	1,485	0,757	NO	0,883	0,286	NO

Individual peptide ratios for all differentially regulated candidates were examined manually (data not shown). Seventy-two proteins differentially expressed after treatment with DHT as compared to control cells. Treatment with EST resulted in 22 differentially expressed proteins compared to control cells. As shown in the Venn diagram, 3 proteins were differentially regulated by both male and female sex hormones. In turn, 22 proteins were differentially regulated between DHT- and EST-treated cells (Figure 82A).

Log2 transformed normalized ratios are shown as heat maps for all DHT/CONT, EST/CONT and EST/DHT differentially regulated proteins (Figure 83).

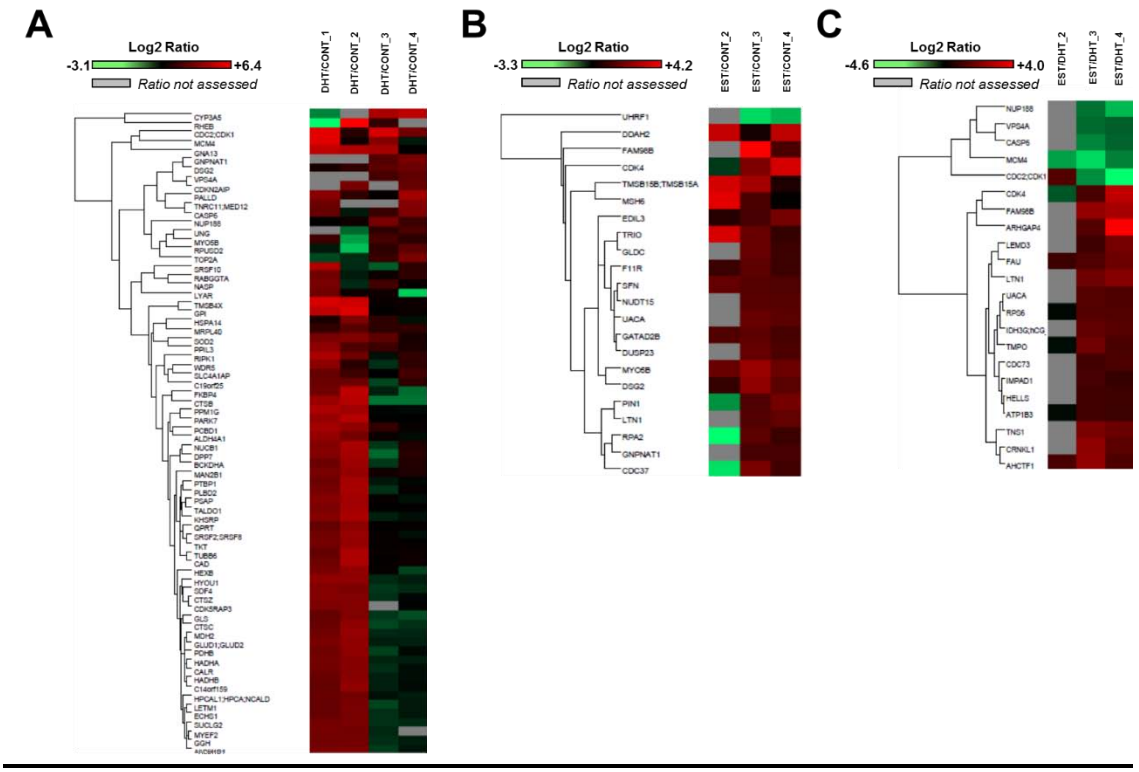

Figure 83. Heat map representation of sex-regulated proteins in PTEC. Heat maps were constructed using Perseus software and reflect the value of Log2 transformed normalized DHT/CONT (A), EST/CONT (B) and EST/DHT (C) ratios for each individual protein (rows) in each experiment (columns). The color intensity of red and green boxes correlates with the degree of protein over- and under expression, respectively. Grey boxes indicate that the ratio was not assessed for that particular protein in that particular experiment.

Interestingly, all DHT-regulated proteins were up-regulated relative to control (Figure 83A, Table 22). Similarly, only RING-finger type E3 ubiquitin ligase (UHRF1), an important nuclear protein that that plays critical roles in regulating various processes such as DNA methylation maintenance and G1/S transition[512], was found to be downregulated after EST treatment (Figure 83B, Table 22). Among 22 proteins differentially expressed when comparing the two sex hormone treatments, 17 proteins

showed higher expression and only 5 proteins were lower in EST- as compared to DHT-treated cells (Figure 83C, Table 22). The intrinsic variability across passages is also reflected in the values of the ratios between conditions, as replicates 1 and 2 represent passage 4, and replicates 3 and 4 represent passage 5.

5.E.II.5. Gene ontology and molecular pathway analysis

We next evaluated Gene Ontologies of our proteins differentially regulated by sex hormones. Some of the most relevant and significant biological processes enriched among all DHT-regulated proteins were fatty acid beta-oxidation (FAO), glutamine metabolic process, N-acetylglucosamine metabolic process, glucose catabolic process, tricarboxylic acid (TCA) cycle, and response to hydrogen peroxide, indicating DHT-induced alterations in energy metabolism (Figure 84). In this sense, gene ontology revealed mitochondrion as one of the most enriched cellular organelles (Table 23).

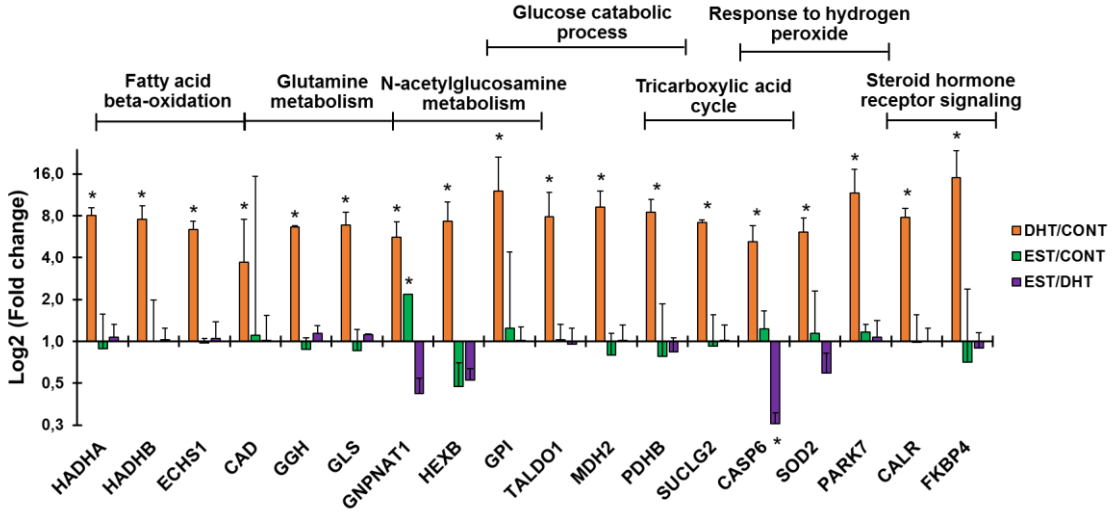

Figure 84. Enriched biological processes among the 72 proteins differentially regulated by DHT. Bar graphs illustrating the Log2 transformed DHT/CONT, EST/CONT and EST/DHT ratios of several DHT-regulated proteins involved in the most representative, informative and significantly enriched biological processes according to gene ontology analysis using BinGO plugin in Cytoscape. An asterisk indicate that these protein was significant by significance A with $p<0.01$ in at least 2 experiments

Steroid hormone receptor signaling biological process was also significantly enriched by DHT treatment (Figure 84). Indeed, positive regulators of androgen signaling pathway such as protein deglycase DJ-1 (PARK7)[513,514], calreticulin (CALR)[515] and heat shock protein 90 cochaperone FKBP52 (FKBP4) [516–518] were up-regulated, providing further confirmation of the PTEC biological response to DHT treatment. Biological processes linked to apoptosis were also significantly enriched in the analysis of both DHT- and EST-regulated proteins (Table 23).

Table 23. Most representative and biologically relevant gene ontology terms that were significantly enriched among DHT/CONT regulated proteins.

Gene ontology classification: BIOLOGICAL PROCESS			
Gene ontology term	**p value**	**Corrected p value**	**Genes**
Carboxylic acid metabolic process	$2.19e^{-5}$	$1.89e^{-3}$	*BCKDHA, HADHB, ALDH4A1, GPI, HADHA, ECHS1, MDH2, QPRT, CAD, GGH, GLS*
Glutamine metabolic process	$3.98e^{-5}$	$2.51e^{-3}$	*CAD, GGH, GLS*
Coenzyme metabolic process	$4.82e^{-5}$	$2.86e^{-3}$	*MDH2, QPRT, TALDO1, SUCLG2, PDHB, SOD2*
Glucose catabolic process	$7.50e^{-5}$	$3.79e^{-3}$	*GPI, MDH2, TALDO1, PDHB*
N-acetylglucosamine metabolic process	$8.00e^{-5}$	$3.79e^{-3}$	*GPI, HEXB, GNPNAT1*
Apoptotic chromosome condensation	$1.07e^{-4}$	$4.42e^{-3}$	*TOP2A, CAD*
Tricarboxylic acid cycle	$1.07e^{-4}$	$4.42e^{-3}$	*MDH2, SUCLG2, PDHB*
Fatty acid beta-oxidation	$2.49e^{-4}$	$7.39e^{-3}$	*HADHB, HADHA, ECHS1*
Cellular respiration	$7.43e^{-4}$	$1.59e^{-2}$	*MDH2, SUCLG2, PDHB, SOD2*
Response to hydrogen peroxide	$2.67e^{-3}$	$4.78e^{-2}$	*CASP6, PARK7, SOD2*
Gene ontology classification: MOLECULAR FUNCTION			
Gene ontology term	**p value**	**Corrected p value**	**Genes**
Enoyl-CoA hydratase activity	$1.48e^{-6}$	2.07e-4	*HADHB, HADHA, ECHS1*
Carbon-oxygen lyase activity	$8.21e^{-5}$	$3.28e^{-3}$	*HADHB, HADHA, ECHS1, PCBD1*
Transferase activity of aldehyde or ketones	$1.07e^{-4}$	$3.34e^{-3}$	*TALDO1, TKT*
Oxidoreductase activity	$1.42e^{-4}$	$3.98e^{-3}$	*BCKDHA, HADHB, ALDH4A1, HADHA, ALDH1B1, MDH2, PCBD1, PARK7, PDHB, SOD2, CYP3A5*
Sugar binding	$1.77e^{-4}$	$4.51e^{-3}$	*HEXB, PSAP, GNPNAT1, TALDO1, MAN2B1, CALR*
Cysteine-type endopeptidase activity	$2.66e^{-4}$	$5.50e^{-3}$	*CASP6, CTSZ, CTSC, CTSB*
Aldehyde dehydrogenase (NAD) activity	$6.36e^{-4}$	$9.89e^{-3}$	*ALDH4A1, ALDH1B1*
Nucleotide binding	$2.20e^{-3}$	$2.57e^{-2}$	*TOP2A, MYEF2, CAD, VPS4A, HSPA14, HADHB, GNA13, PTBP1, HADHA, TUBB6, RHEB, MYO5B, MCM4, SUCLG2, RIPK1, HYOU1, TKT, FKBP4, SRSF10*
Double-stranded RNA binding	$8.22e^{-3}$	$4.51e^{-2}$	*SLC4A1AP, CDKN2AIP*
Gene ontology classification: CELLULAR COMPONENT			
Gene ontology term	**p value**	**Corrected p value**	**Genes**
Mitochondrion	$2.12e^{-7}$	$2.44e^{-6}$	*BCKDHA, C14ORF159, ECHS1, MDH2, PARK7, PDHB, SOD2, GLS, UNG, HADHB, ALDH4A1, LETM1, HADHA, MRPL40, ALDH1B1, PSAP, SUCLG2, RIPK1, CTSB*
Lytic vacuole	$3.19e^{-7}$	$3.21e^{-6}$	*DPP7, HEXB, CTSZ, PSAP, GGH, MAN2B1, CTSC, PLBD2, CTSB*
Lysosome	$3.19e^{-7}$	$3.21e^{-6}$	*DPP7, HEXB, CTSZ, PSAP, GGH, MAN2B1, CTSC, PLBD2, CTSB*
Fatty acid beta-oxidation multienzyme complex	$1.50e^{-5}$	$1.27e^{-4}$	*HADHB, HADHA*
Cytosol	$4.50e^{-3}$	$2.50e^{-2}$	*DPP7, CASP6, RHEB, QPRT, CAD, TALDO1, GGH, RIPK1, PARK7, CALR, TKT, FKBP4*

Deregulated metabolism is a key factor in many kidney diseases[415]. In DN, increased intracellular glucose metabolism leads to excessive activation of hexosamine and protein kinase C pathways, as well as accentuated non-enzymatic glucose oxidation to advanced glycation end products[3]. As a consequence, mitochondrial oxidative phosphorylation and reactive oxygen species (ROS) release are promoted. Increased FAO and acetyl-CoA production in TCA cycle accentuate these processes in the mitochondria[519]. DHT alone was able to deregulate processes that are also altered by diabetes such as glucose metabolism, N-acetylglucosamine metabolism (a relevant step in hexosamine biosynthetic pathway, HBP), and FAO. Thus, we selected GPI, GNPNAT1 and HADHA as candidates for validation that represented each one of these three processes. It is remarkable that GNPNAT1 protein expression was increased in both DHT- and EST-treated PTEC as compared to control cells. Figure X illustrates the role of the most representative DHT and EST up-regulated proteins in cellular energy metabolism pathways.

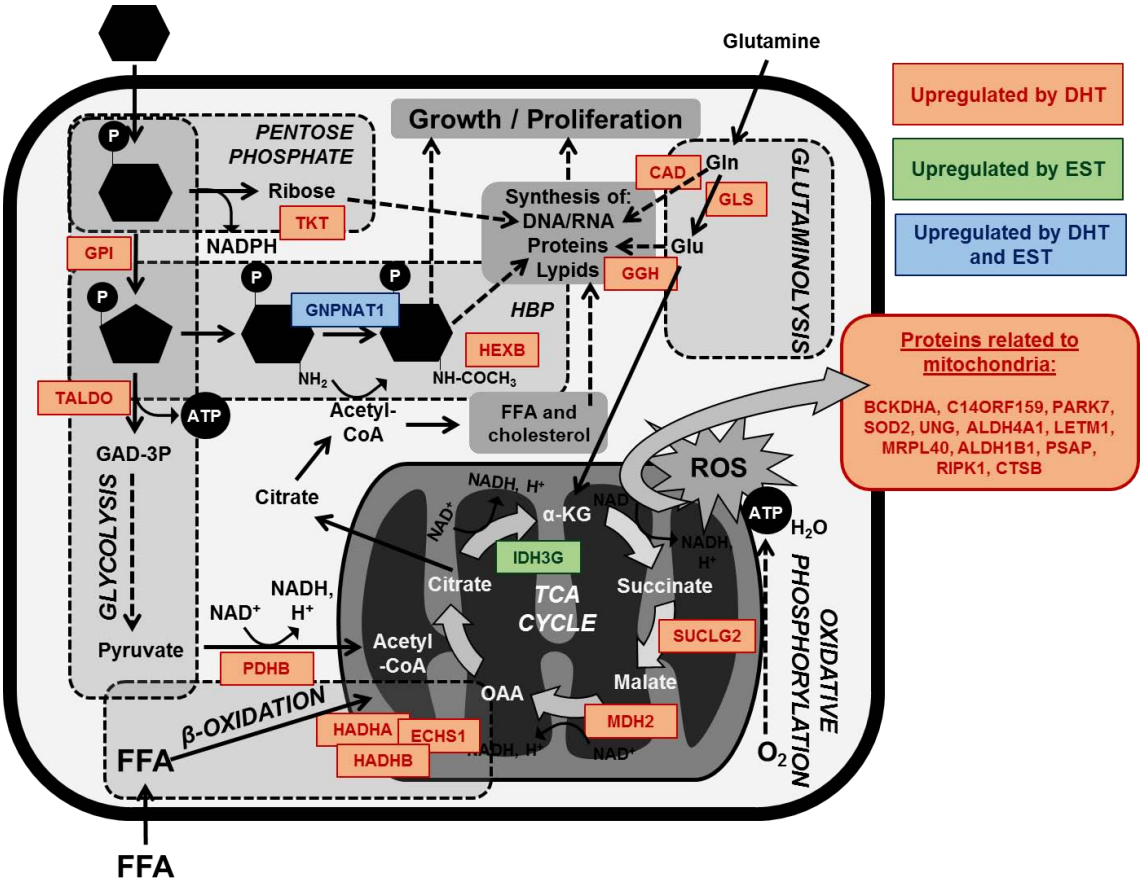

Figure 85. Role of DHT- and EST-regulated proteins in energy metabolism. The figure illustrates a simplification of several processes related to energy metabolism and mitochondrial compartment. Proteins that appeared to be up-regulated by DHT (orange), EST (green) or both DHT and EST (blue) are also represented. GAD-3P, glyceraldehyde-3-phosphate; FFA, free fatty acids; HBP, hexosamine biosynthetic pathway; Gln, glutamine; Glu, glutamate; ROS, reactive oxygen species; α-KG, alpha-ketoglutarate; OAA, oxaloacetate.

5.E.III. *In vitro* and *in vivo* validation

We next aimed to confirm SILAC ratios by Western Blot analysis in the same protein extracts used for the proteomic study. In consistence with our findings from SILAC, Western blot analysis in treated PTEC confirmed a significant up-regulation of HADHA, GPI and GNPNAT1 by DHT. To a lesser extent, these proteins were also up-regulated by EST (Figure 86).

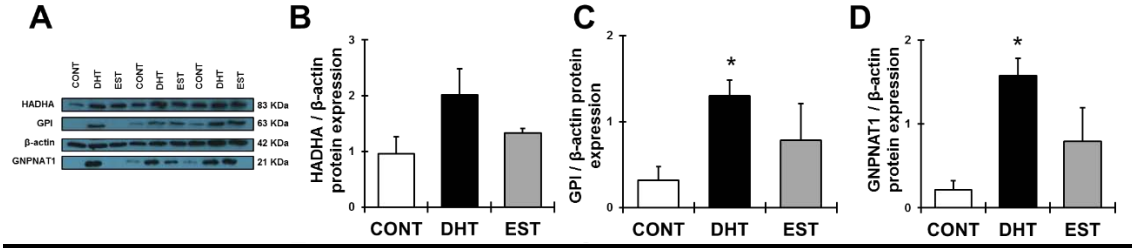

Figure 86. *In vitro* verification studies for HADHA, GPI, and GNPNAT1. Panel A shows the immunoblots representing HADHA, GPI, and GNPNAT1 protein expression in the same treated PTEC

used for the spike in SILAC study. Intensities for HADHA (B), GPI (C) and GNPNAT1 (D) were calculated and normalized to β-actin (B, C, D). Densitometry analysis of each band was performed using Image J software. Data are expressed as mean±SEM. *P<0.05 compared to control cells.

We next examined whether these observations were consistent in new PTEC stimulation experiments, at both passages studied in SILAC experiments. Cells at passage 4 and 5 were thus serum-starved for 18h and then treated with control, DHT or EST for 8h (n=5-6 in each passage). Expression of proteins HADHA, GPI and GNPNAT1 was numerically increased in DHT-treated cells at passage 4 (Table 25). At passage 5, both DHT- and EST-treated PTEC exhibited a significant increase in GNPNAT1 protein expression, a result concordant with SILAC protein expression data. However, HADHA and GPI at passage 5 were not up-regulated by DHT, simulating our SILAC experiments (Table 24).

Table 24. HADHA, GPI and GNPNAT1 protein expression normalized to β-actin in CONT, DHT and EST treated PTEC. *p<0.05 vs CONT.

	Passage 4 (n=6)			Passage 5 (n=6)		
	CONT	DHT	EST	CONT	DHT	EST
HADHA vs. β-actin protein expression	1.00 ± 0.07	1.15 ± 0.09	1.12 ± 0.05	1.00 ± 0.08	0.79 ± 0.21	1.84 ± 0.47
GPI vs. β-actin protein expression	1.00 ± 0.03	1.10 ± 0.07	1.04 ± 0.12	1.00 ± 0.18	1.03 ± 0.11	1.57 ± 0.28
GNPNAT1 vs. β-actin protein expression	1.00 ± 0.15	1.16 ± 0.20	1.06 ± 0.16	1.00 ± 0.22	1.53 ± 0.10*	2.37 ± 0.46*

We next aimed to examine whether our *in vitro* observations in PTEC have relevance *in vivo*. With this purpose, we determined expression of HADHA, GPI and GNPNAT1 proteins in the kidney of healthy female and male mice by immunohistochemistry. As shown in Figure 87, both sexes showed strong positive staining for all three candidates in cells from the proximal tubule and other tubular segments. These findings suggest that changes in renal HADHA, GPI and GNPNAT1 across sexes will be mostly ascribed to sex-specific regulation of these proteins in the tubular compartment, strengthening the significance of our *in vitro* observations.

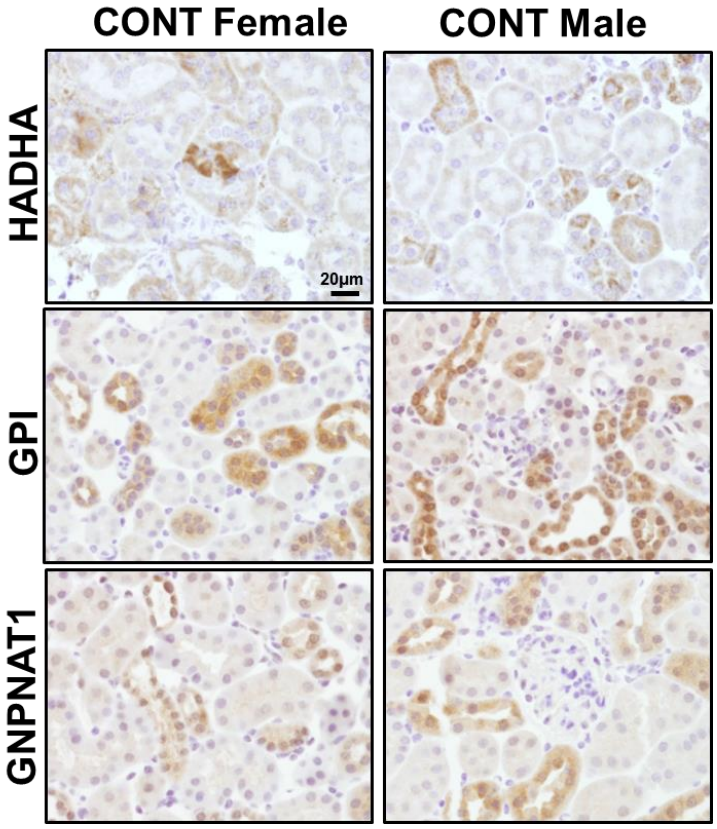

Figure 87. Localization of the top candidate proteins in the mouse kidney. The renal distribution of HADHA, GPI, and GNPNAT1 was evaluated in kidney sections from healthy female and male mice. As depicted in the microphotographs, these proteins were clearly expressed in the tubular compartment of both sexes. Scale Bar=20µm. Original magnification x40.

In concordance with our results from SILAC proteomics, Western Blot analyses revealed that, under physiological conditions, renal HADHA and GPI were significantly increased in males as compared to females. In contrast, GNPNAT1 was not significantly different between female and male mice (Figure 88).

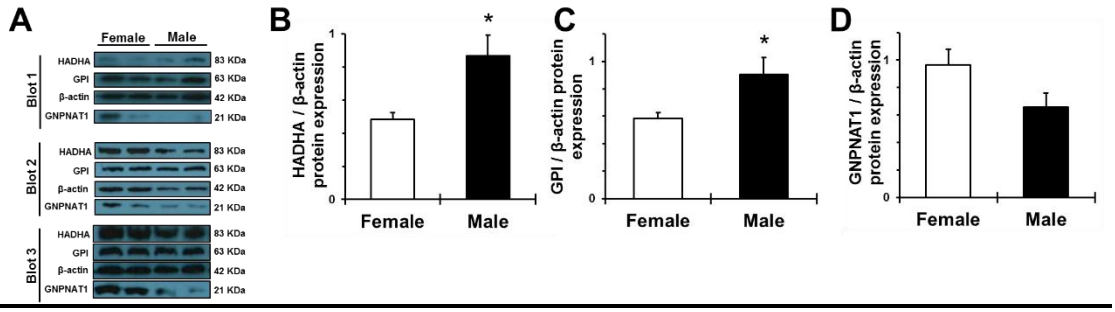

Figure 88. *In vivo* validation studies for HADHA, GPI, and GNPNAT1. Panel A shows the immunoblots representing HADHA, GPI, and GNPNAT1 protein expression in the kidney of healthy female and male mice. Densitometry analysis of each band was performed using Image J software. Intensities for HADHA (B), GPI (C) and GNPNAT1 (D) were calculated and normalized to β-actin (B, C, D). For these experiments, 6 animals were analyzed in each group. Data are expressed as mean±SEM. *P<0.05 compared to control cells.

Expression of HADHA and GPI renal proteins strongly and significantly correlated with animals' kidney weights (r=0.675, p=0.023; r=0.772, p=0.005; respectively) which were significantly increased in males as compared to females (Table 25).

Table 25. Physiological parameters at the end of the study. *p<0.05 vs female

Study group	Blood glucose (mM)	Body weight (g)	Kidney Weight (g)	KW/BW (%)
Female	9.80 ± 0.41	20.89 ± 0.79	0.25 ± 0.00	1.19 ± 0.03
Male	10.45 ± 0.15	29.09 ± 0.75*	0.33 ± 0.01*	1.12 ± 0.04

5.E.IV. Biological significance: Validation of top candidates in the diabetic kidney

Since our top candidate proteins belong to biological processes critical for DN[3], namely glycolysis, HBP and FAO, we evaluated the effect of sex on renal HADHA, GPI and GNPNAT1 protein expression in female and male mice of two different models of diabetes: the STZ-induced and the Akita ($Ins2^{WT/C96Y}$) models of type 1 diabetes. Interestingly, both STZ-induced and $Ins2^{WT/C96Y}$ diabetic males showed accentuated hyperglycemia compared to females, as well as a more severe renal hypertrophy in terms of KW and kidney to body weight ratio (Table 26).

Table 26. Physiological parameters at the end of the study. *p<0.05 vs female

Study group	Blood glucose (mM)	Body weight (g)	Kidney Weight (g)	KW/BW (%)
STZ female	306 ± 31.7	21.24 ± 0.43	0.24 ± 0.02	1.13 ± 0.08
STZ male	492 ± 41.4*	27.62 ± 0.66*	0.35 ± 0.02*	1.27 ± 0.07
$Ins2^{WT/C96Y}$ female	15.38 ± 2.05	20.11 ± 0.40	0.24 ± 0.01	1.20 ± 0.05
$Ins2^{WT/C96Y}$ male	32.50 ± 0.78*	26.14 ± 0.71*	0.53 ± 0.02*	2.03 ± 0.08*

In the setting of type 1 diabetes, male sex was associated to increased HADHA, GPI and GNPNAT1 protein expression as compared to females (Figure 89). Specifically, renal HADHA was significantly increased, whereas GPI and GNPNAT1 were modestly higher, in STZ males as compared to females (Figure 89A-D). We demonstrated that the expression of these three proteins was predominantly in renal tubules, similar to the control animals (Figure 89E). These findings were further validated in diabetic Akita mice, a genetic model of type 1 diabetes. Akita males showed significantly higher protein levels of HADHA and GNPNAT1, as well as a modest increase in GPI protein expression (Figure 89F-I). Correlation analyses in all the studied diabetic mice revealed a moderate but significant association between HADHA protein expression and KW (r=0.471, p=0.013).

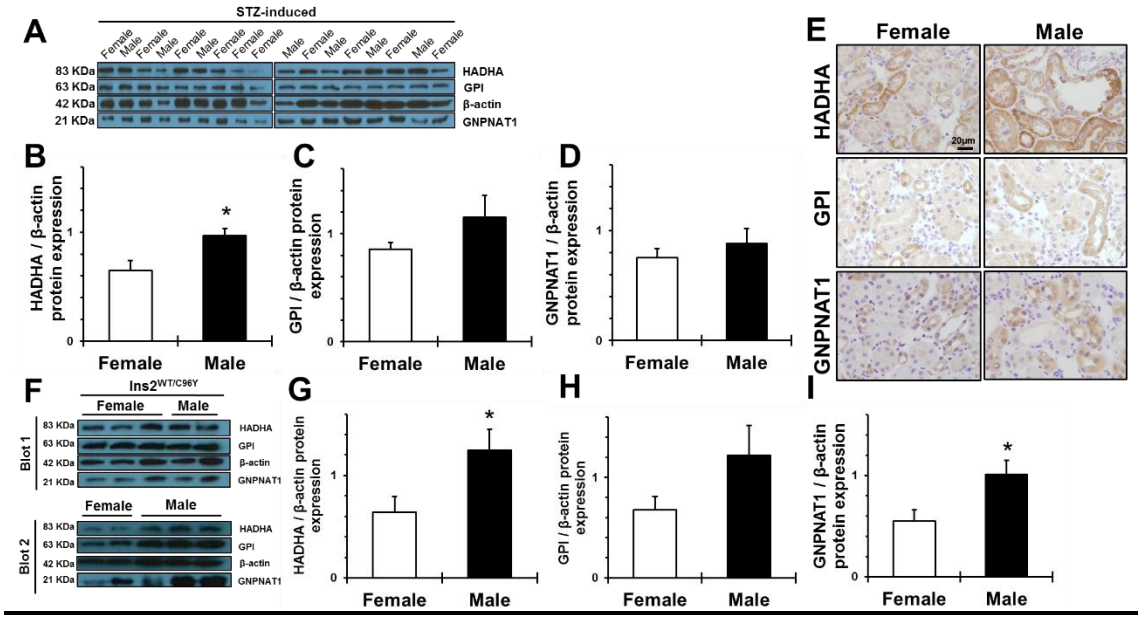

Figure 89. Protein expression and localization of HADHA, GPI, and GNPNAT1 in the mouse diabetic kidney. The expression of the 3 candidate proteins was evaluated in the renal cortex of female and male diabetic STZ-induced (A-E) and Ins2WT/C96Y (F-I) mice. Densitometry analysis of each band was performed using Image J software. Intensities for HADHA (B, G), GPI (C,H) and GNPNAT1(D,I) were calculated and normalized to β-actin. For these experiments, 5-10 animals were analyzed in each group. Data are expressed as mean±SEM. *P<0.05 compared to females.

5.E.V. Enriched functional category analysis

To elucidate if the perturbations in renal energy metabolism associated with DHT and male sex exerted deleterious effects on the kidney, we explored enriched biological processes in our SILAC data that were reproducible in prior studies of diabetes. We thus employed Enrichment Map plugin in Cytoscape and evaluated functionally enriched genes between our sex hormone proteomic dataset and previous transcriptomic datasets in kidney tissue[520,521] . Specifically, we superimposed a network of enriched GO terms among our 72 proteins up-regulated by DHT with the lists of genes up-regulated in human diabetic vs control kidneys[521] and in male vs female mice kidneys[520], and we found that several processes associated with oxidative stress were significantly enriched in both datasets (Figure 90). Specifically, response to gamma radiation, to inorganic substance, to hydrogen peroxide, and to reactive oxygen species, were significantly enriched in both proteomic and transcriptomic datasets. Nothing significant was shared after superimposing our list of EST-regulated proteins to the subsets of differentially expressed genes from female kidneys (data not shown).

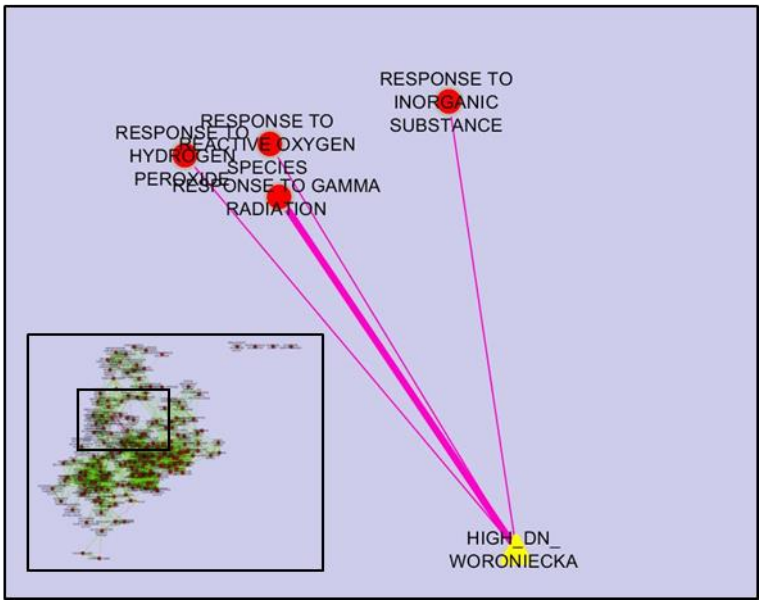

Figure 90. Functional enrichment of oxidative stress among our DHT-regulated proteins. The enrichment map (EM) was constructed imposing our list of DHT-regulated proteins to renal transcriptomic data sets from male mouse kidneys and human diabetic kidneys in Cytoscape. EM is depicted in the bottom, with a square indicating the zoomed in area in the panel. Each circle represents an enriched GO term, with red color indicating significance. Green edges indicate that up-regulated proteins are shared by the two GO terms they connect. The analysis revealed that functional groups associated to oxidative stress were shared with our data set. The pink edge represents overlap between the target gene set and the enriched biological processes from our experiment.

Given the recognized importance of oxidative stress in diabetic nephropathy, and its link to our dataset of DHT regulated proteins in kidney cells, we next examined whether oxidative stress was increased in male compared to female mouse kidneys. Examination of kidney tissues of male and female control mice demonstrated significantly increased nitrotyrosine staining in male kidneys (Figure 91A,B). Similarly, nitrotyrosine staining was significantly increased in kidneys of diabetic males as compared to females (Figure 91A,B).

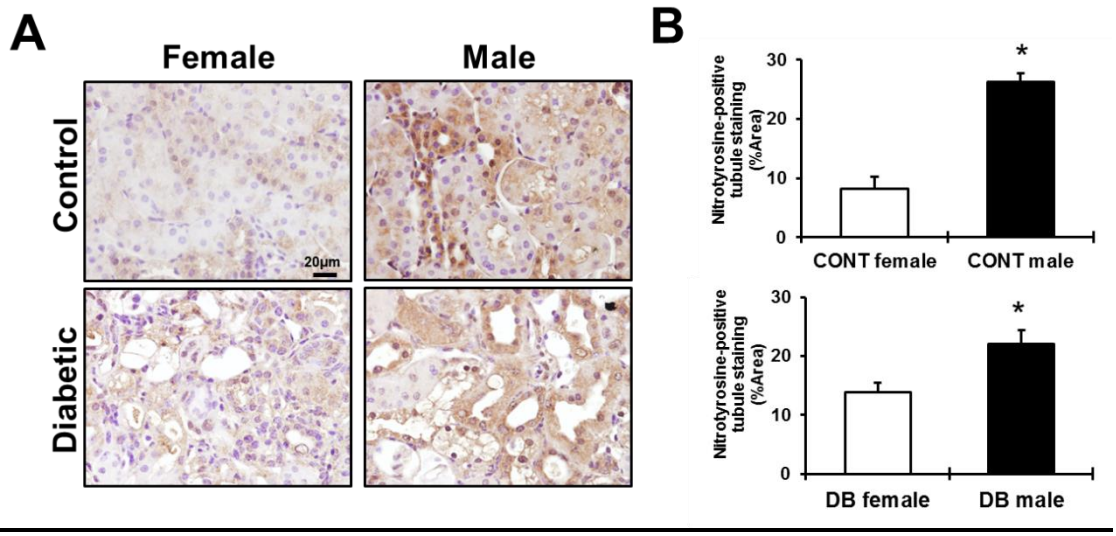

Figure 91. *In vivo* validation of the functional enrichment of oxidative stress. To validate the link between male sex and renal oxidative stress, nitrotyrosine immunostaining was used to evaluate superoxide and peroxynitrite levels in kidney sections from female and male, control and STZ-diabetic mice (A). Scale Bar = 20µm. Original magnification x40. Brown-stained areas were quantified with ImageJ software (B). Data are expressed as means ± SEM of positive area fraction (%). *P<0.05 compared to females.

5.E.VI. Additional bioinformatics analyses

5.E.VI.1. Enrichment of glycosphingolipid metabolism

Glycosphingolipid (GSL) metabolism also emerged as a significantly enriched functional group between our DHT-stimulated proteins and the transcriptomics data sets of diabetic and male kidneys (Figure 92A). The two key enzymes involved in GSL metabolism that were present in our list of DHT up-regulated proteins were beta-hexosaminidase subunit beta (HEXB) and prosaposin (PSAP).

Previous studies suggest that HEXB plays a role in the pathogenesis of DN[522]. Thus, we decided to validate the effect of sex on renal HEXB expression in our control and STZ-induced mice. In concordance with our bioinformatics findings, Western Blot analysis revealed that HEXB protein expression was higher in the renal cortex of control males as compared to females (Figure 92B). Cytoplasmic localization of this enzyme was observed by immunostaining in the tubules of both, males and females. In males, HEXB positive staining was also observed in the brush border of tubules with high degree of vacuolization. Furthermore, diabetic males showed increased cortical expression of HEXB as compared to females (Figure 92C).

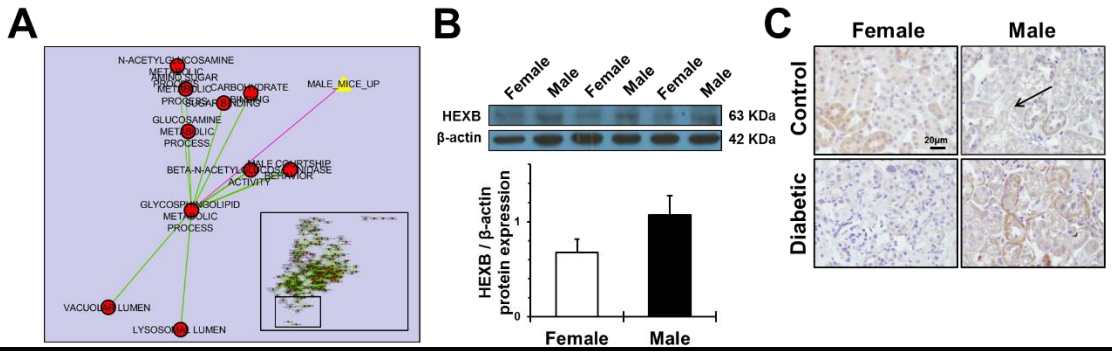

Figure 92. Functional enrichment analysis of DHT-regulated proteins unmasked a link between male sex, diabetes and glycosphingolipid metabolism in the kidney. The analysis revealed that functional groups associated to GSL metabolism were shared with our data set (A). The entire enrichment map is depicted in the right bottom of the image, with a square indicating the zoomed in area in the panel. Each circle represents an enriched GO term, with red color indicating significance. Green edges indicate that up-regulated proteins are shared by the two GO terms they connect. The pink edge represents overlap between the target gene set and the enriched biological processes from our experiment. To validate the link between male sex and renal GSL metabolism, Western Blot (B) and immunohistochemistry (C) for HEXB were performed. The black arrow indicates HEXB localization in the brush border of a proximal tubule. Scale Bar = 20μm. Original magnification x40. For these experiments, 4-6 animals were analyzed in each group. Data are expressed as mean±SEM.

5.E.VI.2. Enzyme-metabolite network analysis

Using Metscape plugin in Cytoscape, we visualized the connections between our DHT-regulated proteins in PTEC and a list of human serum metabolites that showed significant differences between men and women obtained from Krumsiek and coauthors metabolomics data set[523]. The analysis revealed association between our subset of proteins and several metabolites related to TCA cycle (Figure 93A) and the metabolism of several amino acids such as glutamate, glycine (Figure 93A), serine, leucine, isoleucine, valine (Figure 93B), and proline (Figure 93).

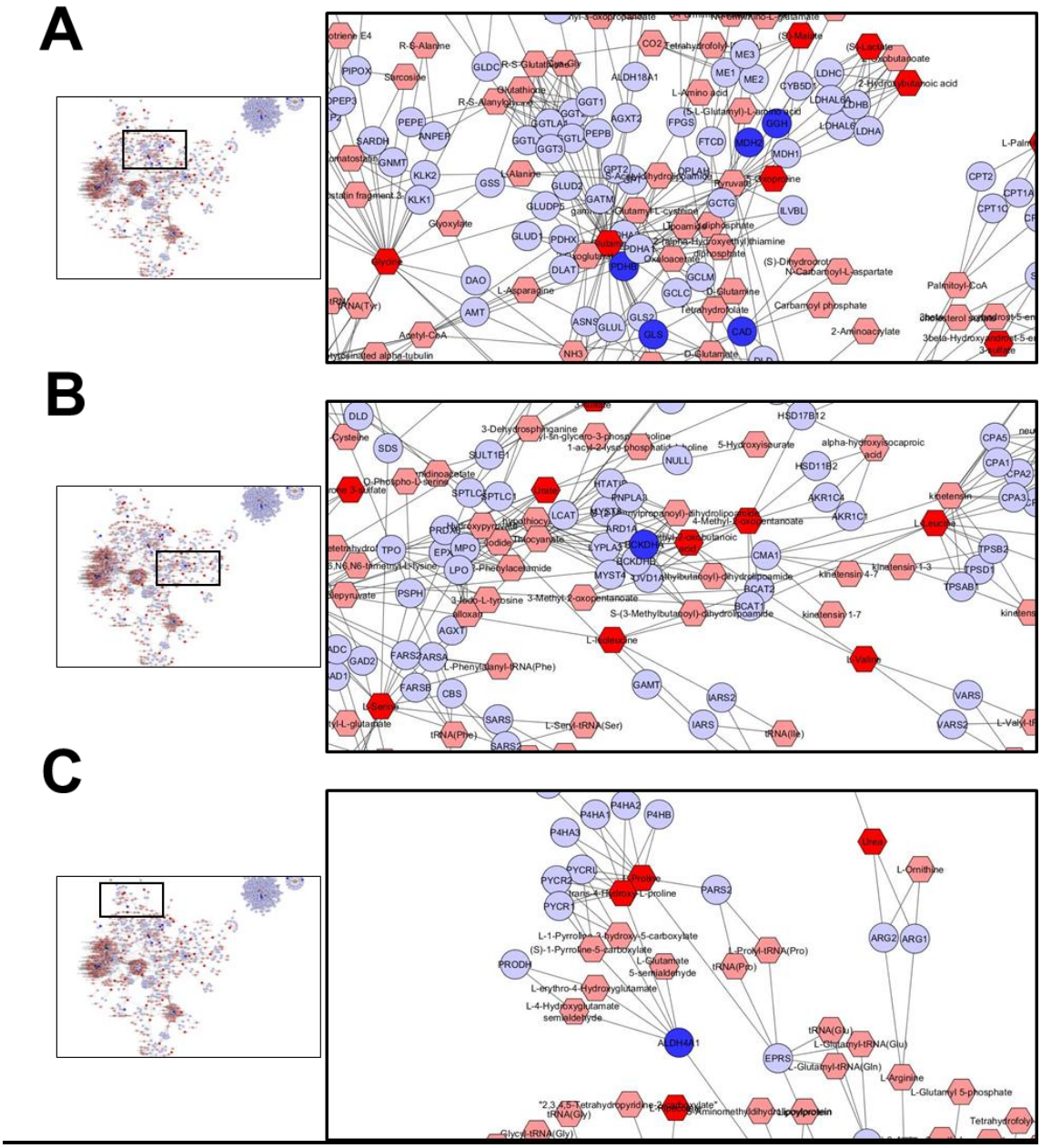

Figure 93. DHT-induced alterations in tricarboxylic acid cycle and amino acid metabolism are linked to sex-related changes in the human serum metabolome. Using Metscape plugin in Cytoscape, we visualized the connections between our DHT-regulated proteins in PTEC (intense blue circles) and many human serum metabolites that showed significant sex differences as previously reported (67) (intense red hexagons). The enzyme/metabolite network is depicted to the left of each image, with a square indicating the zoomed in area in the panel. The analysis revealed association between our subset of proteins and several metabolites related to TCA cycle (A) and the metabolism of several amino acids such as glutamate, glycine (A), serine, leucine, isoleucine, valine (B), and proline (C).

6. DISCUSSION